LECTURE NOTES   1

Muscle/Bone Interactions in the Musculo-Skeletal System

Joseph Mizrahi

Department of Biomedical Engineering
Technion Israel Institute of Technology
Haifa, Israel

a b i o m e d

Centre of Excellence for
Applied Biomedical Modelling and Diagnostics

WARSAW 2004

ABIOMED LECTURE NOTES

Series Editors:

Executive Committee of ABIOMED:
  J. Joachim Telega (*Scientific Coordinator*)
  Tomasz A. Kowalewski
  Tomasz Lekszycki
  Andrzej Nowicki

Contents

Foreword to the Series ABIOMED Lecture Notes

Main aims of the Centre of Excellence for Applied Biomechanical Modelling and Diagnostics (ABIOMED) can be summarized as follows:

- organising international conferences,
- organising a series of specialised lectures, conferences, workshops, and mini-symposiums,
- enhancing the international co-operation of the Institute of Fundamental Technological Research with European Universities and biomedical research centres.

Conferences, lectures and similar scientific events will be documented by publishing books in the series ABIOMED Lecture Notes. This series is intended to cover a broad spectrum of currently important topics in solid and fluid biomechanics as well as ultrasounds in medicine and biomedical engineering.

The present volume, written by Prof. Joseph Mizrahi (Head of the Department of Biomedical Engineering, Technion, Israel Institute of Technology, Haifa) is the first in the Series and presents lectures delivered by this author in September – October, 2003. The lectures were focused on impacting loads on the human body, the role of functional electrical stimulation in the presence od musculo-skeletal deficiencies, modelling and predictability of forces in stimulated muscle, and biomechanical interaction between muscle and bone.

Józef Joachim Telega
Scientific Coordinator of ABIOMED
Editor-in-Chief

Preface

Muscles and bones act together in the locomotor machine of the human body. The bones provide the structural basis and support. They are divided into segments separated by articular joints to provide the multiple degrees of freedom required to generate motion for mechanical daily activity. Muscles are attached to the bones and, by acting across the joints provide the torques required to either stabilize the multi-segmental structure (under static conditions) or to act as dynamic actuators for generating motion.

Due to their small lever arms relative to the joint's center of rotation, the muscle forces responsible for exerting the required torques are particularly high. Thus, contracting muscles do act as load amplifiers and are thus greatly responsible for the high-intensity loading of the bones and joints. This has special relevance to dynamic loading, particularly impact loading, which occurs, for instance, at heel-strike during walking or running. More severely, it is found in fast or impulsive walking, stair climbing, jumping, falling down or in collision. The shock impacts from each walking or running cycle are transmitted from the feet vertically upwards the skeleton to the different parts of the body and are often associated with damage.

Apart from its function as a joint actuator, muscle acts also as an active shock absorber, capable of attenuating impact loads. This property somewhat compensates for the severe loading burden that muscles put on the bones and joints. Another positive mechanical effect of muscle contraction on bone lies in the frequency spectrum of the load signal, having substantial components within the range of 10–50 Hz. While this frequency component is an extremely low frequency from the electromagnetic point of view, it is considered very high from mechanical aspects. Interestingly, dynamic loading applied at this frequency has been found to be beneficial in bone remodeling. With normal daily activities occurring at a frequency of around 1 Hz, only muscle can provide the 10–50 Hz mechanical components, which are beneficial for bone remodeling. Thus, in addition to exerting high-intensity loads on the bone

and joint systems, muscles have two beneficial roles: (a) provide the high frequency components of the mechanical loading, which are important for mediating the physiologic response of bone tissue, and (b) shock absorption.

Muscle fatigue hampers the muscles from effectively fulfilling the important role of attenuating impact shocks therefore protecting the skeleton and joints from damage. Fatigue may be considered to be a muscle deficiency. While this usually is a temporary deficiency, more permanent deficiencies such as in situations of post-stroke, lower limb amputation and deterioration related to aging, muscle impairment presents a high-risk situation that may endanger the skeleton and joints.

In the presence of musculo-skeletal deficiencies, a common consequence is the reduction of smoothness of motion, which characterizes normal gait. Stiff gait accompanied with bi-lateral asymmetry appears. Furthermore, previous studies have indicated that following disability on one side of the body, there is a developing tendency to transfer loading forces from this affected side to the contra-lateral side. This leads to a two-fold problem: due to reduced loading, osteoporosis is likely to develop on the affected side, while joint degeneration and osteoarthritis develop on the over-loaded contra-lateral side. Moreover, due to the stiffer nature of locomotion higher dynamic components contribute to increased impact loading, contributing to enhanced joint degeneration. Further studies have indicated substantial damage also to the spine. Thus, the primary disability provides a predisposition for a secondary disability, both creating a vicious circle of severing the locomotion abilities.

The following question may then be asked: Are there means to *enhance muscle activity* so as to increase its protective action under *fatigue* or other *conditions of muscle deficiency*?

Artificial activation of muscles by functional electrical stimulation (FES) may alter the loads on bones and joints. For instance, by activation of the tibialis anterior, tensile stresses can be reduced in the tibia. Moreover, activation of antagonistic muscles can modify the type of stresses on bone, depending on the modes of activation, e.g. symmetric, asymmetric or anti-symmetric. Thus, muscles can be activated either as limb actuators, or as shock absorbers. In the first case, activation may achieve better loading balance between the 2 legs by enhancing weakened functions. In the second case, muscle activation may serve to reduce impact loads. An interesting additional issue is whether electrical stimulation at 20–50 Hz compensates for the reduced muscle activity in that frequency?

The present book addresses these questions by combining the knowledge and experience gained in the author's laboratory in the following two areas: dynamic loading of the musculo-skeletal system in human locomotion and FES of muscles. The first chapter presents a treatise on the biomechanical implications of impacting loads on the human body. The concept of mechanical impedance is used to quantify the factors involved in body protection from dynamic loading. The second chapter introduces the phenomenon of electrical stimulation of muscles, particularly by discussing two associated key issues: muscle recruitment and muscle fatigue. The third chapter presents the work accomplished on modeling and force predictability in electrically stimulated muscle. Mechanical, myoelectric and metabolic manifestations of the contractile engine are used to set a comprehensive structural/phenomenological model. The fourth and last chapter ties together the issues discussed in the previous chapters. First, it analyses the mechanical manifestations of muscle fatigue, particularly in relation to shock load transmission. Muscle fatigue is further treated as an example of muscle deficiency. Additional contributors to muscle deficiency are also discussed. Finally, the prospective of the application of FES to enhance muscle activity and bone remodeling and reduce bone and joint loading are discussed.

Joseph Mizrahi, D.Sc.
Pearl Milch Professor of Biomedical Engineering Sciences
Head, Department of Biomedical Engineering,
Technion, Israel Institute of Technology
Haifa 32000, Israel

Chapter 1

Impacting Loads on the Human Body: Impedance Nonlinearities and their Role in Body Protection

1.1. Impact

Impact loading on the human body takes place at foot strike during walking and running and, more dramatically, during jumping. In fact, vertical jumping and landing are an important element in locomotion, sporting and other activities. With the development of biomechanical models of human body motion, it has become possible to simulate vertical jumping in order to gain insight into the intermuscular coordination and to elucidate control strategies of the musculoskeletal system. A common method to deal with this type of problems is to lump together elements of the human body e.g., muscles, tendons, ligaments, bones and joints so that the overall musculoskeletal system is represented as a damped elastic mechanism.

Impact loading is a high intensity load occurring in short durations. Exposure of the lower limbs to unusually high impact loads, as happens during landing from free fall may under certain conditions lead to one of the two following consequences:

1. Short-term damage, e.g., fracture of bones or rupture of tendons at their insertions (short-term fatigue) [Welsh, 1979]. This occurs due to progressing disproportion between load and strength of the musculo-skeletal tissues, which do not have sufficient time to adapt to the increasing mechanical stresses.

2. Long-term damage through joint degeneration [Radin et al., 1972], known as osteoarthritis of the joints.

The above listed consequences can be avoided by decreasing the impulsive forces transmitted to the body, which can be done by adequate shock absorption. There exist two types of mechanisms of shock absorption: one passive and one active.

In the passive mechanism, shock attenuation is achieved by the bone and soft tissues. Radin et al., [1970] suggested that trabecular bone has a major role in this mechanism, explaining that attenuation of dynamic peak forces is a function of the ability to deflect under these forces. As compared to synovial fluid and articular cartilage, bone deforms a little, but because it exists in much larger amounts, bone acts altogether in a more meaningful way. Fracture of the trabeculae is the most effective way to absorb energy. Moreover, as has been shown by Ducheyne et al. [1977], the process of fracture of the trabeculae is localized and gradual, which allows only minimal rupture during shock loading. This damage is restored in the living bone unless multiple overloading occurs, in which case progressive collapse of the trabecular structure may occur.

The active mechanism is far more significant than the passive one and it essentially relies on lengthening of muscles under tension, accompanied by joint motion. This mechanism can be easily demonstrated in walking on the heels, with the ankles and knees extended and the muscles tight, causing a jolt in each step, mainly because the active mechanism cannot function. A more extreme example was given by Smith as early as in 1953, who showed that a free fall of an 80 kg man from one meter height with a 'knee-locked situation' is likely to produce severe damage of the head and the neck of the femur or will push the head of the femur through the acetabulum.

It follows then that the main part of kinetic energy acquired by the body is dissipated by the muscles. It should however be remembered that the active mechanisms are under control of the reflexive neuro-muscular system and that there is a measurable time for this reflexive action. For instance, the time required for reflex activity from the otoliths to activate antigravity muscles in man ranges from 70 to 100 ms [Radin, 1974; McMahon and Greene, 1979; Isakov et al., 1986]. It can thus be concluded that, if rapid enough, loading will normally be unaccompanied by reflex accommodation.

Ideally, both shock-absorbing mechanisms complement each other. When deformation starts in the passive mechanisms, then according to Finlay and Repo, [1979] a neurological feedback system senses the resulting increased force and so brings muscles into play before the forces have time to reach

destructive levels. It should, however, be kept in mind that reflex mechanisms can be fatigued, as may happen with individuals performing repetitive tasks [Radin, 1974]. The ability to pre-program muscle action and joint motion therefore has major importance when reflex activity has not yet appeared. To make use of this ability, the parameters related to it should be investigated.

Among these parameters, the mechanical impedance plays an important role. In general, mechanical impedance expresses the 'ratio' between the mechanical inputs (usually generalized loads) and outputs (usually generalized displacements). Due to time delays and to time and inertia dependencies, this quantity may be complex in nature.

Why is it important to know about joint impedances in particular when subjected to impact forces? The answer is that mechanical impedance provides a means for expressing the extent to which the joint will be exposed to, or protected from, impact forces. In addition, when using control strategies based on the *impedance* approach the continuous *nonlinear behavior* of the joints is required.

1.2. Problem Statement

Of the several paradigms used for studying impact loading, free-fall motion is worth noting [Mizrahi and Susak, 1982 a,b].

Figure 1.1 shows typical time-history data of the foot-ground reaction forces (FGR), joint angles of the lower limb and vertical displacement of the center of gravity (c.g.) during a free-fall experiment. Impact loading usually demonstrates two significant peaks taking place shortly after the onset of foot contact with the ground. The subsequent peaks are of substantially lower intensity and are to a great extent related to the motion of the body segments relative to each other. By comparing the FGR curve to the monotonic c.g. curve, it becomes obvious that the ratio between these two quantities is clearly *nonlinear*. This ratio expresses the average overall vertical stiffness of the human body in falling motion or, more generally, the mechanical impedance.

Several factors are involved in determining the characteristics of impact loading. These include, among others:

1. Energy of impact, which is related to the height of fall. The higher the impacting energy, the higher the forces will be.
2. Body configuration, which affects the usage of the body's flexibility e.g. landing on the balls of the feet versus landing with the feet flat.

(a)

(b)
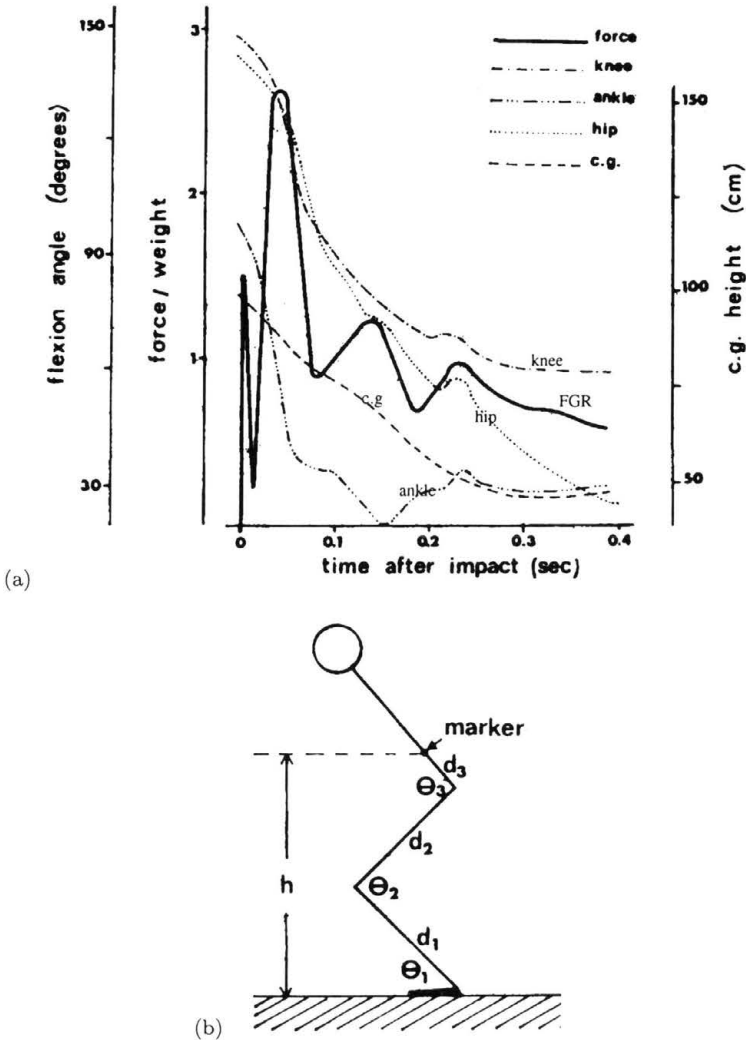
Figure 1.1. Free-fall experiment: (a) time-history data of the foot-ground reaction forces (FGR), joint angles of the lower limb and vertical displacement of the center of gravity (c.g.); (b) body configuration and definition of coordinates

For instance, landing with FF increases the first peak of the FGR and decreases the range of ankle flexion compared to landing on the balls of the feet.

3. Footwear, which determines the amount of attenuation provided by the cushioning action between body and ground. Cushioning was reported to decrease the intensity of the second (main) peak.

1.3. Evaluation of Mechanical Impedances from Data Obtained Experimentally

The following discussion describes biomechanical models for the evaluation of mechanical impedances from experimentally obtained data as solved by computer simulation (*in silico*). *In silico* evolutionary stages of handling the nonlinear problem of impedance estimation include:

- Linearisation of the problem by isolating position and other dependencies;

- Quasi-Linear solution done for 1-DOF motion;

- Piecewise Linear solution for a multi DOF by using nonlinear parameter estimation

- More general nonlinear expression reduced to first order nonlinearity, established using multicollinearity diagnostics algorithms.

1.3.1. Linear Solution

Several reports on the transmission of dynamic forces into or through the human body can be found in the literature. A common method of investigation involves measurement of the acceleration at one location on the body in response to a known force applied elsewhere on the body. This can be done either in a vibration test, in which an impact force is applied by an instrumented hammer [Saha and Lakes, 1977; Streitman and Pugh, 1978], or by impedance and resonance test, in which a sinusoidal excitation force is applied [Jurist, 1970; Selle and Jurist, 1966; Thompson, 1973]. By using accelerometers, the combined impedance of bone and soft tissue can be measured with acceptable reproducibility. Care should however be taken to properly position and attach them with a sufficiently high preload force [Streitman and Pugh, 1978; Thompson, 1973].

Usage of either the vibration or impedance - resonance methods has been done in the past to non-invasively assess the mechanical characteristics of dynamic force transmission of the human ulna [Jurist, 1970; Orne, 1974; Orne and Mandke, 1975] or that of the human tibia [Streitman and Pugh, 1978; Streitman et al., 1979]. However, in order to solve the required properties, material assumptions have to be made. Several models describing the landing phase of running, hopping or jumping can be found in the literature [Greene and McMahon, 1979; Mizrahi and Susak, 1982a; Ozguven and Berme, 1988;

Kim et al., 1994; Farley et al., 1998; Spagele et al., 1999]. These models are usually characterized by the presence of elastic springs and viscous dampers, with constant properties and provide a reasonable prediction of the maximal vertical foot/ground reaction force.

Although nonlinear models have been suggested [Muksian and Nash, 1974], it has been shown that linear viscoelastic representations yield satisfactory results [Orne and Mandke, 1975; Greene and McMahon, 1979; McMahon and Greene, 1979].

An example for a linear solution is now presented. The subject under investigation is the *in-vivo* transmission of impact forces from the foot through the entire straight leg to the level of the greater trochanter [Mizrahi and Susak, 1982a]. A two-degree of freedom linear mathematical model was employed to describe the mechanical behavior of both bone and soft tissue of the leg and of the rest of the body. Landing from a fall from short height, $h < 10$ cm, (Fig. 1.2) was barefoot on the right leg with a straight knee while the hip and ankle were kept in the neutrally anatomical position. The foot-ground reaction (FGR) force $F(t)$ served as input and the hip acceleration (attached to the greater trochanter) as output. Mass m_1 represents the lower legs from foot to hip and mass m_2 represents the rest of the body. This approach allows determine the in-vivo impedance of any portions of the leg, from the foot to a pre-selected level on leg, in which the output acceleration
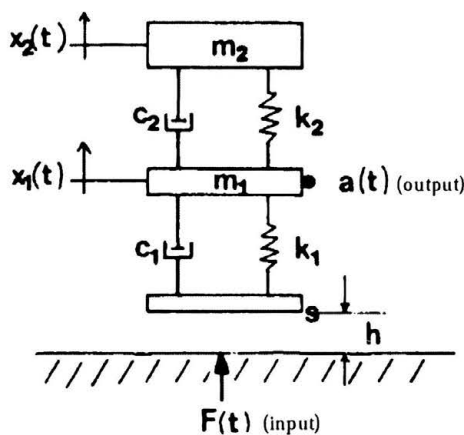

FIGURE 1.2. A two degree-of-freedom linear model for landing from a fall from short height (see text)

is being measured. The foot-ground force is written as

$$F(t) = k_1 X_1 + C_1 \dot{X}_1, \tag{1.1}$$

with k_1 and C_1 being the stiffness and damping properties of the leg, to the level of the hip.

The boundary conditions for the falling motion read:

$$t = 0, \quad X_1(0) = 0,$$
$$\dot{X}_1(0) = (2gh)^{1/2}. \tag{1.2}$$

And the equations of motion are:

$$m_1 \ddot{X}_1 + (C_1 + C_2)\dot{X}_1 + (k_1 + k_2)X_1 - C_2\dot{X}_2 - k_2 X_2 = 0,$$
$$m_2 \ddot{X}_2 + C_2(\dot{X}_2 - \dot{X}_1) + k_2(X_2 - X_1) = 0. \tag{1.3}$$

From numerical iterations, the best-fit solution values of elastic stiffness, damping constant and damping ratio ζ_1 ($\zeta = C/(2m\omega_n)$) are summarized in Table 1.1.

TABLE 1.1. Best fit solution values of elastic stiffness, damping constant and damping ratio ζ_1

Subject	h (cm)	k_1(kN/m)	C_1(kN-s/m)
A	4.06 (0.06)	8.45 (0.38)	0.81 (0.02)
B	5.70 (0.10)	5.32 (0.36)	0.79 (0.03)

Subject	ζ_1	k_2(kN/m)	C_2(kN-s/m)
A	0.52 (0.03)	45.2 (12.7)	0.94 (0.29)
B	0.67 (0.05)	42.3 (15.4)	0.78 (0.24)

Sensitivity analysis showed that the evaluated acceleration was more sensitive to C_1 than it was to k_1. The values presented in Table 1.1 provided good (< 3% difference) prediction for the first two peaks of the acceleration curve. However, for subsequent peaks higher errors in magnitude and phase were obtained. The importance of the first two peaks for the characterization of shock absorption has found expression in Streitman et al., [1979]. It should be noted that the procedure of calculating k_1 and C_l is direct and is based on the measured force and acceleration only. The calculation of k_2 and C_2, on the other hand, is based on assuming that $m_2 \gg m_1$ in the model (refer

to Fig. 1.2), which may explain the bigger variability obtained in these two latter constants.

The technique suggested in this study allows the mechanical impact properties of the leg to be investigated, including hard and soft tissues as well as articular cartilage and synovial fluids. The exact contribution of the different constituents in the leg in the transmission and attenuation of peak forces remains, however, undetermined. Clearly, the advantage of linearization is that it arrives to constant impedance coefficients, capable of providing reasonable prediction. The validity of the obtained coefficients should, however, be regarded in accordance with the restrictions imposed by the experiment and model, namely: (a) they represent gross lumping of the system, from foot to hip level; (b) no flexion of the joints takes place; (c) analysis limited to low-height jumping.

1.3.2. Quasi-linear Solution for 1-DOF Motion (sudden inversion of the foot relative to the shank)

In conditions of sprain of the ankle joint, the foot is subjected to sudden inversion relative to shank. In a previous study, Isakov et al., [1986] found that in unexpected and sudden inversion motion of the foot, the stretch reflex of the peroneal muscles remains unelicited for approximately 70 ms from the onset of motion. It is thus important to quantify the kind of anatomical passive restraints involved in the joint. With the purpose to measure these restraints the dynamic properties of the human subtalar joint in sudden inversion were studied in vivo on a specially designed apparatus [Mizrahi et al., 1990]. The subtalar joint was modelled as a second order system, from which the elastic stiffness and damping coefficient of the joint, as well as the natural frequency of the foot and its moment of inertia about the joint were evaluated under inversion-eversion motion.

During the experiments the tested leg stood on the swiveling platform and the opposite leg stood on a forceplate which served to adjust the weight bearing distribution between the legs (Fig. 1.3).

The quasi-linear model of joint impedance is written as follows

$$M_L(\theta) = \int \kappa(\theta)\theta d\theta + \int c(\theta)\dot\theta d\theta, \qquad (1.4)$$

where

θ – inversion angle of joint,
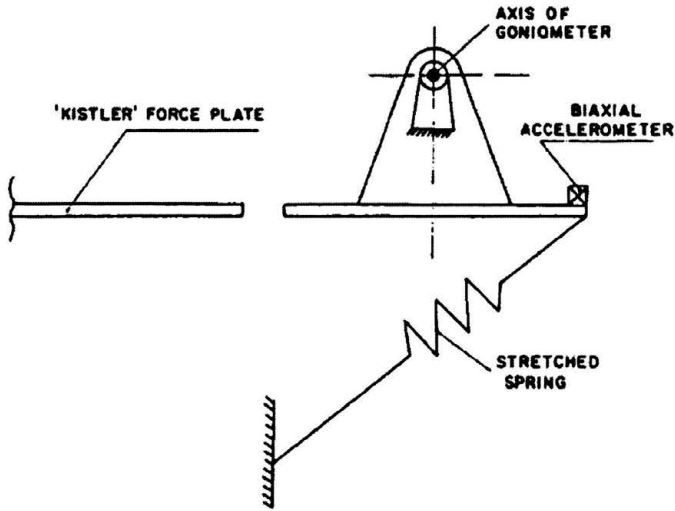
FIGURE 1.3. Schematic description of apparatus to measure the dynamic properties of the subtalar joint in sudden inversion of the foot

$\kappa(\theta)$ – stiffness coefficient,

$c(\theta)$ – damping coefficient.

Note the angle (or time) dependency of $\kappa(\theta)$ and $c(\theta)$. Stretching of the driving spring was such that the complete rotation motion ($\simeq$40 deg.) was completed in less than 42 ms [Isakov et al., 1986], ensuring that reflex-evoked contractions did not take part during the complete inversion motion, as shown in Fig. 1.4.
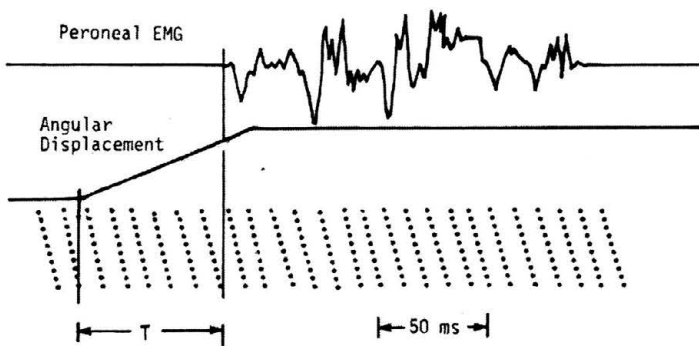
FIGURE 1.4. Time delay between onset of peroneal activity and initiation of sudden inversion of the foot
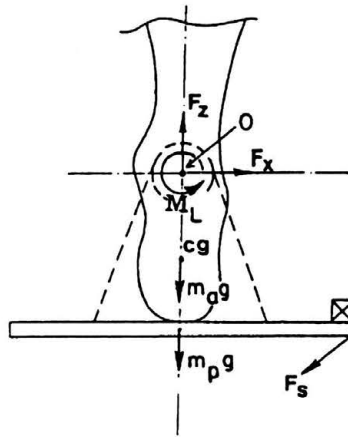
FIGURE 1.5. Loads on the foot segment during sudden inversion motion

As seen from Fig. 1.5, summation of the torques about axis O of the swiveling platform (also coinciding with the subtalar axis) yields:

$$\sum M_0(\theta) = M_s(\theta) + M_p(\theta) + M_a(\theta) + M_L(\theta), \qquad (1.5)$$

where

M_s – torque due to the driving spring,

M_p – opposing torque due to platform inertia,

M_a – opposing torque due to foot inertia,

M_l – opposing torque due to joint tissues (only unknown in above equation).

The following equation of motion can be written

$$\sum M_0 = (I_p + I_a)\ddot{\theta}, \qquad (1.6)$$

where I_p, I_a denote the moments of inertia of the platform and foot, respectively, about point O.

The following quantities may also be defined:

Overall stiffness

$$k_1(\theta) = M_L(\theta)/\theta(t), \qquad (1.7)$$

and natural frequency

$$w_n = [k(\theta)/(I_p + I_a)]^{1/2}. \qquad (1.8)$$

The results obtained were as follows. Table 1.2 shows the average and standard deviation (STD) results obtained from 6 tested subjects for overall

TABLE 1.2. Effect of inversion angle on overall stiffness, actual stiffness, damping and natural frequency

Ankle Inversion Angle (deg.)	M (Nm)	k_1 (Nm rad^{-1})	k (Nm rad^{-1})	C (Nm s rad^{-1})	w_n (Hz)
9	9.11 (3.0)	51.56 (8.5)	8.33 (2.5)	2.96 (0.75)	55.70 (3.6)
18	14.22 (3.0)	46.98 (5.7)	20.55 (5.0)	1.68 (0.50)	83.85 (8.2)
26	18.01 (3.2)	39.53 (6.3)	31.66 (5.5)	0.88 (0.20)	104.12 (10.1)
31	22.02 (2.5)	39.53 (5.7)	36.11 (5.0)	0.53 (0.11)	111.23 (8.3)
35	22.40 (3.5)	33.80 (11.4)	37.55 (4.0)	0.41 (0.20)	112.40 (7.5)

stiffness, actual stiffness, damping and natural frequency. Note that while overall stiffness decreases with rotation angle, the actual stiffness increases with this angle. The latter is associated with the material behavior of the joint tissue. It should be reminded that overall stiffness describes the mere ratio between joint torque and joint displacement, whereas actual stiffness expresses the elastic component only, after dissociation of the damping contribution to torque. It is also noted that with increasing angle the natural frequency increases while damping decreases.

The effects of weight-bearing, foot dominance and footwear protection on ankle torque, overall stiffness, actual stiffness and damping are summarized in Table 1.3. It is noted that a higher stiffness results with increasing weight bearing on the tested leg and with addition of protective footwear. The increase of elastic stiffness with weight bearing may be attributed to the

TABLE 1.3. Effects of supporting load on foot, foot dominance and footwear on ankle torque, overall stiffness, actual stiffness, damping and natural frequency

	M (Nm)	k_1 (Nm rad^{-1})	k (Nm rad^{-1})	C (Nms rad^{-1})
Reference condition	30.01 (8.5)	67.4 (22.0)	51.76 (12.5)	1.32 (0.50)
75% W-Bearing	37.7* (2.7)	96.5* (5.5)	69.01* (2.5)	2.81*(0.06)
25% W-Bearing	23.2* (4.6)	62.3* (9.2)	10.6* (5.8)	2.83 (0.20)
Opposite foot	23.0 (2.2)	48.0 (6.3)	34.6 (5.3)	1.30 (0.16)
High boots	31.6 (2.8)	67.6 (4.9)	51.8 (4.4)	1.08 (0.29)
High boots + Elastic dressing	43.5 (1.7)	105.5* (5.5)	84.1* (7.1)	1.92 (0.50)

*– Statistically significant difference from the reference condition ($p < 0.05$)

increase in muscle tone, necessary for the extra weight bearing, as well as for the maintenance of balance of the joint in this condition. Increase of stiffness in the presence of well-fitted high boots was reported to be accompanied by the reduction of ligamentous load on the joint [Johnson, 1976].

The limitations of the above results can be related to the following problems:

1. Anatomical coupling existing between the subtalar and talo-crural joints, affecting the purity of motion about subtalar an axis directed in the antero-posterior direction.

2. Possible errors in positioning/repositioning of the foot in the comparison of the intra- and inter-subject data.

3. Inaccuracy in weight-bearing maintenance during the experiment.

The proposed method has, nevertheless, several advantages which can be summarized as follows:

1. The model and data provide sufficient means to solve for the foot anthropometry, in addition to the stiffness, damping and natural frequency. This provides means for comparison between data-base estimation and model solution of anthropometry.

2. Muscle activation-free dependence due to the high deformation-rate.

3. While results on inversion motion had not been published before, the results obtained can be compared to those of the talo-crural joint due to the earlier mentioned coupling between the two joints. As demonstrated

TABLE 1.4. Comparison of ankle properties obtained from different groups

Parameter compared	Mizrahi et al. (1990)	Kearney and associates* (1982, 86)	Agarwal and Gottlieb** (1977, 78)
Range of motion (deg)	10 – 35	−51 – +17	± 12
Moment (Nm)	8 – 30	5 – 35	0 – 12
Elastic stiffness (Nm/rad)	3 – 52	0 – 100	13 – 54
Damping coefficient (Nms/rad)	0.3 – 2.9	0.6 – 1.0	0.2 – 0.7
Natural frequency (Hz)	58 – 125	10 – 20	5

*, ** for talocrural joint

in Table 1.4, the results are in the expected range and compare well with other results from the literature [Agarwal and Gottlieb, 1977; Kearney and Hunter, 1982; Weiss et al., 1986].

1.3.3. Piecewise Linearization

The next step in the evolution of impedance modeling is the inclusion of several degrees of freedom [Daily, 1998]. A four-degree of freedom biomechanical model is represented for the simulation of the stance phase of human running (Fig. 1.6). The data measured include the acceleration time-course at two levels: shank and sacrum. Specifically, the first 44 ms from foot-strike are being modeled. The various segments in the model are m_1, m_2, m_3, m_4, representing the foot, shank, thigh and rest of the body, respectively.

With m representing the mass of the body, then [Winter, 1990]

$$
\begin{aligned}
m_1 &= 0.0145m, \\
m_2 &= 0.0465m, \\
m_3 &= 0.100m, \\
m_4 &= m - (m_1 + m_2 + m_3) = 0.839m.
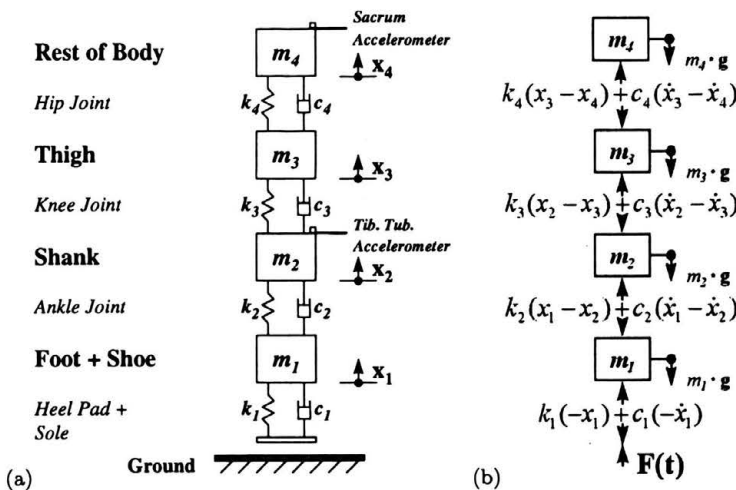\end{aligned}
\tag{1.9}
$$

FIGURE 1.6. Four degree-of-freedom biomechanical model for the simulation of the stance phase of human running: (a) lumping of segments; (b) free body diagram of lumped segments

The following model equations are written for the multi-segmental system:

$$
\begin{aligned}
m_1\ddot{x}_1 =& - k_1 x_1 - c_1\dot{x}_1 - k_2(x_1 - x_2) - c_2(\dot{x}_1 - \dot{x}_2) - m_1\mathbf{g}, \\
m_2\ddot{x}_2 =& k_2(x_1 - x_2) + c_2(\dot{x}_1 - \dot{x}_2) - k_3(x_2 - x_3) \\
& - c_3(\dot{x}_2 - \dot{x}_3) - m_2\mathbf{g}, \\
m_3\ddot{x}_3 =& k_3(x_2 - x_3) + c_3(\dot{x}_2 - \dot{x}_3) - k_4(x_3 - x_4) \\
& - c_4(\dot{x}_3 - \dot{x}_4) - m_3\mathbf{g}, \\
m_4\ddot{x}_4 =& k_4(x_3 - x_4) + c_4(\dot{x}_3 - \dot{x}_4) - m_4\mathbf{g},
\end{aligned}
\tag{1.10}
$$

with assigned boundary conditions for the accelerations $\mathbf{a}_2$, $\mathbf{a}_4$ at the shank and sacrum, respectively, and with the following initial conditions:

$$
x_i(0) = 0, \quad \dot{x}_i(0) = v_0 = -1\,\mathrm{m/s}, \quad i = 1, 2, 3, 4.
\tag{1.11}
$$

These initial conditions state that, at the instant of foot strike, the body segments fall at the uniform downward velocity of $1\,\mathrm{m/s}$, i.e., with no relative velocity between the segments. While this assumption consists of a simplification of the model formulation, it does not affect the generality of the formulated method. Its verification, however, would necessitate accurate information about the kinematics of the segments.

The consistency of measured acceleration was studied by re-measuring the signals and checking for reproducibility. It was also interesting to note any possible effect of the attachment preload of the accelerometer strips. The results for the shank acceleration are demonstrated in Fig. 1.7 and for the sacrum in Fig. 1.8. It is noted that while the shank reproducibility was good, it was less satisfactory in the case of sacrum acceleration.

The method of solution consisted of nonlinear parameter estimation using the Gauss-Marquardt method [Bard, 1974]. Numerical integration was performed using the Runge Kutta method using Weighted Least Squares (WSL) target function, with assigned boundary conditions for the accelerations $\mathbf{a}_2$, $\mathbf{a}_4$, at the shank and sacrum, respectively.

Stiffness was assumed to be piecewise linear in 2 zones, of $22\,\mathrm{ms}$ each. Fig. 1.9 demonstrates the prediction of tibial tuberosity acceleration obtained for a 1-zone linear stiffness versus a 2-zone piecewise linear stiffness. It is clearly seen that for satisfactory model results the 1-zone stiffness is not satisfactory and that a 2-zone stiffness is essential. The 2-zone estimation gave the following stiffnesses: for zone 1: $k_1 \simeq 19\,\mathrm{kN/m}$; $k_2 \simeq 11\,\mathrm{kN/m}$, and for zone 2: $k_1 \simeq 140\,\mathrm{kN/m}$; $k_2 \simeq 17\,\mathrm{kN/m}$.
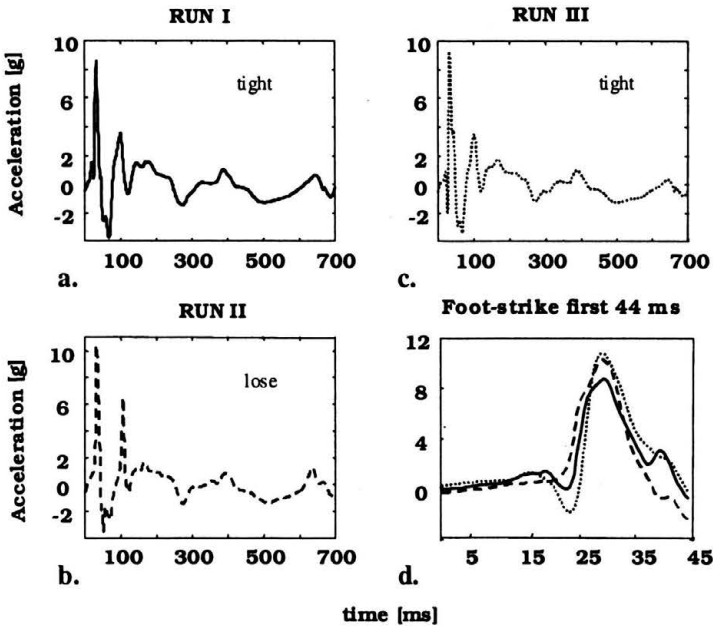
FIGURE 1.7. Consistency of measured acceleration on the shank
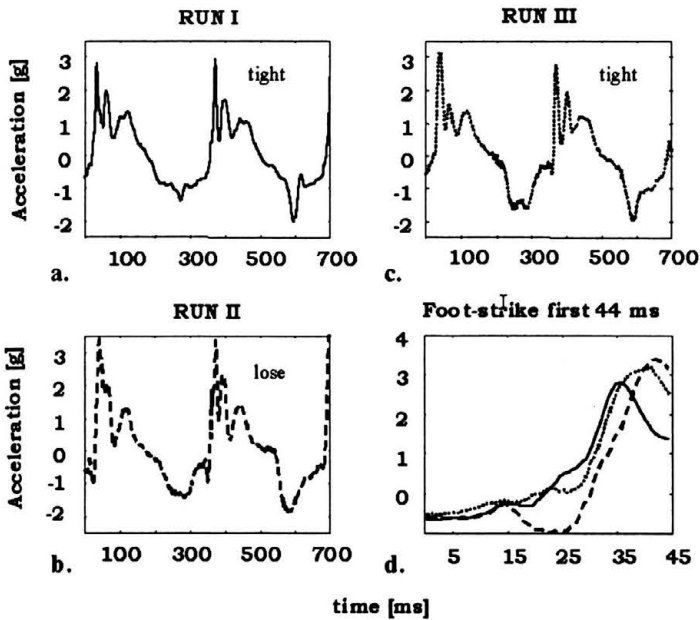
FIGURE 1.8. Consistency of measured acceleration on the sacrum
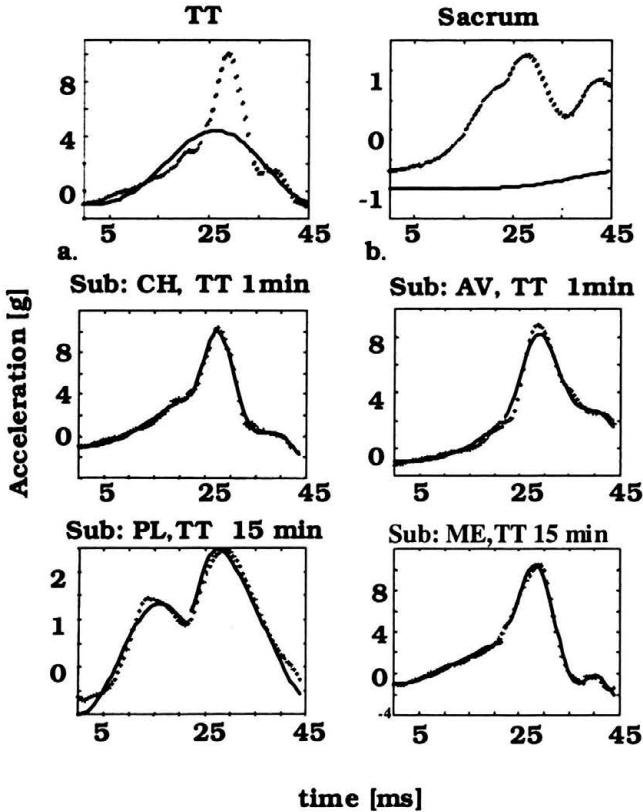
FIGURE 1.9. Comparison between measured (dotted curves) and model-prediction accelerations in the tibial tuberosity (TT) and sacrum levels; In the two upper panels the comparison is for a 1-zone linear stiffness, for the first minute of running. In the middle and lower panels the comparison is for a 2-zone piecewise linear stiffness, for the first minute (1 min) and the 15th min. of running for the different subjects (Sub): CH, AV, PL and ME.

From the results it may be concluded that there is a substantial increase in stiffness with deformation (zone 2 versus zone 1). While the model is capable of predicting the stiffnesses of the foot, ankle and knee, a high variability between the subjects was noted.

The problems in this model can be attributed to a number of factors including, among others, the errors in anthropometric estimations such as the segment masses. The following can be attributed to problems of kinematical source: assumption of zero relative velocities between the segments at foot strike, accuracy of landing velocity value of 1 m/s, unreliable sacrum acceleration measurement, accurate determination foot-strike instant. Clearly,

these questions could be improved by the more accurate measurements of kinematics, with higher time and space resolution. It would also be beneficial if the FGR could be measured, to augment the amount of input data to the model.

1.3.4. Nonlinear Solution for Impedance

In repetitive physical activity, such as in running, hopping, and trotting, the subject bounces on the ground in a spring-like manner [Cavagna et al., 1964, 1977; Blickhan and Full, 1987; Alexander, 1988; Blickhan, 1989; McMahon and Cheng, 1990; Farley and Morgenroth, 1999]. Depending on the range of joint flexion and on the frequency of motion, a considerable amount of elastic energy can be stored and re-used. It has been shown that the dissipated energy in muscles increase when the amplitudes of joint movement are increased [Thys, 1978]. Bosco and Komi, [1979] also commented on the utilization of stored elastic energy stating that this depended on the shortness in latency between the stretch and shortening phases of the muscles. Accordingly, during the ground-contact period of running, hopping and trotting, the leg was modeled as a single linear spring or, in terms of the leg joints, as constant torsional springs for the ankle, knee, and hip joints, with no damping. The stiffness of these springs, termed 'average' stiffness, was defined as the ratio between overall force or moment change to overall vertical displacement or angle change for the leg and joint stiffness, respectively [Farley et al., 1998; Farley and Morgenroth, 1999].

Physiologically, however, the conception of constant mechanical stiffness may not be applicable. For instance, muscular activation, which is believed to be directly related to joint stiffness, varies during the stance phase. For that reason, hopping is not a purely harmonic motion and human joints are not simple mechanical springs. Apart from its ability to store, release and absorb energy, the muscle-tendon complex can also generate energy and, as above-mentioned, its stiffness generally depends on the activation level of the muscle. Thus, it can be expected that the joint stiffness is nonlinear in nature and that damping may be present and that a model accounting for these facts may improve the system's representation and model prediction [Farley and Morgenroth 1999; Seyfarth et al 2001].

Variations of the leg and joint stiffnesses were considered in past models as a result of variation in hopping, or stride, frequency and in ground stiffness

[Farley et al., 1998; Farley and Morgenroth, 1999; Farley et al., 1991; Farley and Gonzalez, 1996; Arampatzis et al., 1999]. It was argued that a stiffer leg leads to a higher stride frequency and shorter stride length at a given speed. Variation of the mechanical impedance in the subtalar joint was also considered to vary with joint angle in sudden inversion motion of the foot [Mizrahi et al., 1990]. Rotational springs with nonlinear stiffnesses were recently studied in a three-segment leg modeling of repulsive tasks like human running and jumping [Seyfarth et al., 2001]. Variability of the impedances of the leg joints during the stance phase of hopping was recently reported [Rapoport et al., 2003]. This requires the nonlinear solution of the impedance for a multi-degree of freedom model of human hopping.

The model is demonstrated in Fig. 1.10. This is a two-dimensional hopping model in the sagittal plane was used, consisting of four linked rigid segments identified as the feet, shanks, thighs, and HAT (head, arms and trunk) [Barin, 1989; Pandy and Zajac, 1990; Gerritsen et al., 1995; Selbie and Caldwell, 1996]. Each of the ankle, knee and hip joints was considered to be a frictionless hinge, representing the joint action of the paired human legs. The foot was
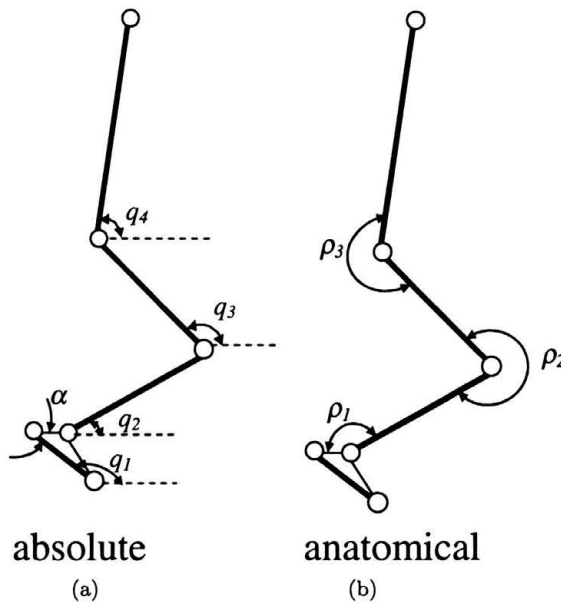

FIGURE 1.10. Two-dimensional hopping model in the sagittal plane consisting of four linked rigid segments identified as the feet, shanks, thighs, and HAT (head, arms and trunk): (a) absolute coordinates; (b) anatomical coordinates

considered to establish contact with the floor through a virtual hinge located at the tip of the toe. The segments are interconnected by three mechanical impedances, representing the functional behavior of the joints [Farley and Morgenroth, 1999]. Each of these impedances includes a nonlinear torsional stiffness, connected in parallel to a nonlinear torsional damper.

It was assumed that during the stance phase, motion takes place in the sagittal plane and is accomplished by pure rotation of the segments around the mentioned four joints. The kinematics of the multi-body system can thus be described in terms of the absolute angles q_1, q_2, q_3, and q_4 (Fig. 1.10a) of the foot, shank, thigh, and HAT, respectively, measured from the horizontal line and represented by the generalized coordinate vector $\mathbf{q}$:

Thus, the generalized coordinate vector is

$$\mathbf{q} = [q_1 \quad q_2 \quad q_3 \quad q_4]^{\mathsf{T}}, \tag{1.12}$$

and for the joint angles ρ_j, the coordinate transformation reads:

$$\begin{aligned}
\rho_1 &= q_1 - q_2 + \alpha, \\
\rho_2 &= q_3 - q_2 + \pi, \\
\rho_3 &= q_3 - q_4 + \pi.
\end{aligned} \tag{1.13}$$

Figure 1.11 demonstrates angular displacements of the hip, knee and ankle and ankle power during hopping at a frequency of 1.53 Hz. It is seen that the motion is coordinated between joints during the stance phase. The braking (negative) energy is roughly equal to the pushing (positive) energy. Angle ranges were 15, 60 and 90 deg. for the hip, knee and ankles, respectively.

The Newton-Euler inverse-dynamics method is applied and the following objective function is minimized:

$$J_j = \sum_{l=1}^{n} (\tau_{jl} - M_{jl})^2, \tag{1.14}$$

where τ_j and M_j denote the inverse-dynamics and model results torques.

The following constraints apply:

- Positivity of stiffness and damping coefficients:

$$K_{jl} \geqslant 0, \tag{1.15}$$

$$B_{jl} \geqslant 0. \tag{1.16}$$
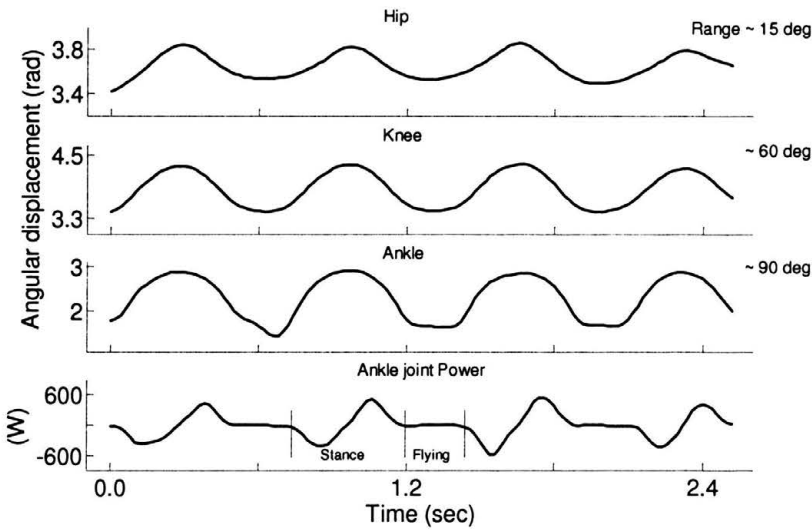
FIGURE 1.11. Angular displacements of the hip, knee and ankle and ankle power during hopping at a frequency of 1.53 Hz

- Positive potential elastic energy:

$$\int_{E_{sj0}}^{E_{sjl}} dE_{sj} = \int_{\rho_{j0}}^{\rho_{jl}} M_{sj} d\rho_j', \tag{1.17}$$

$$E_{sjl} \geqslant 0.$$

- No energy storage in damper:

$$P_{djl} = - M_{djl}\omega_{jl}, $$
$$P_{djl} \leqslant 0. \tag{1.18}$$

The mechanical properties of biological material are, in general, multiple variable-dependent. Specifically stiffness, in addition to its being nonlinear e.g. strain dependent, often depends on the deformation rate. This is the case with bones [Wright and Hayes, 1980; Peterson et al., 1987], tendons and ligaments [Peterson et al., 1987], cartilage [Li et al., 1983] and muscle [Herzog and Leonard, 1991]. Similarly with damping, which can be position-dependent. Accordingly, stiffness and damping during the stance phase of hopping can be represented by a second order regressive function. However, by using multicollinearity analysis to reveal dependencies between the coefficients the stiffness and damping order can be reduced.

Multicollinearity diagnostic criteria were applied to reveal and eliminate redundancies. This was achieved by the deletion of offending predictor variable from regression model without impairing the ability to predict the system's response. Multicollinearity diagnostic criteria combined with F-test [Slinker and Stanton, 1985] were thus used to reveal dependencies and eliminate redundancies in the numerical solution of the stiffness and damping coefficients. The Hessian matrix was first formed. Its elements are the second derivatives of the objective function with respect to each of the parameters of the model. Singularity of the Hessian matrix can signify multicollinearity, i.e. relative dependence between the parameters and redundancy of information.

Thus, reduction of the model yields:

1. Linearly variable stiffness

$$K_j(\rho_j) = k_{0j} + k_{1j}(\rho_j - \rho_{j0}).\qquad(1.19)$$

2. Constant damping

$$B_j = b_{0j}.\qquad(1.20)$$

Figure 1.12 shows typical moment/angle and stiffness curves of the joints during the ground-contact phase as well as their variations with frequency. The joint moments were computed from inverse dynamics. The maximal moments take place at maximum joint flexion and they increase with increasing frequency (rightmost curves). The joint moments and angular displacements were smallest in the hip, and largest in the ankle. It is noted that the rotational stiffness at all joints increases with hopping frequency.

As shown in Table 1.5, the variable stiffness model was closer to the inverse dynamics solution than the constant stiffness model (* indicates $P < 0.05$, in comparison of errors), indicating that the former solution was preferable for the prediction of joint torques.

As seen from Fig. 1.13, the stiffness behavior was similar in the ankle, knee, and hip joints. As shown in this figure, max rotational stiffness occurs at midstance when the jumper's joints are maximally flexed. It is also noticed that at the touchdown and take-off instants of the stance phase the stiffness values are both non-zero, indicating that activity is preprogrammed. Figure 1.14 shows that the initial stiffness is proportional to the maximal stiffness, revealing the paradigm of pre-activation.

While departing from the stiffness constancy concept, the above model revealed that the correct and sufficient variability of the joint stiffness is of first
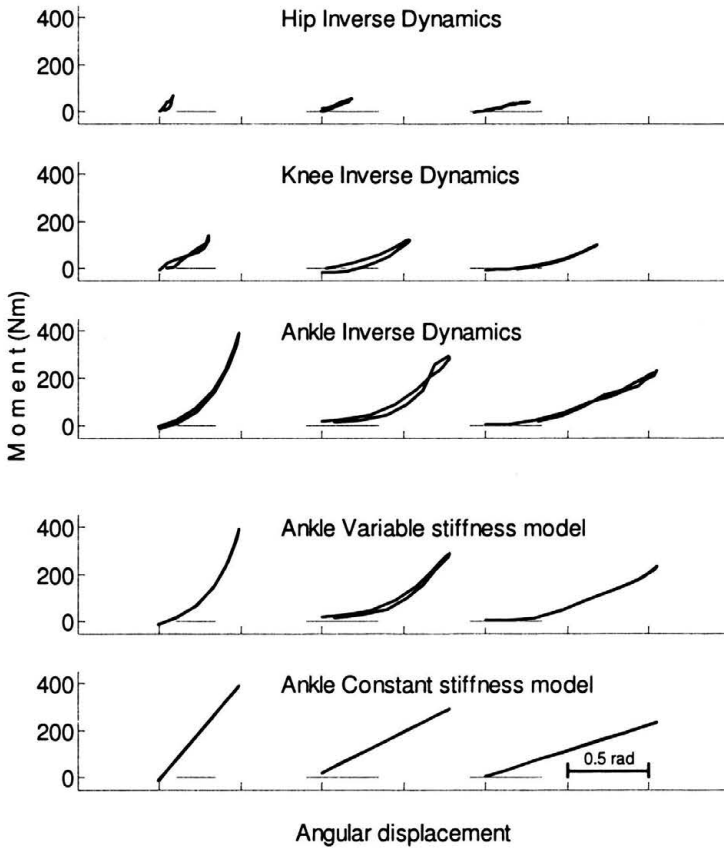
FIGURE 1.12. Moment/angle and stiffness curves of the joints during the ground-contact phase as well as their variations with frequency. Left curves (dotted) = 2.20 Hz, central curves (dashed) = 1.87 Hz, right curves (solid) = 1.53 Hz)

order, as described by equation (1.19). This was obtained after eliminating redundancies in the numerical solution, using multicollinearity diagnostic algorithms, indicating that a higher order of nonlinearity is not necessary. This result should be considered meaningful in those problems where the constant stiffness representation is not sufficient and in cases where the system's representation has to be improved. The variable stiffness obtained solution also provides, through the obtained stiffness profiles, an insight into the patterns of the muscular activation in the legs' joints.

The fact that the simple model of a linearly variable stiffness can predict major features of the jumping exercise makes it an effective tool for future

TABLE 1.5. Comparison of the error of the joints moment over time between the Inverse Dynamics (reference) model and each of the constant stiffness and variable stiffness models (Mean(SD), n=8); The values presented were calculated from the formula $\frac{SSE \times 10^{-3}}{N} \times$ FR, where N is the number of points in the stance phase ($N = 22$, 18 and 14 for LF, MF and HF, respectively) and FR($= 50$) is the frame rate of the camera.

Frequency	Models	Ankle	Knee	Hip
HF	Inverse dynamics, versus Variable stiffness model	12.16 (16.21)	0.20 (0.22)	0.09 (0.10)
	Inverse dynamics, versus Constant stiffness model	239.1* (227.9)	39.00* (23.84)	21.77 (31.86)
MF	Inverse dynamics, versus Variable stiffness model	3.74 (2.66)	0.12 (0.11)	0.57 (1.01)
	Inverse dynamics, versus Constant stiffness model	95.70* (62.01)	88.98 (89.63)	0.81 (0.65)
LF	Inverse dynamics, versus Variable stiffness model	5.16 (4.06)	1.31 (2.57)	0.17 (0.28)
	Inverse dynamics, versus Constant stiffness model	32.05* (29.80)	20.41* (20.40)	1.44* (1.11)

* Denotes a significant difference ($P < 0.05$) between the Inverse dynamics (reference) and Constant stiffness models.
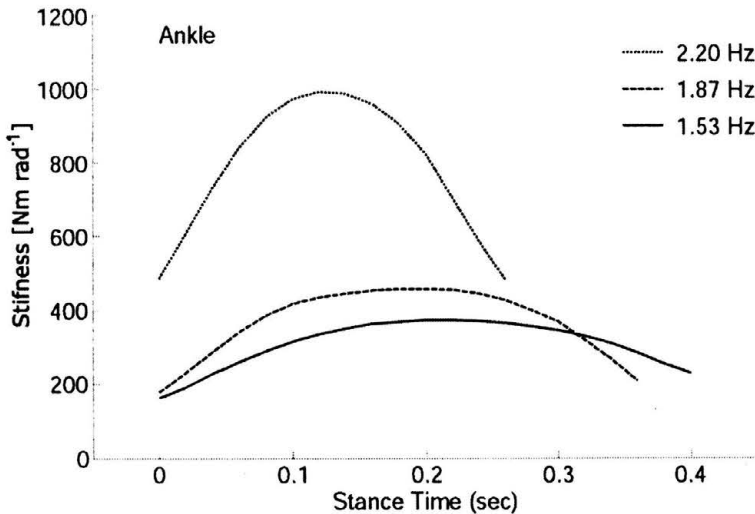
FIGURE 1.13. Stiffness behavior during the stance phase of hopping in the ankle joint
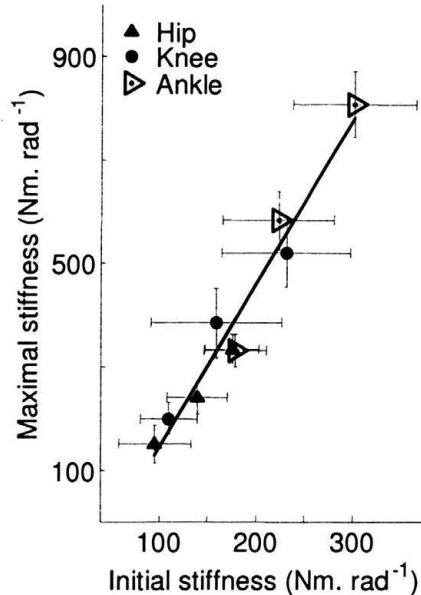
Figure 1.14. Relation between the initial stiffness and the maximal stiffness

designing of artificial legs and robots and also for the development of more accurate control strategies.

1.3.5. Wobbling Mass Model

In all previous models the human body was considered as consisting of rigid segments. The following question may however be asked: what is the significance of rigid body based estimates of joint moments and forces, considering the non-rigid nature of the human motor system?

This brings us back to the initial problem of landing from a vertical drop, except that now we introduce the effect of soft tissues surrounding the skeletal elements [Langzam, 2002]. These types of models are called Wobbling Mass models. Figure 1.15 shows segment separation into two rigid sub-bodies: skeleton and soft tissue. While the soft tissue is connected to the adjacent skeletal segment, the skeletal segment is connected to its adjacent skeletal segment. The linkage between soft tissue and skeletal segments is composed of translational and rotational elements representing passive linear stiffness and damping mechanism. Stiffness and damping are assumed to have constants properties during the whole simulation sequence (Fig. 1.15b,c).
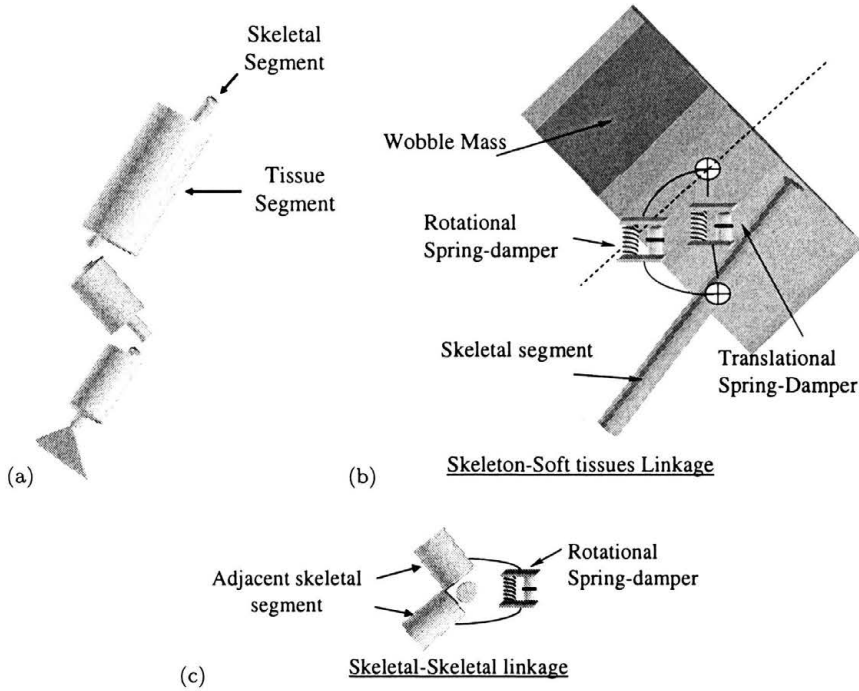
FIGURE 1.15. Wobbling mass model representation: (a) skeleton & soft tissue segments; (b) skeleton/soft tissue linkages; (c) skeleton/skeleton linkage

Skeletal-skeletal linkages are assumed to take place via rotational elements only. The assumptions made in the model treated are: symmetric drop (2D motion); passive mechanisms only (i.e., no muscle activation is involved); body modeled as seven rigid bodies; shank, thigh and HAT are modeled as wobble masses i.e., with separate skeletal+soft tissues (Fig. 1.15a); foot is treated as combining together the skeletal and soft tissues; the first 50 ms after ground hit are being modeled.

Joints are assumed to behave as exponential torsional springs, with constant coefficients, as follows (Fig. 1.16):

$$T_i = \begin{cases} -(\exp(k_{\phi j} \cdot |\phi_j - \phi_{j0}|) - 1) - c_{\phi j}\dot{\phi}_j, & \phi_j - \phi_{j0} > 0, \\ (\exp(k_{\phi j} \cdot |\phi_j - \phi_{j0}|) - 1) - c_{\phi j}\dot{\phi}_j, & \phi_j - \phi_{j0} < 0, \end{cases} \qquad (1.21)$$

where

ϕ_j – joint angle,

$k_{\phi j}$ – stiffness coefficient,

$c_{\phi j}$ – damping coefficient.
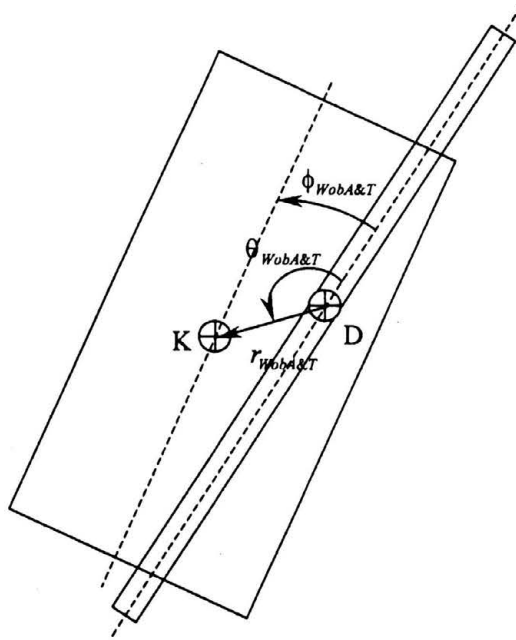
FIGURE 1.16. Angle definitions of joints in wobble mass model

Foot-Ground interface
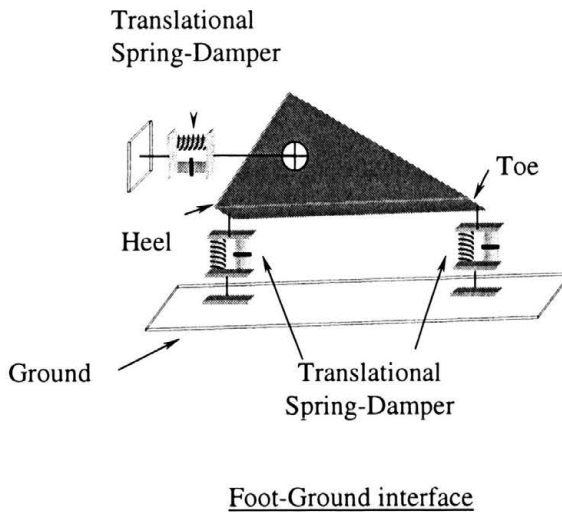
FIGURE 1.17. Interaction of the foot segment with the ground

The foot segment is assumed to interact with the ground via two mechanisms at the heel and the toe for the vertical forces and one mechanism at the foot CG for horizontal forces (Fig. 1.17).

Parameter estimation was carried out using an optimization procedure via a *Genetic Algorithm* [Srivinias and Patanaik, 1994]. The essence of this method lies in a process of natural search and selection, whereby the fittest parameter survives. This method is especially successful in reaching the global optimum of optimization. The disadvantages, however are that it is not very suitable for continuously variable problems; requires large computations and is sensitive to operator parameter values (needs customization procedures). The fact that the wobble-mass model predicts better than the rigid body model as demonstrated in Fig. 1.18, confirming that the former model is preferable.
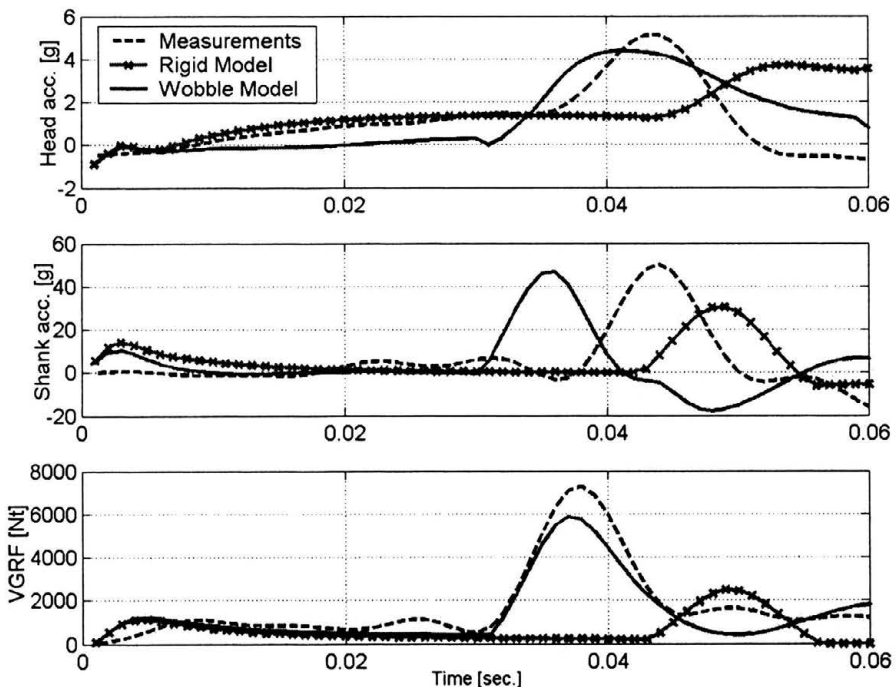
FIGURE 1.18. Comparison of predictions from wobble model versus rigid body model

1.4. Future Work

Future work should extend 'wobble-mass' concept to include other activities than vertical jump, such as locomotion. Stiffness and damping should not be restricted to constant properties only. As has been previously demonstrated, these properties are highly dependent on joint angles, weight bearing intensity and muscle activation; thus variable coefficient models should be developed in conjunction with the wobble mass concept. An additional generalization of wobble mass models is to extend the quasi-rigid segmentation used beyond two sub-segments. Finally, the provision of more comprehensive data including high-speed kinematics and EMG data should be attempted for improved estimation of the model parameters.

References for Chapter 1

1. G.C. AGARWAL and G.L. GOTTLIEB, *Compliance of the Human Ankle Joint*, J. Biomech. Eng., **99**:166–170, 1977.

2. R.McN. ALEXANDER, *The Spring in your Step: the Role of Elastic Mechanism in Human Running*, Free University Press, Amsterdam, pp. 17–25, 1988.

3. A. ARAMPATZIS, G.-P BRUGGEMANN, and V. METZLER, *The Effect of Speed on Leg Stiffness and Joint Kinetics in Human Running*, J. Biomech., **32**:1349–1353, 1999.

4. Y. BARD, *Nonlinear parameter estimation*, Academic Press Inc., New York, 1974.

5. K. BARIN, *Evaluation of a Generalized Model of Human Postural Dynamics and Control in the Sagittal Plane*, Biological Cybernetics, **61**:37–50, 1989.

6. R. BLICKHAN and R.J. FULL, *Locomotion Energetics of the Ghost Crab. II. Mechanics of the Centre of Mass during Walking and Running*, J. Experimental Biology, **130**:155–174, 1987.

7. R. BLICKHAN, *The Spring-Mass Model for Running and Hopping*, J. Biomech., **22**:1217–1227, 1989.

8. C. BOSCO and P.V. KOMI, *Mechanical Characteristics and Fiber Composition of Human Leg Extensor Muscles*, European J. Appl. Physiology, **41**:275–284, 1979.

9. G.A. CAVAGNA, F.P. SAILBENE, and R. MARGARIA, *Mechanical Work in Running*, J. Appl. Physiology, **19**:249–256, 1964.

10. G.A. Cavagna, N.C. Heglund, and C.R. Taylor, *Mechanical Work in Terrestrial Locomotion: Two Basic Mechanisms for Minimizing Energy Expenditure*, American Journal of Physiology, **233**:R243–R261, 1977.

11. D. Daily, *Mechanical factors in shock transmission in the human body: effect of muscle fatigue*, MSc thesis submitted to the Technion, Israel Institute of Technology, Haifa, Israel (supervisors: J.Mizrahi & Y. BenHaim).

12. P. Ducheyne, L. Heymans, M. Martens, E. Aernoudt, P. De Meester, and J.C. Mulier, *The Mechanical Behaviour of Intracondylar Cancellous Bone of The Femur at Different Loading Rates*, J. Biomech., **10**:747–762, 1977.

13. C.T. Farley, R. Blickhan, J. Saito, and C.R. Taylor, *Hopping Frequency in Humans: Test of How Springs Set Stride Frequency in Bouncing Gaits*, J. Appl. Physiology, **71**:2127–2132, 1991.

14. C.T. Farley, and O. Gonzalez, *Leg Stiffness and Stride Frequency in Human Running*, J. Biomech., **29**:181–186, 1996

15. C.T. Farley, H.H.P. Houdijk, C. van Strien, and M. Lourie, *Mechanism of Leg Stiffness Adjustment for Hopping on Surfaces of Different Stiffnesses*, J. Appl. Physiology, **85**:1044–1055, 1998.

16. C.T. Farley, D.C. Morgenroth, *Leg Stiffness Primarily Depends on Ankle Stiffness during Human Hopping*, J. Biomech., **32**:267–273, 1999.

17. J.B. Finlay and R.U. Repo, *Energy Absorbing Ability of Articular Cartilage During Impact*, Med. Biol. Engng. Comput., **17**:397–403, 1979.

18. G.M. Gerritsen, A.J. Bogert, and B. Nigg, *Direct Dynamics Simulation of the Impact Phase in Heel-Toe Running*, J. Biomech., **28**:661–668, 1995.

19. P.R. Greene and T.A. McMahon, *Reflex Stiffness of Man's Anti-Gravity Muscles During Kneebends While Carrying Extra Weights*, J. Biomech., **12**:881–891, 1979.

20. W. Herzog and T.R. Leonard, *Validation of Optimization Models that Estimate the Forces Exerted by Synergistic Muscles*, J. Biomech., **24**(S1):31–39, 1991.

21. E. Isakov, J. Mizrahi, P. Solzi and Z. Susak, *Response of the Peroneal Muscles to Sudden Inversion of the Ankle During Standing*, Int. J. Sports Biomechanics, **2**(2):100–109, 1986.

22. G.R. Johnson, D. Dowson, and V. Wright, *A Biomechanical Approach to the Design of Football Boots*, J. Biomech., **9**:581–585, 1976.

23. J.M. Jurist, *In Vivo Determination of the Elastic Response of Bone - I. Method of Ulnar Resonant Frequency Determination*, Physics in Medicine and Biology, **15**:417–426, 1970.

24. R.E. KEARNEY and I.W. HUNTER, *Dynamics of Human Ankle Stiffness: Variation with Displacement Amplitude*, J. Biomech, **15**:753–756, 1982.

25. W. KIM, A.S. VOLOSHIN and S.H. JOHNSON, *Modeling of Heel Strike Transients during Running*, Journal of Human Motion Science, **13**:221–244, 1994.

26. E. LANGZAM, *Impact loading attenuation in landing from vertical falls*, MSc thesis submitted to the Technion, Israel Institute of Technology, Haifa, Israel (supervisor J. Mizrahi), 2002.

27. J.T. LI, C.G. ARMSTRONG, and V.C. MOW, *The Effects of Strain Rate on Mechanical Properties of Articular Cartilage in Tension*, Proc Biomechanical Symposium ASME AMD, **56**:117–120, 1983.

28. T.A. MCMAHON and P.R. GREENE, *The Influence of Track Compliance on Running*, J. Biomech., **12**:893–904, 1979.

29. T.A. MCMAHON, G.C. CHENG, *The Mechanics of Running - How Does Stiffness Couple with Speed ?*, J. Biomech., **23**(suppl. 1):65–78, 1990.

30. J. MIZRAHI and Z. SUSAK, *Elastic and Damping Response of the Human Leg to in Vivo Impact Forces*, J. Biomech. Eng. (ASME), **104**:63–66, 1982a.

31. J. MIZRAHI and Z. SUSAK, *Analysis of Parameters Affecting Impact Force Attenuation in Landing of Human Vertical Free Fall*, Engineering in Medicine, **11**(3):141–147, 1982b.

32. J. MIZRAHI, Y. RAMOT, and Z. SUSAK, *The Passive Dynamics of the Subtalar Joint in Sudden Inversion of the Foot*, J. Biomech. Eng., **112**:9–14, 1990.

33. R. MUKSIAN and C.D. NASH, *A Model for the Response of Seated Humans to Sinusoidal Displacements of the Seat*, J. Biomech., **7**:209–215, 1974.

34. D. ORNE, *The In Vivo Driving Point Impedance of the Human Ulna- A Viscoelastic Beam Model*, J. Biomech., **7**:249–257, 1974,

35. D. ORNE and J. MANDKE *The Influence of Musculature on the Mechanical Impedance of the Human Ulna, An In Vivo Simulated Study*, J. Biomech., **8**:143–149, 1975.

36. H.N. OZGUVEN and N. BERME, *An Experimental and Analytical Study of Impact Forces during Human Jumping*, J. Biomech., **21**:1061–1066, 1988.

37. M.G. PANDY and F.E. ZAJAC, *An Optimal Control Model for Maximum-Height Human Jumping*, J. Biomech., **23**:1185–1198, 1990.

38. R.H. PETERSON, M.A. GOMEZ, and S.L.-Y. WOO, *The Effects of Strain Rate on the Biomechanical Properties of the Medial Collateral Ligament: a Study of Immature and Mature Rabbits*, Transactions of the Orthopedic Research Society, **12**:127, 1987.

39. E.L. Radin, I.L. Paul, and M. Lowy, *A Comparison of the Dynamic Force Transmitting Properties of Subchondral Bone and Articular Cartilage*, J. Bone Jt. Surg., **52A**(3):444–456, 1970.

40. E.L. Radin, I.L. Paul, and R.M. Rose, *Role of Mechanical Factors in Pathogenesis of Primary Osteoarthritis*, Lancet:519–521, 1972.

41. E.L. Radin, *Nature of mechanical factors causing degeneration of joints in the hip*, Proc. of the 2nd Open Scientific Meeting of the Hip Society 1974, C. V. Mosby (ed.), St. Louis, pp.76–81, 1974.

42. S. Rapoport, J. Mizrahi, E. Kimmel, O. Verbitsky and E. Isakov, *Constant and Variable Impedance of the Leg Joints in Human Hopping*, ASME Journal of Biomechanical Engineering, **125**:507–514, 2003.

43. S. Saha and R.S. Lakes, *The Effect of Soft Tissue on Wave Propagation and Vibration Tests for Determining the In Vivo Properties of Bone*, J. Biomech., **10**:393–401, 1977.

44. W.S. Selbie and G.E. Caldwell, *A Simulation Study of Vertical Jumping from Different Starting Postures*, J. Biomech., **29**:1137–1146, 1996.

45. W.A. Selle, and J.M. Jurist, *Acoustical Detection of Senile Osteoporosis*, Proceedings of the Society for Experimental Medicine, **121**:150, 1966.

46. A. Seyfarth, M. Gunther, and R. Blickhan, *Stable Operation of an Elastic Three-Segment Leg*, Biological Cybernetics, **84**:365–382, 2001.

47. B.K. Slinker and A.G. Stanton, *Multiple Regression for Physiological Data Analysis: the Problem of Multicollinearity*, American Journal of Physiology, **249**:1–12, 1985.

48. L.D. Smith, *Hip fractures. The Role of Muscle Contraction or Intrinsic Forces in the Causation of Fractures of the Femoral Neck*, J. Bone Jt Surg., **35A**:367–383, 1953.

49. T. Spagele, A. Kistner, and A. Gollhofer, *Modeling, Simulation and Optimization of a Human Vertical Jump*, ASME Journal of Biomechanical Engineering, **32**:521–530, 1999.

50. M. Srivinias and M. Patanaik, *Genetic Algorithms: a survey*, Computer, **27**:17–26, 1994.

51. M. Srivinias and M. Patanaik, *Genetic Search: Analysis Using Fitness Models*, IEEE Transactions on Knowledge and Data Engineering, **8**:120–133, 1996.

52. A. Streitman, A., Miller, and J. Pugh, *The Response of the Lower Extremity to Impact Forces, II. Computerized Mechanical Impedance Measurements*, Bulletin of the Hospital for Joint Diseases, **XL**:120–131, 1979.

53. A. STREITMAN, and J. PUGH, *The Response 'Of the Lower Extremity to Impact Forces. I. Design of an Economical Low Frequency Recording System for Physiologic Waveforms*, Bulletin of the Hospital for Joint Diseases, **XXXIX**(I):63–73, 1978.

54. G.A. THOMPSON, *In Vivo Determination of Bone Properties from Mechanical Impedance Measurements*, Aerospace Medical Association Annual Science Meeting, Las Vegas, Nev., May 7–10, 1973.

55. H. THYS, *Evaluations Indirecte de l'Energie Elastique Utiliseé dans l'Impulsion des Sauts*, Schweizerischen Zeitschrift für Sportsmedizin, 4:169–177, 1978.

56. P.L. WEISS, R.E. KEARNEY, and I.E. HUNTER, *Position Dependence of Ankle Joint Dynamics - 1. Passive Mechanics*, J. Biomech., **19**:727–735, 1986.

57. P. WELSH, *Stress Syndrome in Athletes*, New Zealand Medical Journal, **89**:223–225, 1979.

58. D.A. WINTER, *Biomechanics and motor control of human movement*, 2nd Ed., John Wiley&Sons, New York, 1990.

59. T.M. WRIGHT and W.C. HAYES, *Tensile Testing of Bone over a Wide Range of Strain Rates: Effects of Strain Rate, Micro-Structure and Density*, Medical and Biological Engineering and Computing, **14**:671–680, 1980.

Functional Electrical Stimulation (FES): Muscle Recruitment, Fatigue and Optimization

Functional Electrical Stimulation (FES) of muscles is an artificial way of activating muscles (usually, but not solely, skeletal muscles) for functional purposes. FES has been used to induce contractions of impaired muscles. It is required when the neuro-muscular system is impaired, as in the case of paralysis, for restoring or for enhancing function. Its main purposes are to exercise muscle tissue in order to prevent or decrease atrophy and reduce the incidence of muscular spasm, to improve circulation and increase tissue temperature, to reduce contractures and prevent vein thrombosis [Brooks and Fahey, 1985; Ellison et al., 1985]. FES has been used in spinal cord injury patients as a rehabilitation technique for improving the performance and physical state of spastic paralyzed muscles and for restoring the locomotor abilities [Benton et al., 1981; Kralj et al., 1980a,b; Peckham et al., 1976; Isakov et al., 1985, 1993; Minzly et al., 1993].

Spinal cord injury may disrupt or interrupt contact with the CNS. In many cases and, depending on the level of injury, the peripheral site may remain intact, despite the lack of control from the central nervous system (Fig. 2.1).

2.1. Stimulation Apparatus

Past work on FES has led to the development of stimulation apparatus for the activation of groups of muscle in a sequenced manner, to obtain co-ordination of movement within and between the limbs. Various methods of
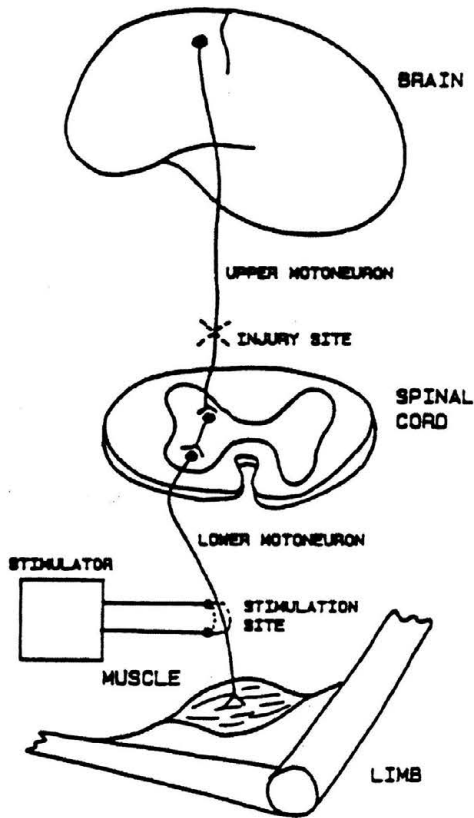
FIGURE 2.1. Central and peripheral nervous systems: note the injury site and the role of FES intervention, as indicated by the 'Stimulator'

stimulation have been developed, particularly in conjunction with the type of electrodes used. These can be: (a) surface electrodes (transcutaneous stimulation); (b) internal, i.e. inside the muscle, but inserted through the skin (percutaneous); or (c) entirely implanted, such as the case of nerve electrodes (Fig. 2.2).

Figure 2.3 shows a six-channel lightweight, portable and computer-controlled stimulator for the functional activation of paraplegic patients [Isakov et al., 1993; Minzly et al., 1993b]. Several basic parameters characterize chronic stimulation. These include: (1) pulse shape; (2) intensity; (3) frequency; (4) pulse width; (5) duration of stimulation train; (6) sequence between the channels. A commonly used pulse shape is the monophasic rectangular one. Stimulation requires to be readjusted due to muscle fatigue.
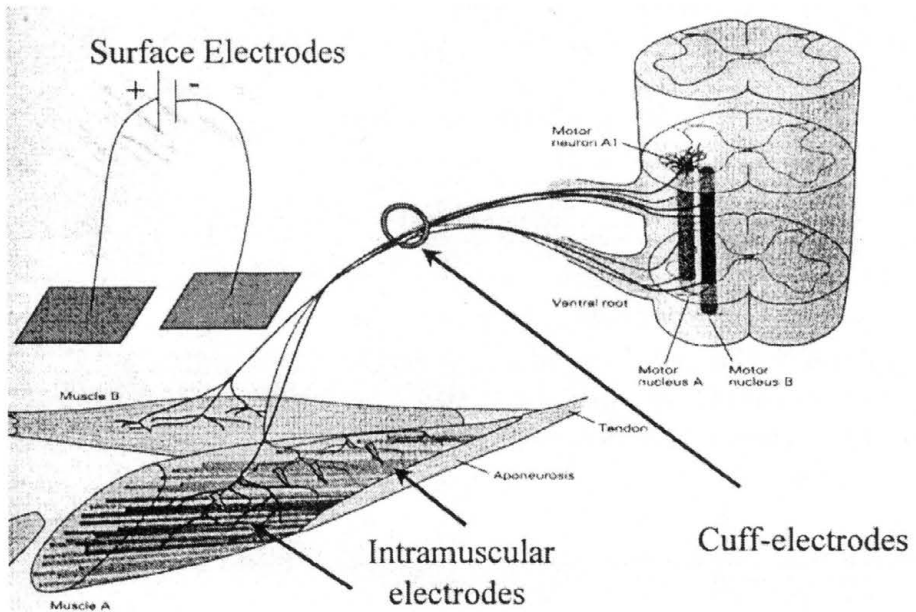
FIGURE 2.2. Schematic illustration of the various modes of stimulation

FIGURE 2.3. A six-channel lightweight, portable and computer-controlled stimulator for the functional activation of paraplegic patients [Isakov et al., 1993; Minzly et al., 1993b]

Modulation can be made either through intensity or pulse width. Duration of stimulation train as well as the sequence is very much determined by the function to be performed.

To enable programming of the various functions, the stimulator is designed to work in a remote-control mode hosted by PC, in addition to its normally used local mode. The pulse trains in each channel consist of rectangular monophasic pulses. The stimulus current characteristics are: 0–400 mA for intensity, with a programmable upper limit, an adjustable frequency of 10–50 Hz and a range of 100–300 μs for pulse width. These parameters are individually adjustable and programmable for each channel. Sequencing of channel activation is also programmable. The power source is 12 V, 500 mAh^{-1}, from 10 rechargeable nickel cadmium batteries, with a run time of 1.5 h for a load of 200 mA per channel if four channels are being used. Various training programmes for the activation of paraplegics in the sitting, standing and walking positions can be selected.

The FES system is essentially a hybrid system, necessitating the conjunction of a walking aid for support and stabilization. A typical system may include a reciprocating-type walker, equipped with two control units to allow the subject to obtain the self-standing and walking functions [Isakov et al., 1993]. The control units are attached to each of the walker handles, positioned on the medial aspect of the handle, enabling the subject to control each with his thumb (Fig. 2.4). Each set includes:

1. A double function joystick, in which the first function is channel selection. Pressing the joystick laterally activates the quadriceps muscles channel, while medial inclination activates the peroneal nerve channel. The second function is dedicated to the adjustment of current intensity: pressing forward results in increment and backward inclination in decrement of the current intensity to the preselected channel.

2. A swing activator button, which when pushed down activates the peroneal nerve channel and assists in swinging the leg forward.

3. A solitary run button, attached either to the left or right handle set. It substitutes the stimulator 'RUN' button, functioning as a program 'standby' position. When pressed, it activates the 'STAND' program. The walker control units are connected to the stimulator and can be also attached to the handles of a pair of Canadian crutches or tripods.

Figure 2.5 a,b demonstrate a patient during the standing up procedure,

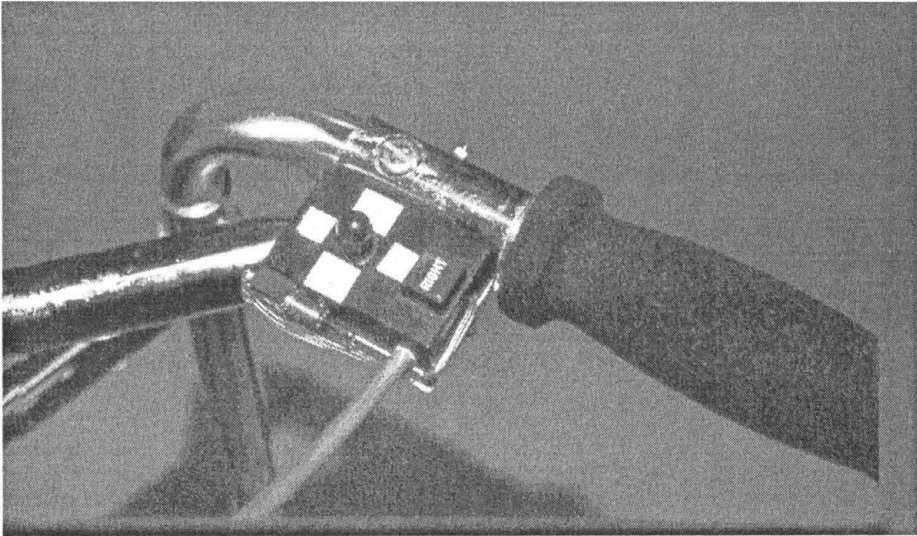FIGURE 2.4. A walker supplements the stimulator to form a hybrid system: control units are attached to each of the walker handles, positioned on the medial aspect of the handle, enabling the subject to control each with his thumb

a   b

FIGURE 2.5. Demonstration of a patient during the standing up procedure, using the hybrid system: stimulator and walker
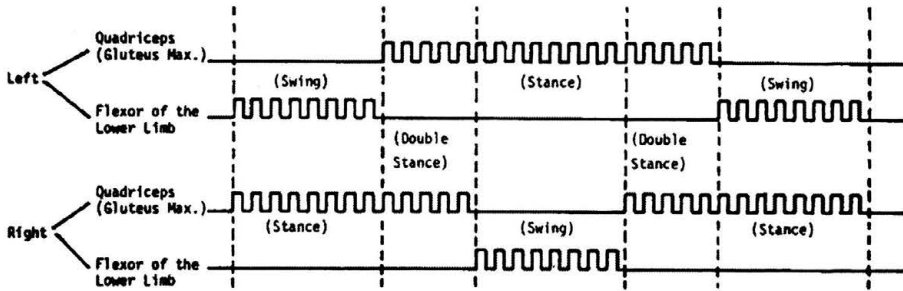
FIGURE 2.6. Sequence used for stepping, or reciprocal walking, using two channels of stimulation for each leg: one for knee extension (quadriceps stimulation) and the other for the flexion reflex (stimulation of the peroneal nerve near the head of the fibula)

using the above-described stimulator. Figure 2.6 demonstrates the sequence used for stepping, or reciprocal walking, using two channels of stimulation for each leg: one for knee extension (quadriceps stimulation) and the other for the flexion reflex (stimulation of the peroneal nerve near the head of the fibula). It should be realized that stepping as obtained by these two functions for each leg is only possible by the supplementary usage of a walking aid for the stabilization of the trunk by means of the upper limbs. As above-described, the walking aid demonstrated in Fig. 2.4 is a walker with finger controls for controlling stimulation sequence and timing, intensity as well as for controlling the main power of the device.

2.2. Issues Associated with the Application of FES

Two major issues associated with functional electrical stimulation (FES) of paralysed muscles are: the mechanism of force generation by means of the recruitment of muscle fibres, and the variation of the muscle force with time as a result of fatigue under sustained stimulation. These issues determine to a great extent the quality of performance.

Modulation of the force produced within the muscle by varying muscle recruitment levels has been studied in the past on experimental animals using intramuscular [Crago et al., 1980], direct neural [Gorman and Mortimer, 1983] and epimysial [Grandjean and Mortimer, 1986] electrical stimulation. Later [Durfee and McLean, 1989], recruitment by nerve stimulation was analyzed by deconvolution methods and by comparing these methods with others previously used.

2.2.1. Recruitment of Muscle

In paraplegic patients, recruitment of the quadriceps muscles has been studied by measuring the torque developed in the knee as a function of stimulation voltage [Kralj et al., 1980b, 1986; Levy et al., 1990].

Figure 2.7 shows recruitment measurements on the quadriceps muscle in isometric stimulation which were made at one of four different muscle lengths, corresponding to 0°, 30°, 60° and 90° of knee flexion angle. The current amplitudes were varied in a ramp-like current input from 30 to 220 mA, within 6 s for recruitment and 6 s for derecruitment (Fig. 2.8). This time interval was judged short enough to avoid possible fatigue within the measurement period. In these experiments the muscle force as evaluated via the foot reaction force was digitized at 20 Hz, and the current amplitude of the FES stimulator was digitized at 10 kHz. Ramp-like current input is shown at the top and the resulting muscle force response – at the bottom of Fig. 2.8, with a noticeable current threshold (of nearly 30 mA) below which there is no measurable force.

When muscles contract isometrically, the tension developed is proportional to the number of crosslinks between the actin the and myosin molecules, with sliding of thin on thick filaments resulting in fibre shortening. In paralysed muscles electrically stimulated via surface electrodes, the tension develo-
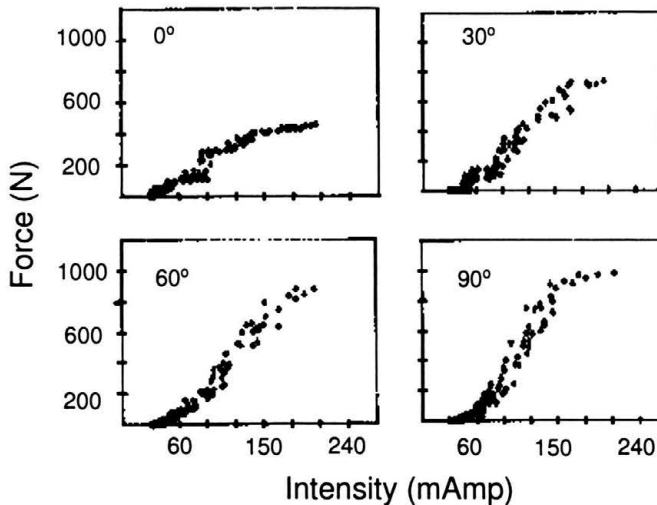

FIGURE 2.7. Recruitment measurements on the quadriceps muscle in isometric stimulation which were made at one of four different muscle lengths, corresponding to 0°, 30°, 60° and 90° of knee flexion angle
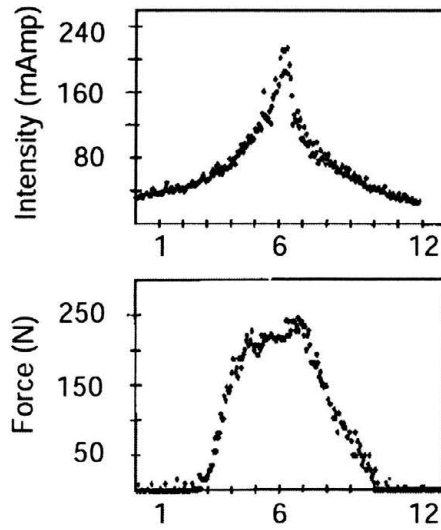
FIGURE 2.8. Current-Force response: ramp-like current input is shown at the top and the resulting muscle force response – at the bottom, with a noticeable current threshold (of nearly 30 mA) below which there is no measurable force

ped increases with pulse intensity. More fibres are recruited by the influence of the local electric field produced. In addition to this direct activation, there is an activation of motor nerve ending in the muscle by electric stimuli [Hultman and Sjoholm, 1983], which also recruits fibres through the motor unit (MU) pattern, resulting in the basic muscle contraction mode, except that it lacks the natural asynchronous MU recruitment mechanism and firing rate regulation observed in normal muscles [Mizrahi et al., 1994]. Moreover, the facilitative effects of cutaneous stimulation observed in healthy subjects [Garnett and Stephens 1981] are absent in the recruitment of paralysed muscles, where no subjective factors are involved.

A great variability was seen among the patients and between the different muscle lengths of the same subject. The maximum quadriceps force at recruitment for the various knee flexion angles for each of the subjects plotted in Fig. 2.7 illustrates this variability. The dependence on muscle length corresponds to previously reported results [Gormann and Mortimer, 1983; Grandjean and Mortimer, 1986]. As in intramuscular stimulation [Crago et al., 1980], the length-tension effects were nearly eliminated in the above case by normalization of the force to the maximal force. The same occurred also in different muscle types. When normalizing the force to the peak values
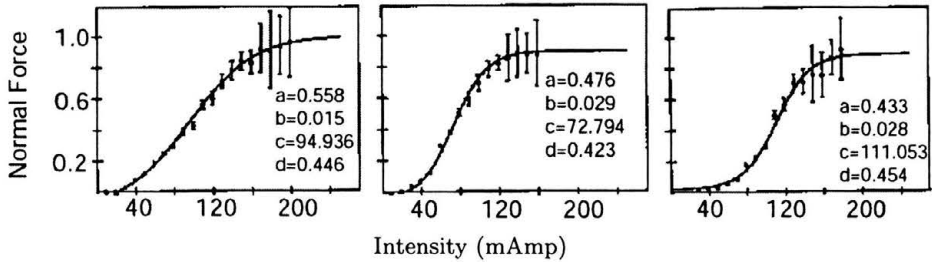
FIGURE 2.9. Recruitment curves for 3 different subjects. A common feature of the recruitment curves is that they are typical and reproducible for each subject. Due to normalization, the curves corresponding to the different flexion angles became similar to one another, enabling us to group them together for every subject

a length-independent ascending twitch force was reported [Wallinga et al., 1980]. Similar length-independent results were obtained in epimysial stimulation when the location of one electrode was varied relative to the muscle motor point [Grandjean and Mortimer, 1986].

A common feature of the recruitment curves is that they are typical and reproducible for each subject as demonstrated in Fig. 2.9. Mean values are represented as dots, with the standard errors of the mean. A tangent hyperbolic regression function was fitted to each subject as follows

$$F = a \tanh[b(x - c)] + d. \tag{2.1}$$

The coefficients a, d represent the translation of axes. The recruitment coefficients are b and c.

The sigmoid-shaped curves obtained had negligible force values at low current intensities until threshold was achieved. A linear-like force increase was thereafter noted. At high current intensities the force levelled-off until the maximum value was reached. This behaviour was noted in all the four muscle lengths studied, with differences in the peak forces. The force values were normalized to the maximal force in each experiment. It should be noted that due to normalization, the curves corresponding to the different flexion angles became similar to one another, enabling us to group them together for every subject. The features which differed between the subjects were the slope of the 'linear-like' portion of the curve, as well as the value of the maximum force.

Electrically stimulated muscle is a highly nonlinear system and is position-dependent [Chizeck et al., 1988]. The recruitment results confirm the non-

linear sigmoidal recruitment curve shapes previously reported in animal experiments during intramuscular (1) and neural (2) stimulation, regardless of the type of stimulus. Nonlinear force addition was also reported when stimulating MU's separately. In the normalized force curves obtained during recruitment in the described experiments, the slope variations could indicate different fatigue resistance among the patients. Threshold and maximal force values were shown to differ from those obtained by other methods, but were both found to be higher in surface FES cases.

In the derecruitment phase which followed recruitment some hysteresis was observed, often with more force in the derecruitment phase suggesting a facilitation process (Fig. 2.10). In animal MU stimulation, the units remaining active during derecruitment produce more force than when recruited [Clamann and Schelhorn, 1988]. It was suggested that in the MU's silenced, passive, elastic elements are unloaded and these may stretch activated units, producing a rise in force, as demonstrated above.
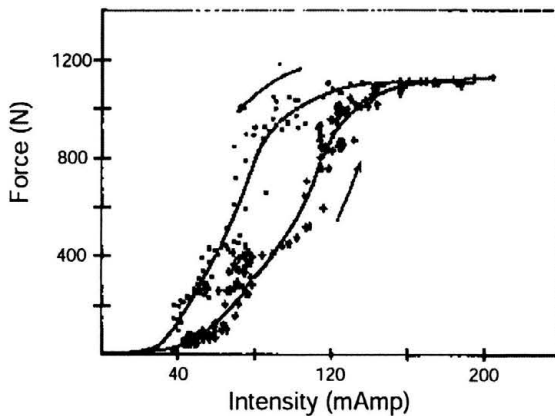
FIGURE 2.10. Derecruitment, following recruitment showing hysteresis, with more force in the derecruitment phase suggesting a facilitation process

2.2.2. Fatigue of Muscle

Muscular fatigue under MVC is probably the closest condition to tetanic contraction by FES. A component of blood flow restriction was reported to be involved due to mechanical compression as a result of enhanced intramuscular pressure, which linearly increases with force up to MVC [Sjogaard et al., 1988]. Besides, potassium and lactate efflux from the exercising muscle may have a crucial influence as with continuity or intermittency of exercise

[Sjogaard et al., 1988]. In electrically stimulated paralysed muscles only peripheral fatigue is present due to complete spinal cord section, avoiding any possible sensory feedback. At the same time, such synchronic stimulation replaces the normal MU firing rate regulation [Mizrahi et al., 1994]. With surface FES, continuous tetanic stimulation of the quadriceps of both legs is needed for standing, which means working under a weight-bearing load in a decreased efficiency mode.

Figure 2.11 shows the typical results of quadriceps force decay at several knee flexion angles of the same subject. The typical behaviour of all the *tests* was characterized by an exponential decay curve, reaching low (non-zero) but functionless values at the end of the three minute test. The force decay observed in fatigued quadriceps under FES corresponds to that reported in studies on animals and normal subjects, with slight differences in its time course. The typical pattern exhibits a double exponential shape; the early part being the acute initial decay and the latter being the asymptotic, low value accommodation. For functional purposes only the first section is the more significant. Indications of partial force recovery in the form of bursts or slight amplitude elevations in the second phase suggest that some of the fibres may have recovered in the process of fatigue. This observation was confirmed from ^{31}P NMR spectroscopy studies [Levy et al., 1993].
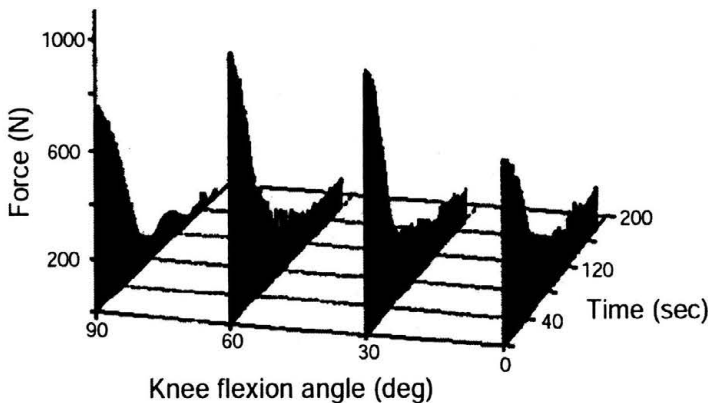
FIGURE 2.11. Quadriceps force fatigue decay at several knee flexion angles of the same subject

2.3. EMG Signals from FES-induced Muscle Contractions

The electromyogram (EMG) of surface-stimulated paralysed muscles by functional electrical stimulation (FES) is of interest if the relationship between the electrical activity and the force within the stimulated muscle is to be investigated. In FES studies, the EMG of surface-stimulated paralyzed muscles was reported to have a repetitive waveform, resulting from the synchronous firing of all the motor units in response to the FES stimulus [Stefancic et al., 1986; Graupe, 1989; Levy et al., 1988; Mizrahi et al., 1994]. This signal was referred to as the compound muscle action potential (CMAP), and is usually preceded by a much stronger stimulus artefact signal (Fig. 2.12). The existence of the artefact is the result of a potential difference developed by the stimulating current between the EMG recording electrodes. Because this potential difference appears as a differential signal, it cannot be rejected by a differential amplifier. This is unlike the common-mode voltages which can be rejected by the EMG amplifier.

In stimulation by surface electrodes, the magnitude of the artefact is especially high (three orders of magnitude higher than the CMAP) for two reasons:

(a) the high stimulation intensities normally required for limb activation,

(b) location of the EMG recording electrodes, usually between the stimulating electrodes, as shown in Figure 2.13.

a = Ml Amplitude
b = Rise time
c = Peak to peak amplitude
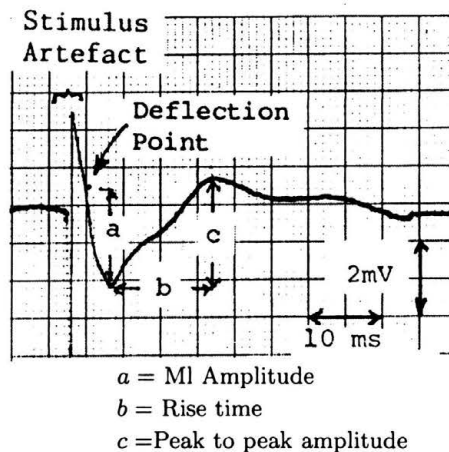
FIGURE 2.12. Electromyographic response of quadriceps to FES: compound muscle action potential (CMAP), preceded by a much stronger stimulus artefact signal
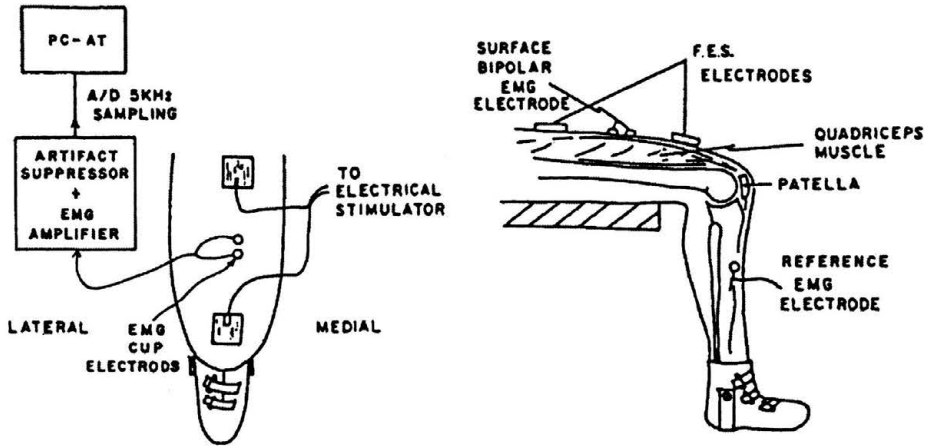
FIGURE 2.13. Detection electrodes placed between the stimulating electrodes. Note the existence of the artifact suppressor in the EMG circuitry

To monitor the stimulus artifact-free compound muscle action potential (CMAP) obtained from the EMG of FES-activated paralysed muscles, it is desirable to synchronise the artefact suppressor with the stimulation pulses of the stimulator. This can be achieved from the EMG electrode themselves. The artefact suppressor [Minzly et al., 1993a] is based on two complementary metal-oxide semiconductor switches that toggle the input of the DC amplifier to earth during the stimulus pulse. The first stage is connected to the patient via three cup electrodes.

The pulse width of the stimulator is typically of the order of 0.3 ms. It is during this time period that the stimulus artifact occurs. Almost immediately after depolarization, the muscle cells begin to repolarize. During repolarization a potential transient is detected between the electrodes. Typically, the repolarization transient is found to last approximately 0.5 ms after the stimulation pulse, amounting together with the pulse width to 0.8 ms from the onset of the pulse. The delay of the first monostable multivibrator is thus set to 1 ms and the measuring window time to 43 ms. Thus for a stimulating frequency of 22 Hz (period of 45.45 ms) a blank time of 1.45 ms results between the end of the measuring time and the next stimulation pulse.

Residual Artefact:

The residual artifact is best assessed by measurement on an unexcitable muscle, e.g., on a flaccid muscle, or on the muscle of a cadaver. Figure 2.14

a. $I = 6\,\text{mA}$ b. $I = 135\,\text{mA}$
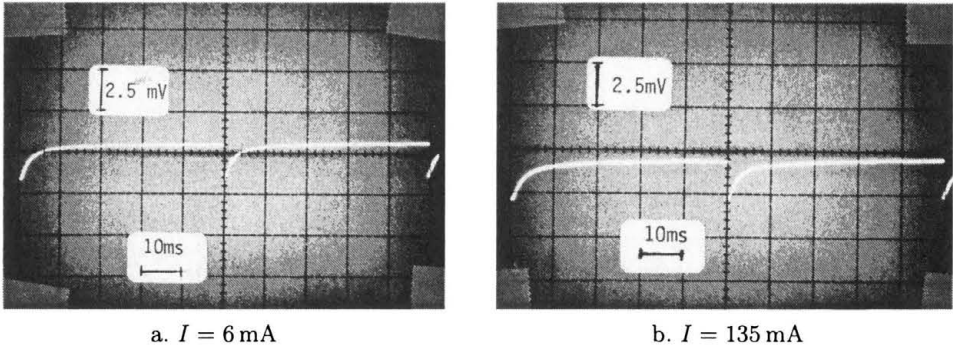
FIGURE 2.14. Suppressed artefact as obtained from measurements made on a cadaver at two stimulation intensities: 6 mA and 135 mA

demonstrates the suppressed artefact as obtained from measurements made on a cadaver at two stimulation intensities: 6 mA and 135 mA. The recording electrodes were aligned between the stimulating electrodes. In both intensities, the suppressed artifact signal had a residual intensity of 3 mV approximately and a recovery time of less than 3 ms. The residual artefact is characterized by a decaying tail, obtained due to the above mentioned time-windowing of the residual component of the repolarization artefact. For stimulation intensities used in FES and usually not exceeding 120 mA, the suppressed artifact signal has a residual intensity of about 3 mV. The recovery time corresponding to this stimulation current was smaller than 3 ms. The exact value of intensity and recovery time was also found to be dependent on the skin-electrode impedance.

An artefact-free CMAP is demonstrated in Fig. 2.15. As seen from Fig. 2.16, the Compound Muscle Action Potential of excited muscle demonstrates deterioration with fatigue.
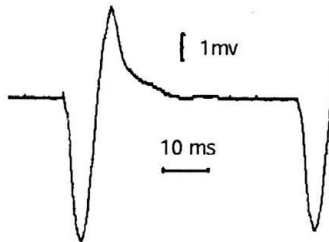
FIGURE 2.15. Artefact-free CMAP

before fatigue   after fatigue
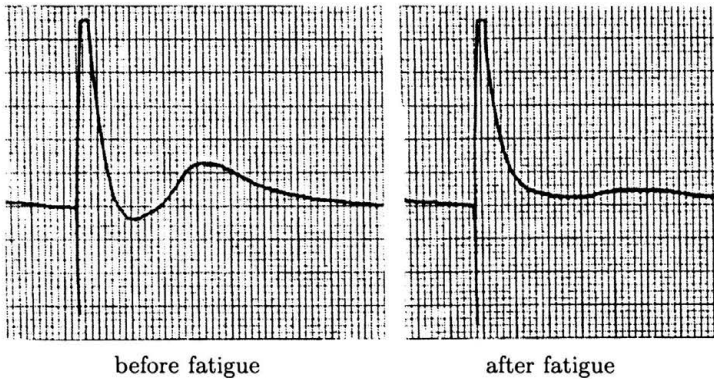
FIGURE 2.16. Compound Muscle Action Potential of excited muscle demonstrates deterioration with fatigue

2.4. Force and EMG Relation in the Course of Fatigue

Typical curves of M-wave peak-to-peak (PTP) amplitude of the M-wave versus muscle force are shown in Fig. 2.17. The PTP is shown to decrease, corresponding to the force developed within the muscle. This behavior was typical of the results for all the four patients tested. An early elevation of the PTP amplitude related to its initial value could often be seen, giving normalized force values greater than unity, and followed by an immediate decrease, corresponding to the force decline. The initial force elevation can be attributed to post-tetanic potentiation [Sinkjaer et al., 1992]. Correlation between force and PTP was made by using the method of least squares and it was found that the data can best be defined by the exponential form. The data presented in Fig. 2.17 were thus fitted as follows

$$y = ax^b \qquad (2.2)$$

where the y axis designated the PTP amplitude and the x axis was for the muscle force (both quantities normalized to their initial values).

It is believed that the very existence of the obtained EMG-force relation in the functional force range allows the use of EMG as a noninvasive monitor of muscular fatigue in isometric conditions. Objective monitoring of fatigue is especially important in paraplegic patients who suffer from lack of sensory feedback from their paralyzed muscles, and it can be used for readjusting stimulation for the prevention of failure. In nonisometric conditions, the changing length of the muscle-tendon structure would increase the
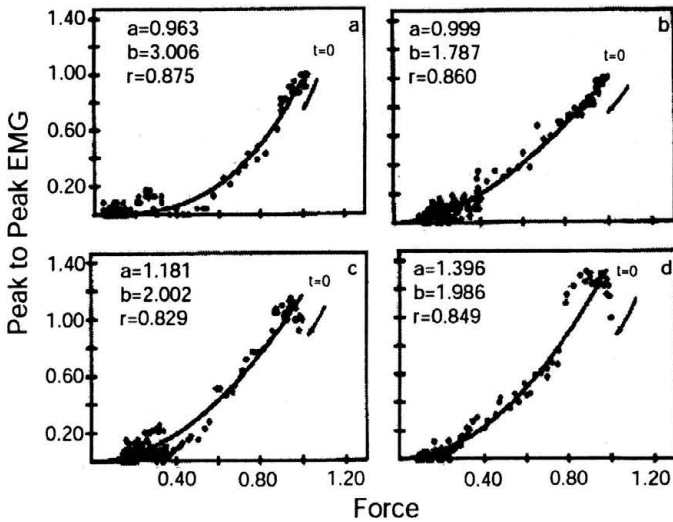
FIGURE 2.17. M-wave peak-to-peak (PTP) amplitude of the M-wave versus muscle force. The data were fitted using $y = ax^b$

number of variable parameters [Giat et al., 1993]. Also, changing geometry of the joints may give rise to changing stretches of the stimulated muscle, which may itself change the force dramatically and nonlinearly [Sinkjaer et al., 1992].

2.5. Training Hypertrophies Muscles

Following spinal cord injury (SCI), paralyzed muscles suffer from atrophy and their fibers transform into type II fast-fatigable fibers [Lieber et al., 1986; Round et al., 1993]. Under such circumstances, the muscle fibers can only generate a limited amount of force and they tend to fatigue rapidly [Miller et al., 1990]. However, when chronic electrical stimulation is applied to the paralyzed muscles of patients with upper motor neuron lesions, the above changes can be reversed [Munsat et al., 1976]. Chronic electrical stimulation was shown to be effective not only in building muscle strength but also in improving fatigue resistance [Peckham et al., 1976; Lieber, 1988]. It should be emphasized, though, that the said improvement in the muscle is reversible if FES training is discontinued [Mizrahi, 1997].

Hypertrophy of the thigh muscles of paraplegics subjected to FES involves an increase in both the diameter and the total number of fibers and,

consequently, in the cross-sectional areas of the entire muscle [Munsat et al., 1976; Neumayer et al., 1995]. The effect of training by FES also involves histochemical changes demonstrated by an increase in the oxidative capacity of the myofibrils [Munsat et al., 1976; Levy et al., 1993; Mohr et al., 1996; Salmons and Sreter, 1976]. The changing condition of the muscle during electrical stimulation with regard to the modification of structure, geometry and function, clearly should be taken into consideration wherever muscle behavior is being studied and modeling is attempted. For instance, force/EMG and/or force/metabolites relations depend on the training status of the muscle [Munsat et al., 1976; Levy et al., 1993; Mizrahi et al., 1997; Moritani, 1993]. Despite the fact that the above factors have been used to evaluate muscle conditioning in subjects with SCI during and following training by FES, it is widely believed that muscle strength and muscle fatigability should be considered as additional important criteria to assess functional rehabilitation in individuals [Mizrahi, 1997; Bajd et al., 1983; Rabischong and Ohanna, 1992; Ragnarsson et al., 1988; Solomonow, 1992].

To estimate the functional changes in the muscle following training by FES an objective measure should be used. Strengthening involves an increase in the muscle force. Since an increase in the dimensions also takes place, a specific index should be established to account for the overall effect of training on the muscle force capacity. A strengthening index was thus proposed as the average muscle force per unit area. This index can express the changes taking place within the muscle. Attention should be paid, though, to the distinction between average muscle force per unit area and muscle specific tension. Whereas the latter reflects an inherent capacity of the muscle fiber, the former is an outcome of several neuromuscular factors, among which is plasticity of the neuromuscular junction and fiber composition of the muscle. It should be noted that evaluation of the average muscle force per unit area requires accurate information on the muscle anthropometry (i.e., cross-sectional area and moment arms). For that, *in-vivo* magnetic resonance imaging (MRI) measurements, in conjunction with biomechanical measurements are used.

Figure 2.18 shows curves of the knee torque during the first 10 s of isometric supramaximal contraction of the quadriceps. Typically, the ascending phase of the activated quadriceps lasted 8 to 10 s after which the torque levelled off. The curves shown in Fig. 2.18 were recorded from the pretrained quadriceps, and at the end of the first and second 4-week periods of training.
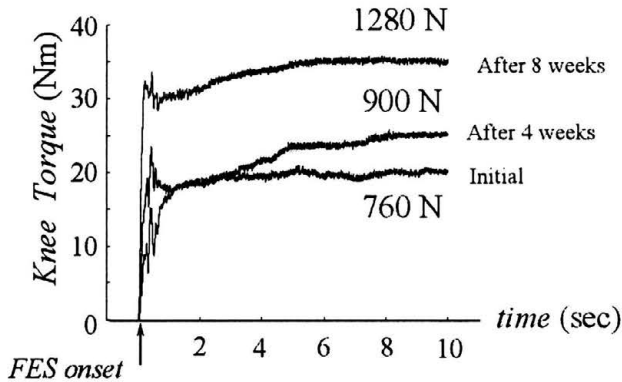
FIGURE 2.18. Knee torque during the first 10 s of isometric supramaximal contraction of the quadriceps; The calculated quadriceps force is shown on each respective curve. Note the training effect on the force.

The calculated peak force in the quadriceps is indicated for each curve. In the first 4-week period, training resulted in an increase of 18% of the peak force of the quadriceps (from 760 at first FES to 900 N at the end of the 4th week). Substantial improvement in the quadriceps force generation capacity occurred during the second 4-week period of training whereas its peak force increased by 42% (up to 1280 N at the end of the 8th week).

Variations of maximal torque (M_{MAX}), residual torque (M_R), force impulse (IMP) and maximal EMG peak-to-peak (PTP) over FES training period are shown in Fig. 2.19.

The solid lines represent linear regressions $y = ax + b$, and the significance of variation of each of the coefficients was tested using the F-test.

The cumulative effect of the 8 weeks of training by FES on the quadriceps group is summarized in Table 2.1. The estimated average force per unit area in the pretrained quadriceps was $27 \, N/cm^2$ (F_{QT}(max) = 760 N; PCSA = $28.2 \, cm^2$). Following the first 4 week of training the estimated average force per unit area increased by only 3.7% ($28 \, N/cm^2$), whereas the peak force levelled at 900 N and the PCSA increased to $31.6 \, cm^2$. A substantial improvement in the force generation capacity of the quadriceps was obtained during the second 4-week training period, where the average force per unit area increased by 43%, from $28 \, N/cm^2$ to $40 \, N/cm^2$ (F_{QT}(max) = 1280 N; PCSA = $32.0 \, cm^2$).
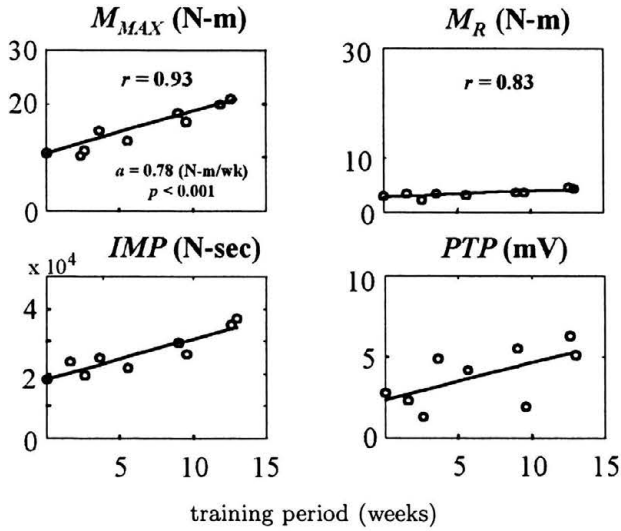
FIGURE 2.19. Variations of maximal torque (M_{MAX}), residual torque (M_{R}), force impulse (IMP) and maximal EMG peak-to-peak (PTP) over FES training period of 12 weeks

TABLE 2.1. Changes in the maximal knee torque $M_K(\text{max})$, maximal quadriceps force $F_{QT}(\text{max})$, quadriceps physiological cross-section area PCSA, and muscle average force per unit area, before training, and after the first 4 weeks and second 4 weeks of training

Training Period [weeks]	$M_K(\text{max})$ [Nm]	$F_{QT}(\text{max})$ [N]	PCSA [cm^2]	muscle average force per unit area [N/cm^2]
Pretrained	20.7	760	28.2	27
End of first 4 weeks	24.7	900	31.6	28
End of second 4 weeks	35.0	1280	32.0	40

It is evident from the results in Table 2.1 that during the 8 weeks training period followed-up, the maximal isometric torque output of the quadriceps increased by almost 70%. However, morphological studies, incorporating magnetic resonance imaging (MRI) of the quadriceps, have confirmed an overall increase of only 13.5% in the physiological cross-sectional area of this muscle over the same training period. This fact may indicate that conditioning of the trained muscle consists also of a general increase in the intrinsic strength of muscle per unit area. Interestingly, only minor variations in the average force capacity per unit area were observed during the first 4 weeks of the training where changes primarily consisted of a general increase in the physiological

cross-sectional area of the muscle (12%). As training proceeded, the muscle average force per unit area changed from $28\,\text{N}/\text{cm}^2$ at the end of the 4th week to $40\,\text{N}/\text{cm}^2$ at the end of the 8th week.

Similarly, strength training performed on able-bodied subjects has demonstrated that when an increase in muscle size occurs, the changes are less prominent than the increase in voluntary strength of the muscle [Moritani, 1993; Moritani and DeVries, 1979; MacDougall et al., 1980]. Ikai and Fukunaga [1970] have demonstrated that an increase in voluntary strength per cross-sectional area was observed both in the trained limb, as well as in the contralateral untrained limb. Moreover, Dons and associates [1979] have demonstrated that the increase in voluntary strength per cross-sectional area was specific to the training (i.e., was pronounced during training but showed no significant changing otherwise). These finding suggest that strengthening may be caused by a neural adaptation rather than by changes in the intrinsic muscle properties [Moritani and DeVries, 1979; Hakkinen and Komi, 1983; Sale, 1986]. In trained muscles, neural adaptation can be attributed to any one, or to a combination of the following processes: (a) increased synchronization of motor unit firing; (b) refitting motor unit recruitment threshold by reversing synaptic efficacy; i.e., increase of high recruitment threshold motor units and reduction of low recruitment threshold motor units [Sale, 1986; Burke, 1986; Kanda et al., 1977]. While increased synchronization of motor unit firing is associated with increases of voluntary control efforts, synaptic efficacy is peripheral in nature and depends on size and structure of the pre-synaptic terminal as well as the post-synaptic receptors. We therefore suggest that in the case where the trained muscles are disconnected from voluntary control, as is the case in FES of paraplegic subjects, neural adaptation should be attributed to an increase in synaptic efficacy of the motor units, and/or preferential enlargement of the nerve axons; thus reduced recruitment threshold of these axons. The latter was found to be significant in muscle fascicles of reinnervated human quadriceps [Munsat et al., 1976]. It can therefore be suggested that specific tension of a single muscle fiber is not affected by training, although the average force per unit area increased from $27\,\text{N}/\text{cm}^2$ before training to $40\,\text{N}/\text{cm}^2$ after 8 weeks of training by FES.

Muscle strengthening may depend on the increase in the number of activated myofibrils, fiber area, myofibrillar area, myofibrillar volume density, and upon ratio of type I (slow oxidative) and type II (fast fatiguable) fibers [Munsat et al., 1976; MacDougall et al., 1980].

Biopsy studies made on able-bodied subjects showed that myofibril cross-sectional area increased significantly following training, while the myofibrillar density, defined as the number of filaments within an enclosed area, remained unchanged. Increase in fiber size was observed in both type I and type II fibers however, in the paralyzed muscles trained by FES, an increase in the size of type II fiber was accompanied by a marked decrease in their relative number [Munsat et al., 1976].

2.6. Metabolic Aspects of FES-induced Muscle Contraction

Fatigue is defined as the failure to achieve or maintain an expected force or power output [Asmussen, 1979]. However, the mechanism by which it is caused during exercise is still unclear. In FES of paralyzed muscles fatigue results only from the activity within the motor unit such as depletion of necessary substances (for instance ATP), accumulation of catabolites caused by the muscle contraction, or problems in excitation contraction coupling [Bigland-Ritchie et al., 1986; Hultman et al., 1986]. Fatigue is influenced also by the specific means of stimulation (continuous or intermittent), since additional intramuscular ischemia may develop in the first case, when maximal contractions are performed, and contribute to the reduction of force, Thus muscular fatigue is obviously not dependent on one single factor, but in all the cases phosphorous metabolites play an important role. Although some research has been done on the mechanical aspects [Peckham et al., 1976; Levy et al., 1990; Susak et al., 1986], relatively little work was done regarding the biochemical and metabolic conditions of paraplegics' muscles. Noninvasive ^{31}P NMR measurements can provide information on the bioenergetics of the fatiguing muscle under FES. This is achieved by monitoring the levels of metabolites at the cellular level.

Thus, force and metabolites of the FES activated muscle had to be measured simultaneously. The experiments were performed using a special apparatus (Fig. 2.20) designed for measurements inside the 1.9 T magnetic field. This apparatus was composed of an experimental shoe, hinged at the ankle level to a cantilever where a load cell was located. This arrangement enabled the foot to perform free flexion-extension. Special care was taken to avoid magnetic materials in the device. The load cell, as well as the rest of the metallic parts, were made of aluminum and attached to a wooden basis
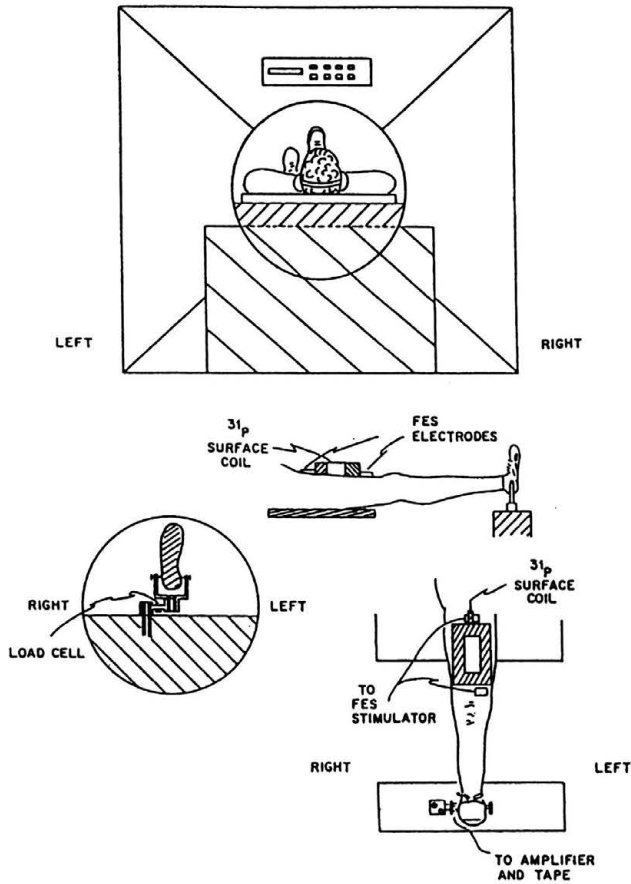
Figure 2.20. Simultaneous measurement of force and metabolites of the FES activated muscle, performed using a special apparatus designed for measurements inside the 1.9 T magnetic field of an MRI/MRS machine

firmly held on the cylindrical bore of the MRI instrument. The electronics and the stimulator were positioned far enough away to avoid any interference from the strong magnetic field.

The continuous stimulation, the force recording, and the ^{31}P NMR measurements were sampled simultaneously within an MR clinical 1.9 T instrument operating at 32.9 MHz for ^{31}P spectroscopy and at 81.3 MHz for ^{l}H imaging. A hydrogen/phosphorus, double tuned, planar, square 11.5×11.5 cm surface coil served for both ^{l}H imaging and ^{31}P spectroscopy. No patient repositioning or hardware change was required when switching between imaging and spectroscopy.

The chemical shift scale was calibrated using $= 0$ for phosphocreatine (PCr) as an internal reference and the intracellular pH was estimated, as described previously [Moon and Richards, 1973; Gadian et al., 1982], from the pH dependent chemical shift of the inorganic phosphate (P_i) peak relative to the pH independent PCr reference, using the following equation [Taylor et al., 1983]:

$$pH = 6.75 + \log(\delta - 3.27)/(5.69 - \delta). \tag{2.3}$$

^{31}P NMR studies of the quadriceps muscle of the paraplegic patients were performed at rest, during 3 min. of stimulated contraction, and during the following recovery period. Normal values were found for the phosphorous metabolite ratios during rest (Fig. 2.21). Average PCr/Pi ratios were in the range for normal subjects [Levy et al., 1993; Jeneson et al., 1990]. In addition, the intracellular pH was 7.1±0.1. These parameters indicate the existence of a normal metabolic state in the paralyzed paraplegic muscle cells. The only difference is the elevated levels of the phosphodiester (PDE) peak, which probably contains mainly glycerophosphocholine (GPC), as previously found for other muscles [Chalovich et al., 1979]. It is interesting to note this relatively enhanced levels of PDE. This may indicate FT to ST transformation,
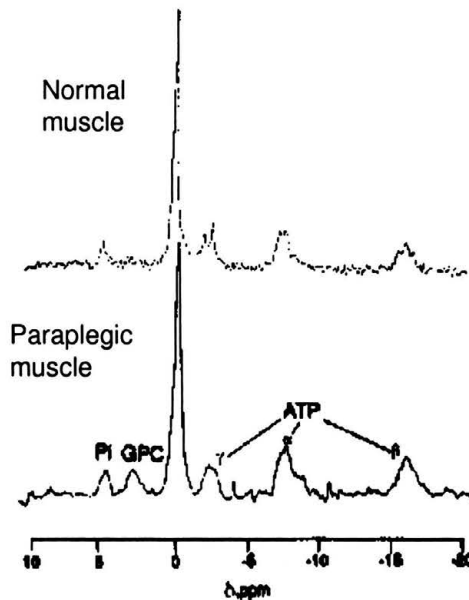
FIGURE 2.21. Normal values were found for the phosphorous metabolite ratios during rest of paraplegic compared to normal muscles

as was found in the case of rabbits under prolonged experimental electrical stimulation [Burt et al., 1982]. It may also be a characteristic marker of paralyzed, inactive muscle, since increased intensity in the PDE region is associated with a variety of diseases of muscles and other tissues [Barany and Siegel, 1989].

The effect of fatigue due to FES is demonstrated in Fig. 2.22, where the top panel describes the resting state and the bottom one describes the state after FES fatigue. Figure 2.23 shows a cascade of spectra obtained: after the rest spectrum there are 3 sets of spectra during fatigue under FES activation, followed by 4 spectra during the period of post-stimulation rest. The individual time-history curves are shown in Fig. 2.24, indicating that during FES pH and PCr decline, whereas Pi and PME increase.

The recovery process of the quadriceps muscle after 3 min. of tetanic contraction is illustrated in right-hand part of the curves of Fig. 2.24. The signals of the various metabolites and the pH returned gradually to their steady state levels at about 35 to 40 min of recovery.
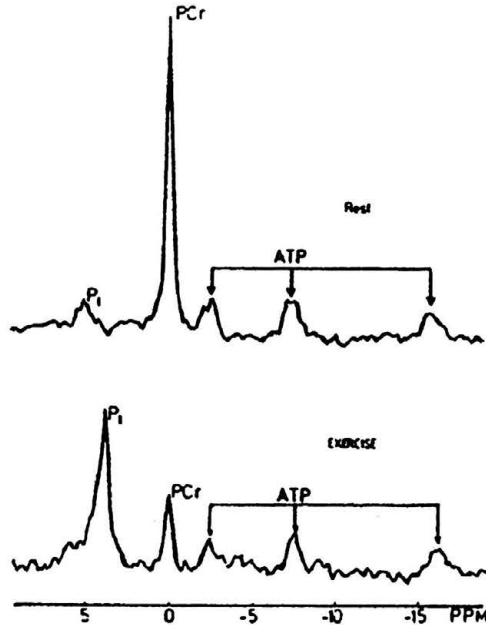
FIGURE 2.22. Effect of fatigue due to FES of paralyzed muscle: top panel describes the resting state and the bottom one describes the state after FES fatigue
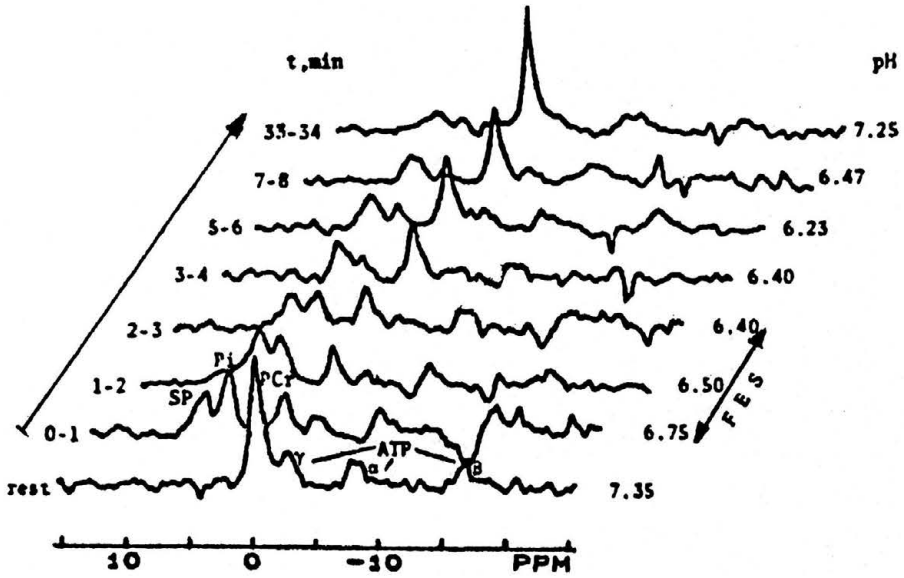
FIGURE 2.23. Cascade of spectra obtained: after the rest spectrum there are 3 sets of spectra during fatigue under FES activation, followed by 4 spectra during the period of post-stimulation rest
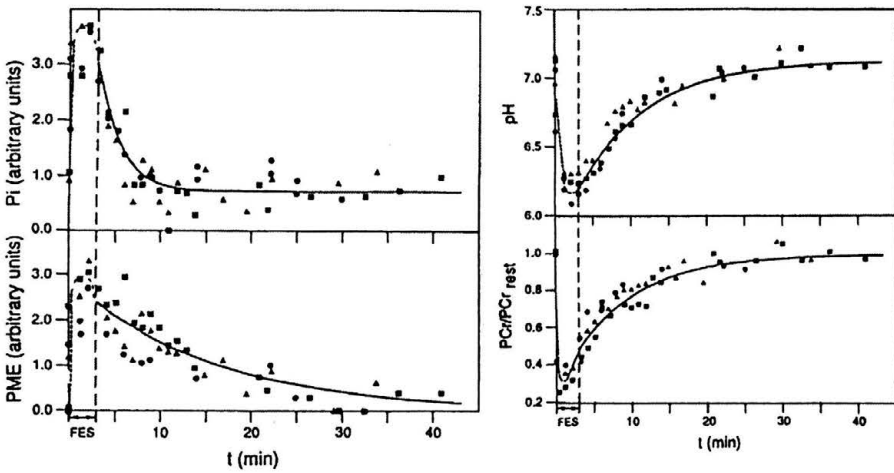
FIGURE 2.24. Individual time-history curves are during FES and recovery of pH, PCr, Pi and PME

2.7. Epilogue

The electrically stimulated paralyzed muscle of the lower limbs of spastic paraplegics constitute a special model of 'isolated' functional contractile tissue. Fatigue in this case is not accompanied by pain, and not affected by voluntary control, and other factors that depend on the interaction with the central nervous system. This is essentially a *peripheral* system due to detachment from CNS following injury (isolated system). Thus, since the central (volitional) component of activation is absent, the parameters treated in this presentation can be used to describe the various aspects of fatigue and related together to obtain relationships between the:

- Mechanical (system),
- Myoelectric (cell/system),
- Metabolic (cell).

This task is achievable via modeling, to be discussed in the next chapter.

References for Chapter 2

1. E. ASMUSSEN, *Muscle fatigue*, Med. Sci. Sports, **11**:313–321, 1979.

2. T. BAJD, A. KRALJ, R. TURK, H. BENKO, and J. SEGA, *The use of a four-channel electrical stimulator as an ambulatory aid for paraplegic patients*, Physical Therapy, **63**:1116–1120, 1983.

3. M. BA'RA'NY, I.M. SIEGEL, P.N. VENKATASUBRAMANIAN, E. MOK, and A.C WILBUR, *Human leg neuromuscular diseases: P-31 MR spectroscopy*, Radiology, **172**:503–508, 1989.

4. B. BIGLAND-RITCHIE, F. FURBUSH, and J.J. WOODS, *Fatigue of intermittent submaximal voluntary contractions: Central and peripheral factors*, J. Appl. Physiol., **61**(2):421–429, 1986.

5. L.A. BENTON, L.L. BAKER, B.R. BOWMAN, and R.L. WALLTERS, *Functional Electrical Stimulation – A Practical Clinical Guide*, (2nd Edition), Rancho Rehabilitation Engineering Program, Rancho Los Amigos Medical Centre, Rancho Los Amigos Hospital, California, 1981.

6. G.A. BROOKS and T.D. FAHEY, in: *Exercise Physiology. Human Bioenergetics and its Applications*, Macmillan Publishing Co., New York, 1985.

7. R.E. BURKE, *The control of muscle force: Motor unit recruitment and fatigue patterns*, in: J. Norman, N. McCartney, and A. McComas (Eds): Human Muscle Power, Human Kinetics Publishers Inc., U.S.A, pp.97–109, 1986.

8. C.T. BURT, M.G. PLUSKAL, and F.A. SRETER, *Generation of phosphodi-esters during fast-to-slow muscle transformation. A 31P-NMR study*, Biochem. Biophys. Acta, **721**:492–494, 1982.

9. J.M. CHALOVICH, C.T. BURT, M.J. DANON, T. GLONEK, and M. BA'RA'NY, *Phosphodiesters in muscular dystrophies*, Ann. N.Y. Acad. Sci., **317**:649–669, 1979.

10. H.J. CHIZECK, R. KOBETIC, E.B. MARSOLAIS, J.J. ABBAS, I.H. DONNER, and E. SIMON, *Control of functional neuromuscular stimulation systems for standing and locomotion in paraplegics*, Proc. IEEE, **76**:1155–1165, 1988.

11. H.P. CLAMANN and T.B. SCHELHORN, *Nonlinear force addition of newly re-cruited motor units in the cat hind limb*, Muscle and Nerve, **11**:1079–1089, 1988.

12. P.E. CRAGO, P.H. PECKHAM, and G.B. THROPE, *Modulation of muscle force by recruitment during intramuscular stimulation*, IEEE Trans. Biomed. Engng., **27**:679–684.

13. B. DONS, K. BOLLERUP, F. BONDE-PETERSEN, and S. HANCKE, *The effect of weight-lifting exercise related to muscle fiber composition and muscle cross-sectional area in humans*, Europe. J. App. Physiol., **40**:95–106, 1979.

14. W.K. DURFEE and K.E. MACLEAN, *Methods for estimating isometric recruit-ment curves of electrically stimulated muscle*, IEEE Trans. Biomed. Engng., **36**:654–667, 1989.

15. A.E. ELLISON, A.L. BOLAND, P. GRACE, K.E. DEHAVEN, G.A. SNOOK, and H. CALEHUFF, in: *Athletic Training and Sport Medicine*, p.115, American Academy of Orthopaedic Surgeons, Chicago, 1985.

16. D.G. GADIAN, G.K. RADDA, M.J. DAWSON, and D.R. WILKIE, in: *Intracel-lular pH: Its Measurement, Regulation and Utilization in Cellular Function*, R. Nuccitelli, D.W. Deamer (Eds.), p.61, Liss, New York, 1982.

17. R. GARNETT and J.A. STEPHENS, *Changes in the recruitment threshold of motor units produced by cutaneous stimulation in man*, J. Physiol., **311**:463–473, 1981.

18. Y. GIAT, J. MIZRAHI and M. LEVY, *A musculo-tendon model of the fatigue profiles of paralyzed muscle under FES*, IEEE Trans. Biomed. Eng., **40**(7):664–674, 1993.

19. P.H. GORMAN and J.T. MORTIMER, *The effect of stimulus parameters on the recruitment characteristics of direct nerve stimulation*, IEEE Trans Biomed Engng., **30**:407–414, 1983.

20. P.A. GRANDJEAN and J.T. MORTIMER, *Recruitment properties of monopolar and bipolar epimysial electrodes*, Ann. Biomed. Engng., **14**:53–66, 1986.

21. D. GRAUPE, *EMG pattern analysis for patient-responsive control of FES in paraplegics for walker-supported walking*, IEEE Trans. Biomed. Eng., **36**:711–719, 1989.

22. K. HAKKINEN and P.V. KOMI, *Electromyographic changes during strength training and detraining*, Medicine and Science in Sport and Exercise, **15**:455–460, 1983.

23. E. HULTMAN and H. SJOHOLM, *Electromyogram, force and relaxation time during and after continuous electrical stimulation of human skeletal muscle in situ*, J. Physiol., **339**:33–40, 1983.

24. E. HULTMAN, L.L. SPRIET, and K. SODERLUND, *Biochemistry of muscle fatigue*, Biomed. Biochim. Acta, **45**:S97–106, 1986.

25. M. IKAI, and T. FUKUNAGA, *A study on training effect on strength per unit cross-sectional area of human muscle by means of ultrasonic measurement*, Europe. J. App. Physiol., **28**:173–180, 1970.

26. E. ISAKOV, J. MIZRAHI, D. GRAUPE, E. BECKER, and T. NAJENSON, *Energy cost and physiological reactions to effort during activation of paraplegics by functional electrical stimulation*, Scand. J. Rehabil. Med., **12**(Suppl.):102–107, 1985.

27. E. ISAKOV, and J. MIZRAHI, *FES system for self-activation: An electrical stimulator and instrumented walker*, Clinical Rehabilitation, **7**:39–44, 1993.

28. J.A.L. JENESON, R.W. DE BORE, J.W. VAN TEEFFELEN, G.J. AMELINK, R.R. BAR, C.J.A. VAN ECHTELD, M. DURAN, and W.B.M. ERICH, 10th Annu. Meeting Soc. Magn. Reson. Med., N. Y. 1222, 1990.

29. K. KANDA, R.E. BURKE, and B. WALMSLEY, *Differential control of fast and slow twitch motor units in the decerebrated cat*, Exp. Brain Res., **29**:57–74, 1977.

30. A. KRALJ, T. BAJD, and R. TURK, *Electrical stimulation providing functional use of paraplegic patient muscles*, Med. Prog. Technol., **7**:3–9, 1980a.

31. A. KRALJ, T. BAJD, and R. TURK, *The influence of electrical stimulation on muscle strength and fatigue in paraplegia*, Proc. Int. Conf. Rehab. Engng., Toronto, Canada, 1980b.

32. A. KRALJ, T. BAJD, R. TURK, and H. BENKO, *Posture switching for prolonging functional electrical stimulation standing in paraplegic patients*, Paraplegia, **24**:221–230, 1986.

33. M. LEVY, J. MIZRAHI, Z. SUSAK, and P. SOLZI, *Fatigue of quadriceps muscles continuously activated by functional electrical stimulation in paraplegics*, in: Electrophysiological kinesiology. Wallinga, W., Boom, H. B. K., De Vries, J. (Eds.), Elsevier Science Publishers BV (Biomedical Division), pp.65–68, 1988.

34. M. LEVY, J. MIZRAHI, and Z. SUSAK, *Recruitment, force and fatigue charac-teristics of quadriceps muscles of paraplegics isometrically activated by surface functional electrical stimulation*, J. Biomed. Eng., **12**:150–156, 1990.

35. M. LEVY, T. KUSHNIR, J. MIZRAHI, and Y. ITZCHAK, *In-vivo 31P NMR stu-dies of paraplegics' muscles activated by functional electrical stimulation*, Mag-net. Reson. Med., **29**:53–58, 1993.

36. R.L. LIEBER, J.O. FRIDEN, A.R. HARGENS, E.R. FERINGA, *Fiber type trans-formation in rat slow and fast muscle one year after spinal cord transection*, 32nd Annual ORS, New Orleans, Louisiana, Feb. 17–20, p.256, 1986.

37. R.L. LIEBER, *Comparison between animal and human studies of skeletal muscle adaptation to chronic stimulation*, Clin. Orthop. Res., **233**:19–24, 1988.

38. J.D. MACDOUGALL, G.C.B. ELDER, D.G. SALE, J.R. MOROZ, J.R. SUT-TON, *Effects of strength training and immobilization on human muscle fibres*, Europe. J. App. Physiol., **43**:25–34, 1980.

39. R.G. MILLER, A.T. GREEN, R.S. MOUSSAVI, P.J. CARSON, and M.W. WEINER, *Excessive muscular fatigue in patient with spastic paraparesis*, Neu-rology, **40**:1271–1274, 1990.

40. J. MINZLY, J. MIZRAHI, N. HAKIM, and A. LIBERSON, *A stimulus artifact suppressor for EMG recording during FES by a constant current stimulator*, Medical and Biological Engineering and Computing, **31**:72–75, 1993a.

41. J. MINZLY, J. MIZRAHI, E. ISAKOV, Z. SUSAK, and M. VERBEKE, *Computer controlled portable stimulator for paraplegic patients*, J. Biomedical Engineering, **15**:333–338, 1993b.

42. J. MIZRAHI, M. LEVY, H. RING, E. ISAKOV, and A. LIBERSON, *EMG as an indicator of fatigue of isometrically FES-activated paralyzed muscles*, IEEE Trans. Rehab. Eng., **2**:57–65, 1994.

43. J. MIZRAHI, O. LEVIN, A. AVIRAM, E. ISAKOV, and Z. SUSAK, *Muscle fa-tigue in interrupted stimulation: Effect of partial recovery on force and EMG dynamics*, J. Electromyogr. Kinesiol., **7**:51–65, 1997.

44. J. MIZRAHI, *Fatigue in muscles activity by functional electrical stimulation*, Critical Reviews in Physical and Rehabilitation Medicine, **9**:93–129, 1997.

45. T. MOHR, P. TORNOE, F. BIERING-SORENSEN, J. PODENPHANT, J. ANDER-SEN, A. WAGNER, H. GALBO, and M. KJAER, *Long term electrically induced cycling in SCI - a pilot study*, in: A. Pedotti, M. Ferrarin, J. Quintern, and R. Riener (Eds.): Neuroprosthetics, from Basic Research to Clinical Applications, pp.569–577, Springer, Berlin, 1996.

46. R.B. MOON and J.H. RICHARDS, *Determination of intracellular pH by 31P magnetic resonance*, J. Biol. Chem., **248**:7276–7278, 1973.

47. T. MORITANI, H.A. DEVRIES, *Neural factors vs. hypertrophy in time course of muscle strength gain*, Am. J. Physical Med.&Rehab., **85**:115–130, 1979.

48. T. MORITANI, *Neuromuscular adaptations during the acquisition of muscle strength, power and motor tasks*, J. Biomechanics, **26**(Suppl):95–107, 1993.

49. T.L. MUNSAT, D. MCNEAL, and R. WATERS, *Effects of nerve stimulation on human muscle*, Arch. Neurol., **33**:608–617, 1976.

50. C.H. NEUMAYER, W. HAPPAK, H. KERN, and H. GRUBER, *Hypertrophy and transformation of muscle fibers in paraplegic patients*, in: 5th Vienna International Workshop on Functional Electrostimulation: Basics, Technology, Clinical Application. Vienna, Austria, August 17–19, pp.75–78, 1995.

51. P.H. PECKHAM, J.T. MORTIMER, E.B. MARSOLAIS, *Alteration in the force and fatigability of skeletal muscle in quadriplegic humans following exercise induce by chronic electrical stimulation*, Clin. Orthop., **114**:326–334, 1976.

52. E. RABISCHONG and F. OHANNA, *Effects of functional electrical stimulation (FES) on evoked muscular output in paraplegic quadriceps muscle*, Paraplegia, **30**:467–473, 1992.

53. K.T. RAGNARSSON, S. POLLACK, W. O'DANIEL, R. EDGAR, J. PETROFSKY, and M. NASH, *Clinical evaluation of computerized functional electrical stimulation after spinal cord injury: a multicenter pilot study*, Arch. Phys. Med. Rehabil., **69**:672–677, 1988.

54. J.M. ROUND, F. BARR, B. MOFFAT, and D.A. JONES, *Fiber areas and histochemical fiber types in the quadriceps muscle of paraplegic subjects*, J. Neurological Sciences, **116**:207–211, 1993.

55. D.G. SALE, *Neural adaptation in strength and power training*, In: J. Norman, N. McCartney, A. McComas (Eds): Human Muscle Power. Human Kinetics Publishers, Inc. U.S.A, pp.289–308, 1986.

56. S. SALMONS, F.A. SRETER, *Significance of impulse activity in the transformation of skeletal muscle type*, Nature, **263**:30–34, 1976.

57. T. SINKJAER, N. GANTCHEV, and L. ARENDT-NIELSEN, *Mechanical properties of human ankle extensors after muscle potentiation*, Electroencephalography and Clinical Neurophysiology, **85**:412–418, 1992.

58. G. SJOGAARD, G. SAVARD, and C. JUEL, *Muscle blood flow during isometric activity and its relation to muscle fatigue*, Eur. Appl. Physiol., **57**:327–35, 1988.

59. M. SOLOMONOW, *Biomechanics and physiology of a practical functional neuromuscular stimulation powered walking orthosis for paraplegics*, in: R.B. Stein, P.H. Peckham, and D.P. Popovic (Eds.): Neural Prosthesis, Replacing Motor Function After Disease or Disability. Oxford University Press, New York pp.202–232, 1992.

60. Z. SUSAK, M. LEVY, J. MIZRAHI, and E. ISAKOV, *The duration of isometric muscle contraction while using FES with stimuli of different parameters*, Proc. 2nd Vienna Int. Workshop Functional Electrical Stimulation, Austria, pp.75–78, 1986.

61. M. STEFANCIC, A. KRAL, R. TURK, T. BAJD, H. BENKO, and J. SEGA, *Neurophysiological background of the use of functional electrical stimulation in paraplegia*, Electromyogr.&Clin. Neurophysiol., **26**:423–435, 1986.

62. D.J. TAYLOR, P.J. BORE, P. STYLES, D.G. GADIAN, and G.K. RADDA, *Bioenergetics of intact human muscle. A 31P nuclear magnetic resonance study*, Mol. Biol. Med., **1**:77–94, 1983.

63. W. WALLINGA-DE JONGE, H.B.K. BOOM, K.L. BOON, P.A.M. GRIEP, and G.C. LAMMEREE, *Force development of fast and slow skeletal muscle at different muscle lengths*, Am. J. Physiol., **239**:C98–104, 1980.

Chapter **3**

FES: Modeling and Predictability of Force in Stimulated Muscle

As described in Chapter 2, muscle fatigue during FES results in force reduction within the motor units, as well as in an elevation of the excitation threshold of these motor units. This implies that increasingly higher electric stimulation is essential to the fatiguing activated muscle, if the performed task has to be maintained. In open loop control, the muscle is usually overstimulated to ensure safety, which causes the muscle to fatigue even more rapidly [Brown and Burns, 1949; Edwards et al., 1972; Lind and Petrofsky, 1979; Petrofsky, 1979]. Open loop control is inherently poor, not only due to the mentioned fatigue, but also due to the following additional factors: individual and widely variable musculo-skeletal properties, depending on the training status of the muscle; unintended variation in the activation conditions; possible existence of muscle spasticity and possible existence of external disturbances. These introduce substantial unknowns into the system to be controlled. Efforts to improve the control methods have been directed towards (a) closed-loop control of the stimulated muscle [Crago et al., 1980; Cybulski et al., 1984; Chizeck et al., 1988] and (b) modeling of muscle behavior in conjunction with fatigue and recovery.

If muscle fatigue could be modeled and muscle force – predicted, synthesis of an open-loop controller based on feed-forward to the activated muscle could be realized [Popovic, 1992].

On the other hand, closed loop control systems require the development of artificial feedback sensors to replace the lost function of the natural proprioceptive and mechano-receptive sensors [Andrews et al., 1988; Hoffer and Haughland, 1992; Webster, 1992]. More robust control systems should com-
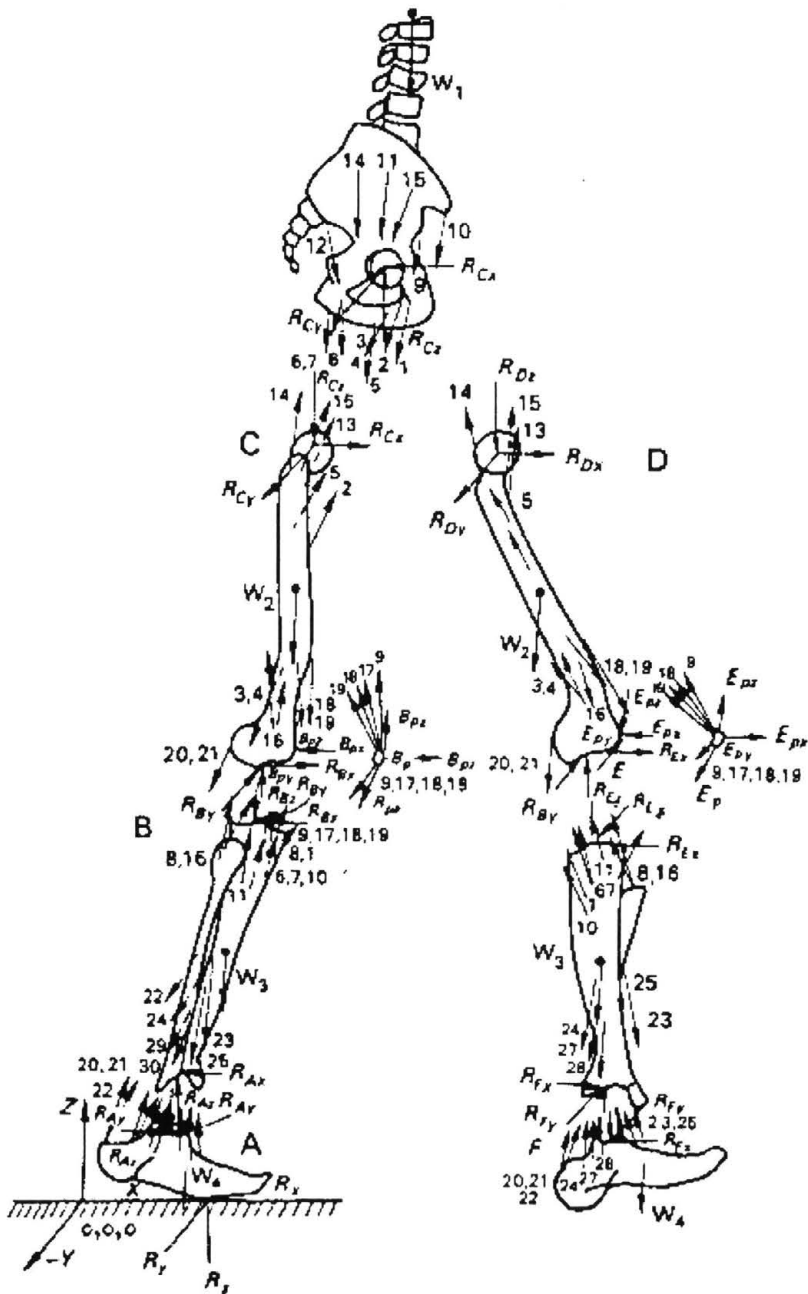
Figure 3.1. In normal locomotion, some 31 active muscle groups have been reported to actively take part in each of the lower limbs imposing the high indeterminacy of the biomechanical system [Seireg and Arvikar, 1975]

bine dynamic modeling of the muscle outputs and a closed loop setting, utilizing sensors for feedback. The dynamic system could thus be used to recalculate the best trajectory to complete the desired task, thus reducing feedback errors and increasing stability of the system [Tashman and Zajac, 1992; Dornay et al., 1994].

The musculoskeletal system of the human limbs of able-bodied subjects is usually treated as dynamically indeterminate if the forces in the individual muscles are to be determined, due to the larger number of unknowns than available dynamic equations [Seireg and Arvikar, 1975]. In normal locomotion, some 31 active muscle groups have been reported to actively take part in each of the lower limbs imposing the high indeterminacy of the biomechanical system (Fig. 3.1). The sequence of muscle activation in the lower limb to be controlled by the CNS during the gait cycle is demonstrated in Fig. 3.2a [Crowninshield and Brand, 1981; Patriarco et al., 1981; Vaughan et al., 1992].

(a)   (b)

FIGURE 3.2. Task complexity of the CNS in controlling the various muscle groups in locomotion: (a) sequence of muscle activation in the lower limb during the gait cycle [Crowninshield and Brand, 1981; Patriarco et al., 1981; Vaughan et al., 1992]; (b) a page from the first movement of Gustav Mahler's $6^t h$ symphony, demonstrating a somewhat close analogy.

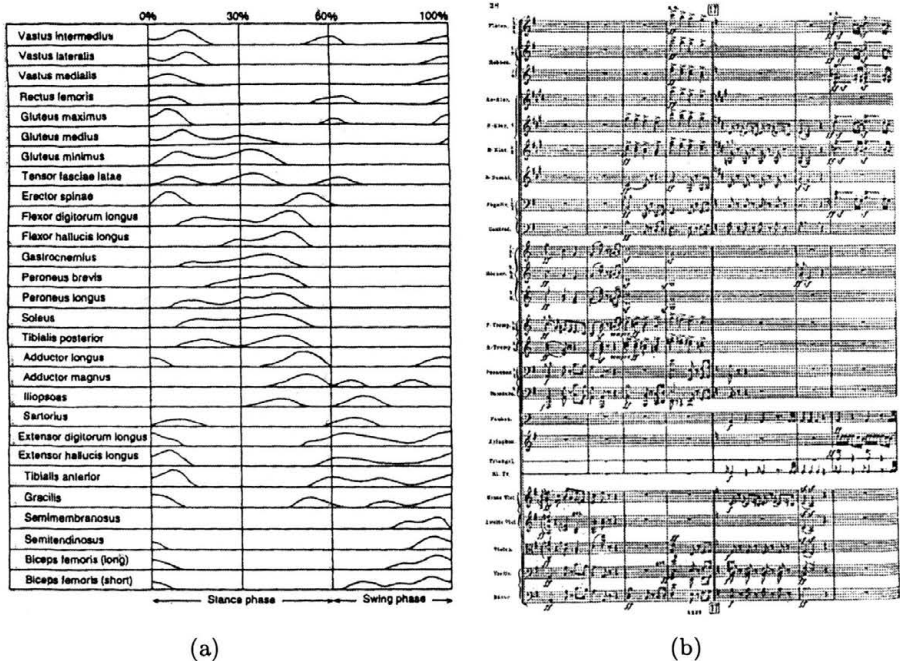A somewhat close analogy to that situation is a symphony orchestra, in which the conductor has to control the temporal roles of the different instruments, e.g., first violins, second violins, flutes, trumpets, percussions and the like. Figure 3.2b shows a page from the first movement of Gustav Mahler's 6th symphony, which is brought here as an example due to the particularly large orchestra required in this symphony and the many roles it presents for the different instruments. From the total of nearly 50 different roles (!), this page exhibits 25, which have to be led by the conductor. The task complexity of the CNS can thus be imagined, as it has to control $31 \times 2 = 62$ different muscle groups in ordinary gait activity.

3.1. Situation in Spinal Cord Injury (SCI)

In SCI the central control of the CNS is disrupted from the limbs, and the 'orchestra' remains with no 'conductor', despite the fact that each muscle can be excited and is capable of producing force. Thus, in the paralyzed limb (with low or no spasticity), all muscles are silent, except those activated by electrical stimulation, reducing the degree of indeterminacy. This is so because the muscles are isolated from voluntary control and the number of activated muscles as well as the level of excitation can be controlled [Giat et al., 1993; Mizrahi et al., 1992; Mizrahi, 1996]. This is a unique situation as it allows us to calculate the actual muscle forces from the externally measured torques and the correlation of this direct muscle output to quantities of another nature, such as metabolic or myoelectric.

Mechanical [Giat et al., 1993; Levy et al., 1990], myoelectric [Mizrahi et al., 1994] and metabolic [Levy et al., 1993] measurements (the latter using ^{31}P MRS) have been reported for the fatiguing quadriceps muscles of paraplegic subjects activated by FES. These formed the basis of a model of muscle fatigue and recovery by which the muscle force can be predicted.

The modeling process starts with the limb in which the muscle is being stimulated. The dynamic analysis allows us, by means of free-body diagram techniques, to connect together external loads and torques to the internal ones, including muscle and joint forces as well as inertial forces. Figure 3.3 presents a sketch of the lower extremity linkage and knee extensor of a paraplegic subject. Of special interest is the resolution of the force within the muscle, which can be analyzed by means of its structural components [Giat et al., 1993, 1996; Mizrahi et al., 1997]. The subject is at the sitting posi-
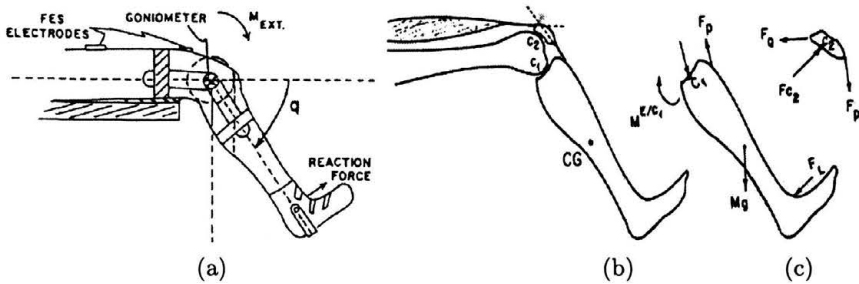
FIGURE 3.3. Lower extremity linkage and knee extensor. In case of a paraplegic subject in whom the quadriceps muscle is activated by FES, all non-activated muscles remain silent.

tion and his thigh is belted to the seat, ensuring that the hip angle remains constant during measurements. The lower leg is hinged at the level of the ankle to a pendulum, which is itself hinged at the level of the knee joint. The pendulum can be locked at any predetermined angle for isometric activation, and the knee torque corresponding to the external force at the ankle level can be measured via an instrumented horizontal cantilever at the lower part of the pendulum arm. Thus,

$$F_L = \frac{r_3}{r_5} F_P - \frac{M^{E/C_1} + r_4 gm \cos q}{r_5} \tag{3.1}$$

where F_L denotes the recorded force at ankle level and F_P is the patella tendon force, r_3, r_4, r_5, denote distances on the shank from the knee contact point to the patellar tendon, to the center of mass of the shank and to the ankle, respectively. The shank mass is denoted by m, q is the knee flexion angle, g is the gravitational acceleration and M^{E/C_1} is the passive torque in the joint due to the elastic tissues.

3.2. The Muscle Model

The most commonly used phenomenological musculo-tendon model consists of 5 elements, as shown in Fig. 3.4. It is assumed that all fibers of the quadriceps muscle are parallel to each other and are oriented at the same pennation angle α [He, 1988]. It should be noted that while pennation provides high force, it causes low displacement and velocity. Since the FES electrodes are positioned over the belly of the rectus femoris, the pennation angle of

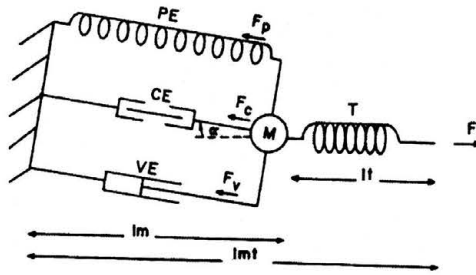FIGURE 3.4. Five-element musculo-tendon model (see text)

this muscle head is selected to represent the quadriceps. Muscle thickness is assumed to remain constant during contraction [Gans and Bock, 1965].

The contractile element (CE) represents the muscle's active element. The passive parallel-elastic element (PE) represents the passive elements in the muscle fiber [Huxley and Simmons, 1971]. The viscous element (VE) represents the viscosity due to presence of the fiber fluids. This element is included into the model for completeness, although previous research has shown that it has a negligible effect on muscle dynamics [Bahler, 1967; Woledge, 1961]. The variable l_m represents the average muscle fiber length.

The portion of the model that represents the tendon is a nonlinear spring for which the length-tension relationship is subdivided into two components: (a) an exponential relationship for shorter lengths, and (b) a linear relationship for longer lengths. Thus, we can write

$$F_t = f_t(l_t) = \begin{cases} A_t[\exp\left(k_{t_e}(l_t - l_{t_0})\right) - 1], & l_{t_0} \leqslant l_t \leqslant l_{t_c}, \\ k_t\left(l_t - l_{t_c} + \frac{F_c}{k_t}\right), & l_{t_c} < l_t, \end{cases} \tag{3.2}$$

where F_t is the tendon force, l_t is the tendon length, l_{t_0} is the tendon length at rest, l_{t_c} is the tendon length at which the tendon force shifts from a nonlinear to a linear curve and F_c is the force that corresponds to the tendon length l_{t_c}. A_t, k_{t_e}, and k_t are stiffness coefficients.

Within the muscle itself, the passive component is represented by a nonlinear spring for the following reasons. The passive stretch of the muscle without activation produces an increase of force with increasing length. It has been shown that the passive muscle fiber force increases exponentially with respect to fiber length (l_m). Thus,

$$F_p = f_p(l_m) = A_p[\exp\left(k_{p_e}(l_m - l_{m_0})\right) - 1], \tag{3.3}$$

where l_{m_0} is the length of the fiber at rest (i.e., $F_p(l_{m_0}) = 0$), and A_p and k_{p_e} are stiffness coefficients.

The damping force F_d due to the viscous muscle fluids has been found proportional to $\dot{l}_m$, the rate of change in the muscle's length [Alexander and Johnson, 1965; Buchtal and Kaiser, 1951; Fung, 1970; Walker, 1960] and is represented by

$$F_d = f_d\left(\dot{l}_m\right) = -k_d\dot{l}_m, \tag{3.4}$$

where k_d is the damping coefficient.

The active component (contractile element) of the muscle produces a force depending on three main factors: (a) fiber length, (b) fiber velocity and (c) timing and level of activation. The relation between muscle length and force is provided by the following nonlinear function

$$F_l = f_l(l_m) = F_z \sin\left(b_1\mathcal{L}_m^2 + b_2\mathcal{L}_m + b_3\right), \tag{3.5}$$

where $\mathcal{L}_m = l_m/l_z$; F_z is the maximum isometric force; l_z is the muscle length at which F_z is achieved; b_1, b_2 and b_3 are curve fitting constants; and F_l is the force level that corresponds to $\mathcal{L}_m$. The reason for the above relation is as follows: at very short lengths, actin filaments of the muscle sarcomere can overlap and interfere with one another, thereby reducing the amount of potential interaction between the myosin cross-bridges and the actin attachment sites. At intermediate lengths, interaction is maximal. It the reduces with increasing lengths until the force drops to zero when the two filaments no longer overlap.

The velocity-tension relationship in the contractile element describes the fiber tension as a function of the shortening or lengthening velocities. This relationship is given by the following equation:

$$F_v = f_v\left(\dot{l}_m\right) = 1 + \arctan\left(c_1\dot{\mathcal{L}}_m^3 + c_2\dot{\mathcal{L}}_m^2 + c_3\dot{\mathcal{L}}_m\right) \tag{3.6}$$

where $\dot{\mathcal{L}}_m = \dot{l}_m/V_{\max}$; $V_{\max}$ is the maximum shortening velocity; and c_1, c_2 and c_3 are curve fitting constants [Giat et al., 1993]. Note that the velocity-tension relationship of a muscle fiber is asymmetric about zero velocity.

3.3. Modeling of Muscle Fatigue under FES

As discussed in the previous chapter, the presence of fatigue during prolonged FES causes a substantial decrease in the quadriceps muscle force output [Levy et al., 1990]. It has been shown that extensive muscular activity

involves the depletion of energy supplying metabolites and the simultaneous accumulation of catabolites. Past ^{31}P measurements (see previous chapter) enabled us to study *in vivo* and non-invasively the variations in the metabolic parameters during stimulation and during recovery. The measured Pcr and Pi levels enabled us to calculate the temporal variations in the intracellular pH from the chemical shift between these levels. Variations of these metabolic parameters during fatigue were correlated with force decay. These metabolic parameters (Pcr, Pi, pH) were also shown to undergo a restoration process in the muscle recovery phase, which followed fatigue. It was assumed that the metabolic parameters reflect the force-producing capability of the FES activated muscle. Initially, the pH level was taken to express fatigue within the contractile element. Thus, to use intracellular pH(t) as a descriptor of fatigue, the curves describing the pH history, force history and pH versus force are necessary.

Decay of pH with time during fatigue is given by

$$pH(t) = d_1 \tanh\left[d_2\left(t - d_3\right)\right] + d_4 \tag{3.7}$$

with constant coefficients d_1, d_2, d_3 and d_4.

Force-pH(t) curve-fitting for prolonged electrical stimulation yields the following [Giat et al., 1993]

$$f_{pH}(pH) = d_5[1 - \exp\left(d_6\left(pH - d_7\right)\right)], \tag{3.8}$$

with constant coefficients d_5, d_6 and d_7.

The importance of incorporating a metabolic parameter, e.g., pH, as an intermediate determinant of force (or as a fatigue descriptor), lies in the possibility to noninvasively measure the metabolic profiles and the availability of these profiles in the fatigue as well as in the recovery processes. Thus, prediction of the FES activated muscle in intermittent stimulation, where fatigue and recovery processes, occur alternately, necessitates the existence of an intermediate determinant of force.

Equation (3.8) is then normalized with respect to the force obtained at t_0, the initial instant of muscular activity where the pH level is assumed to be maximal and where no fatigue has yet taken place. The normalization reveals the following relation:

$$\mathcal{F}_{pH}(pH(t)) = \frac{f_{pH}(pH(t))}{f_{pH}(pH(t_0))} = \frac{d_5[1 - \exp\left(d_6(pH(t) - d_7)\right)]}{d_5[1 - \exp\left(d_6(pH(t_0) - d_7)\right)]}. \tag{3.9}$$

Note that $0 < \mathcal{F}_{pH}(pH(t)) < 1$.

The force balance equation for the muscle mass M gives

$$M\ddot{l}_m \cos\alpha = F_t - F_m \cos\alpha, \tag{3.10}$$

where

$$F_m = F_p + F_d + F_a. \tag{3.11}$$

The force F_a produced by the contractile element is given as

$$F_a(t) = f_l(l_m(t))f_v(\dot{l}_m(t))\mathcal{F}_{\mathrm{pH}}(\mathrm{pH}(t))a(t), \tag{3.12}$$

where $a(t)$ denotes the activation time-trajectory. Upon substituting (3.2)–(3.9), (3.11) and (3.12) into (3.10), the following is obtained

$$\ddot{l}_m(t) = \frac{1}{M\cos\alpha}f_t(l_t(t)) - \frac{1}{M}[f_p(l_m(t)) + f_d(\dot{l}_m(t))$$
$$+ f_l(l_m(t))f_v(\dot{l}_m(t))\mathcal{F}_{\mathrm{pH}}(\mathrm{pH}(t))a(t)], \tag{3.13}$$

where $l_t(t) = l_{mt} - l_m(t)$. Note that the musculo-tendon length l_{mt} is treated here as a measurable constant in isometric experiments. The distinction between muscle length changes and tendon length changes is essential, however, for the more general case where the joint is allowed to rotate. For the particular case where the distance l_{mt} between origin and insertion locations remains constant, the tendon length change is identical but opposite to the muscle length change. Hence, $f_t(l_t(t))$ in (3.13) can be written as $f_t(l_m(t))$.

The activation function satisfies $0 < a(t) < 1$ and, as will be discussed later is responsible for predicting the rising phase of the force.

3.4. Summary of the Model Parameters

The model presented above includes three groups of parameters: (a) five specific parameters, i.e., (=5): l_{m_0}, l_{t_0}, A_m, A_t (muscle and tendon cross section area, respectively), M(muscle mass); (b) non-specific parameters, including: nominal stress-strain relations of tendons and fascia, such as k_{t_e}, k_t and k_{p_e} (c) curve-fitting constants, including: $d_1 \ldots d_7$, etc. A summary of the model parameters is presented in Table 3.1.

3.5. Model Solution

Numerical solution of the equation system presented above provides the force curves presented in Fig. 3.5. A similarity between the model and the experimentally measured curves is noted, especially in the initial and more

Table 3.1. Estimated Model Parameters

Function	Parameter	Knee Angle	Value
pH(t) eq. (3.7)	d_1	0°	−0.5021
	d_2	0°	0.0406
	d_3	0°	−30.0010
	d_4	0°	6.2500
f_{pH} (pH) [eq. (3.8)]	d_5	0°	1136.0000
	d_6	0°	−0.0097
	d_7	0°	6.0934
Muscle stress constant	C_{A_m}	30°	60–64 N/cm^2
Proportionality between muscle slack length and its length *in vivo*	C_{lmt}	0°	0.952
		30°	0.935
		60°	0.920
		90°	0.901
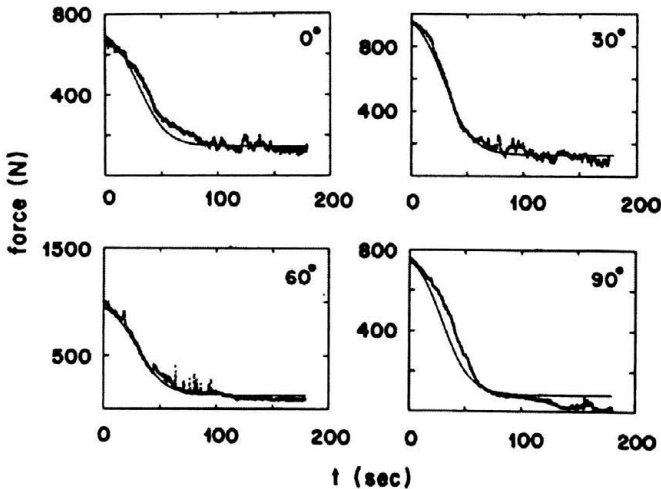
Figure 3.5. Numerical solution of the force curves of the musculo-tendon equation system

important phase, where the force values are still functional. The fatigue parameters, corresponding to the model and including the constants $d_1 \ldots d_7$ are listed in Table 3.1. The values of the estimated muscle stress parameter C_{A_m} (defined as the ratio between muscle strength and its cross-sectional area) and C_{lmt} (defined as the ration between the musculotendon slack length and its length *in vivo*) are also presented in Table 3.1. It is reminded that the product of this parameter and the muscle's cross sectional area reveals the muscle strength F_z.

3.6. Extension of the Musculo-tendon Model to Incorporate Recovery

In most cases FES is used in an intermittent mode, such as during ambulation where the channels are sequenced for the stepping motion (Fig. 2.6, previous chapter). During intermittent stimulation, i.e. when FES contractions are separated by rest periods, a fatigue-recovery algorithm can be constructed. Profile of the metabolites during fatigue and recovery was earlier discussed (Fig. 2.24, previous chapter).

The pH decay or recovery curves can be written as expressed in (3.8), with curve fitting constants for each of the two processes.

Concatenation of pH^F and pH^R to form $pH(a, t)$ (Fig. 3.6), yields the following

$$pH(a, t) = \begin{cases} pH^F(a, t + t_{n_0}^F - d_{n-1}), & d_{n-1} \leqslant t < d'_{n-1}, \\ pH^R(t + t_{n_0}^R - d'_{n-1}), & d'_{n-1} \leqslant t < d_n. \end{cases} \tag{3.14}$$
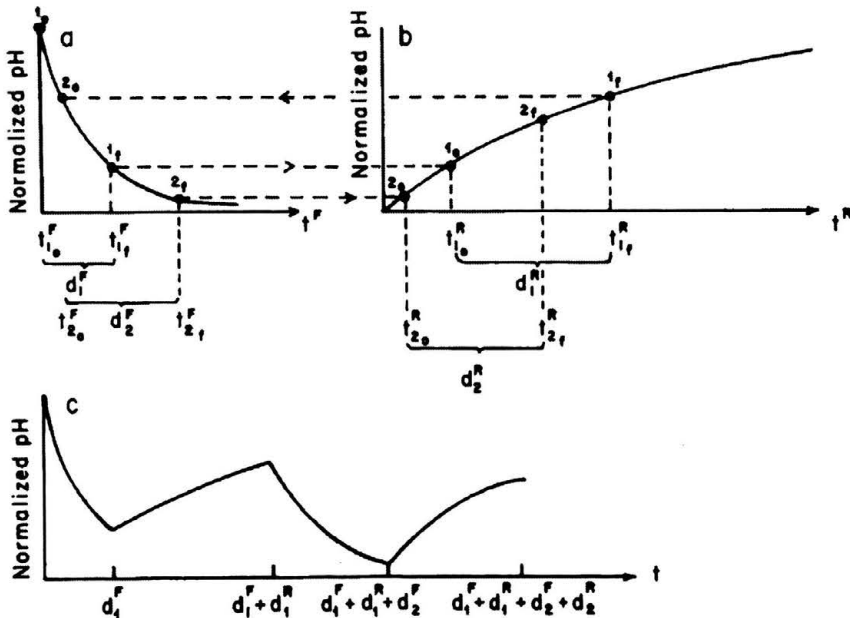
FIGURE 3.6. Concatenation of pH^F and pH^R to form $pH(a, t)$

For each fatigue and recovery cycle, n $(n = 1, \ldots, N)$, where

$$d_n^F = t - d_{n-1}, \quad t_n^F = t_{n_0}^F + d_n^F,$$

$$d_{n-1} = \sum_{i=0}^{n-1} (d_i^F + d_i^R), \quad d_{n-1}' = d_{n-1} + d_n^F,$$

$$t_{n_0}^R = \frac{1}{d_3} \operatorname{arctanh}\left[\frac{\mathrm{pH}^F t_n^F - d_1}{d_2} \right] + d_4,$$

$$d_n^R = t - d_{n-1}', \quad t_n^R = t_{n0}^R + d_n^R, \tag{3.15}$$

$$d_n = d_{n-1} + d_n^F + d_n^R,$$

$$t_{n+1_0}^F = \frac{1}{c_3} \operatorname{arctanh}\left[\frac{\mathrm{pH}^R t_n^R - C_1}{-c_2} \right] + C^4,$$

$$t_{0_f}^F \triangleq t_{0_0}^R \triangleq t_{0_f}^R \triangleq t_{1_0}^F \triangleq 0.$$

3.7. Generalization to Various Fatigue Descriptors

It should be noted that in the above analysis, although muscle intracellular pH was taken to be the fatigue descriptor, other metabolites should also

FIGURE 3.7. A general computation procedure, based on the metabolic histories of the three descriptors pH, Pi and $H_2PO_4^-$

be verified and scored with comparison to one another. Two other metabolites will be checked for the predictability of the force during FES re-activation after a rest period: Pi, $H_2PO_4^-$.
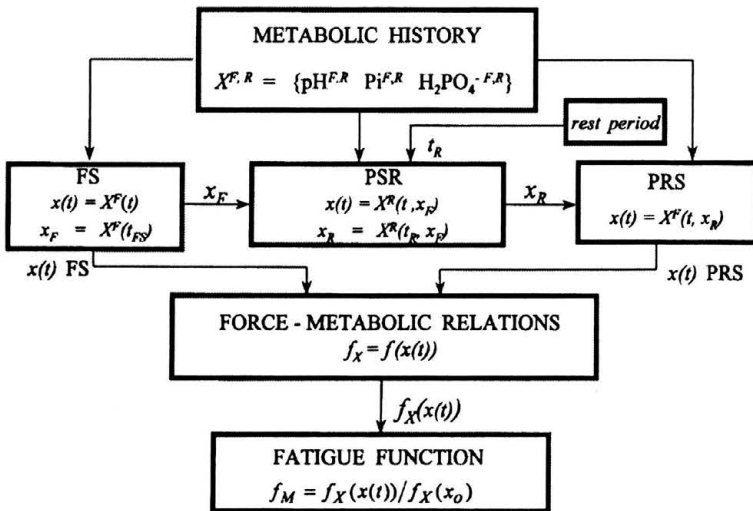
A general computation procedure, based on the metabolic histories of the three descriptors pH, Pi and $H_2PO_4^-$ is presented in Fig. 3.7. In this computation scheme three distinct situations are identified: First Stimulation (FS), where stimulation starts from an unfatigued muscle condition; Post Stimulation Rest (PSR), where recovery takes place after the FS; Post Recovery Stimulation, where FES is applied again, after a given recovery time. Fatigue and recovery metabolite-based functions are given as in (3.14) and (3.15), except that pH can be replaced by any other of the above predictors.

3.8. Inclusion of *Activation* via Measured EMG for the Improved Prediction of Force

It appears that electrolytic and metabolic factors are simultaneously involved in the processes of fatigue and recovery of the muscle during FES. It was therefore concluded that a modified model, based on the simultaneous measurements of force, phosphorus-based metabolites, extracellular K^+ and intracellular Na^+, should form the basis for predicting the expected force after partial recovery [Mizrahi, 1997; Mizrahi et al., 1997]. However, no practical noninvasive means for the *in vivo* monitoring of the electrolytic history is as yet available to provide the separation ability between intra and intercellular free ions. The histories of the above-mentioned electrolytes can, however, be correlated with fatigue and recovery via the M-wave peak-to-peak amplitude [Mizrahi et al., 1994, 1997]. Therefore, the cumulative effect of these electrolytes on the muscle force history may be incorporated into the model by means of the EMG signal.

The EMG M-wave signals are thus taken to indicate the level of neural excitation (neural input) of the muscle. The resultant muscle activation is then resolved through a first order dynamic equation of calcium extrusion and uptake from and into the sarcoplasmic reticulun (SR), and by first order reaction dynamics of calcium and troponin. As before, the predicted decaying phase of the force and the estimated recovery index of the muscle in post-rest stimulation are established by substituting the temporal changes in the levels of the muscle metabolites, including inorganic phosphorus (Pi or $H_2PO_4^-$), or intracellular pH, into a metabolic-based fatigue function. The improved
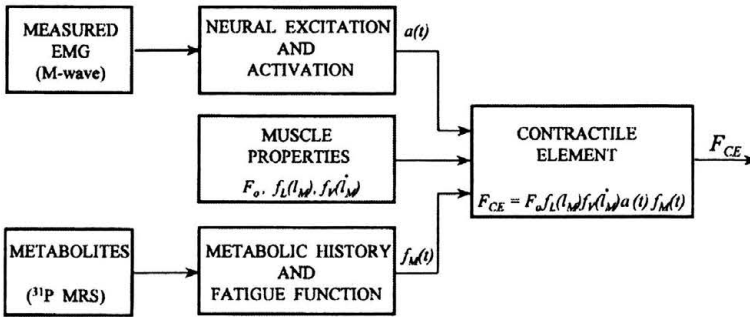
Figure 3.8. Metabolite and neural excitation based force prediction model

model enables us to predict the decaying force during continuous electrical stimulation as well as the recovery capacities of the muscle after different rest periods. A block diagram describing this model is presented in Fig. 3.8.

Excitation-Contraction Coupling and Muscle Activation:

The active state $a(t)$ of the muscle fibers defines the relative amount of calcium (Ca^{+2}) bound to troponin [Ebashi and Endo, 1968], and was evaluated by substituting the muscle neural input $u(t)$, into the activation dynamics model, presented in Fig. 3.9. The development of tension in skeletal muscle involves the release of stored calcium from the sarcoplasmic-reticulum (SR) and the diffusion of calcium across the sarcomere to troponin binding sites. To describe the neural input as a function of the measured EMG, we used a tri-exponential function that expresses the time course of the envelope of the M-wave peak-to-peak amplitude (EMGptp) [Mizrahi et al., 1997], follows:

$$EMG_{ptp}(t) = c_0[1 - c_1 \exp(-t/\tau_1) - c_2 \exp(-t/\tau_2)]$$
$$- c_3 \tanh[(t - t_3)/\tau_3]. \quad (3.16)$$

The first term (with τ_1) describes the rapid and tetanic response of the muscle to stimulation. The second term (with τ_2) describes the slower post-tetanic potentiation due to the enhanced release of presynaptic neuro-transmitter and increased sensitivity of post-synaptic receptors, and in parallel, Ca^{+2} accumulation outside of the sarcoplasmic-reticulum [Sinkjaer et al., 1992]. The latter affects the conductivity of the potassium channels [Sjogaard and McComas, 1995]. The third term (with) represents the decay phase of EMG peak-to-peak amplitude due to changes in the concentrations of the intracellular metabolites and sarcolemma electrolytes.
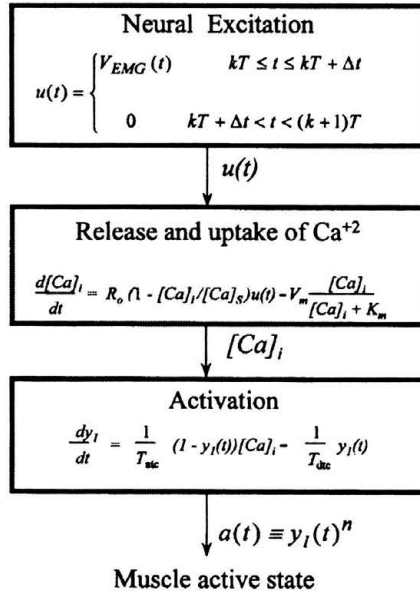
Figure 3.9. Excitation-contraction coupling and muscle activation

The shape and amplitude of the EMG M-wave are affected by the propagation velocity of the action potential across the sarcolemma, the number of active muscle fibers and the amplitude of a single fiber action potential. It has been demonstrated that in the case of low frequency stimulation, as is the case with FES, the time-dependent modifications in the M-wave result primarily from the slowing down of the conduction velocity of the muscle fibers [Sandercock et al., 1985; Juel 1988]. On the other hand, the amplitude of a single fiber action potential shows a small percentage of change during a low frequency stimulation of either: fast fatiguing (FF) or slow oxidative (SO) muscle units [Burke et al., 1973].

Two models of muscle activation were suggested (Fig. 3.10a,b):

A. Amplitude of the neural input function V_{EMG} of the muscle follows that of the actually measured M-wave peak-to-peak in the ascent phase of contraction, but remains unchanged afterwards

This model suggests that muscle recruitment is complete and remains so throughout stimulation. Thus,

$$V_{\text{EMG}}(t) = \begin{cases} \dfrac{\text{EMG}_{\text{ptp}}(t)}{\text{EMG}_{\text{ptp}}(t_{\max\{\text{EMG}\}})}, & 0 \leqslant t < t_{\max\{\text{EMG}\}}, \\ 1, & t_{\max\{\text{EMG}\}} \leqslant t < t_S. \end{cases} \tag{3.17}$$
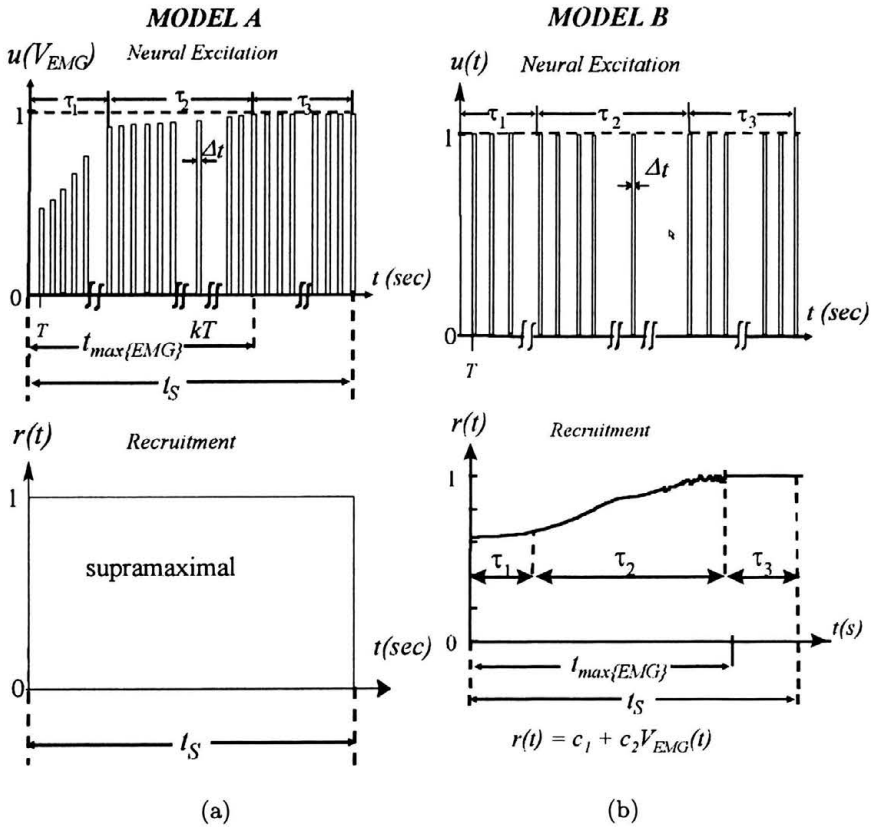
FIGURE 3.10. Models for muscle activation: (a) Amplitude of the neural input function (V_{EMG}) of the muscle follows that of the actually measured M-wave peak-to-peak in the ascent phase of contraction, but remains unchanged afterwards; (b) Action potential waveform $u(t)(=1)$ is taken to be constant, whereas the recruitment function $r(t)$ follows the EMG peak-to-peak amplitude

where $t_{max\{EMG\}}$ designates the time at which the amplitude of the actually measured M-wave peak-to-peak reaches its maximum and t_s expresses the total duration of stimulation. To describe the neural input function $u(t)$, as a product of the EMG envelope and the stimulation frequency f, we derived the following expression:

$$u(t) = \begin{cases} V_{EMG}(t), & kT \leqslant t \leqslant kt + \Delta t, \\ 0, & kT + \Delta t < t < (k+1)T. \end{cases} \qquad (3.18)$$

where $T(=f^{-1})$ is the time interval between two stimuli, k is the number of stimuli, and $t(=5\,ms)$ is the duration of the action-potential that is generated

by each stimulus. The neural input function of the model is depicted in Fig. 3.10a.

It was assumed, for simplicity, that the muscle contraction is limited by calcium kinetics, namely that Ca^{+2} diffusion in the cytoplasm and acto-myosin cross-bridge formations are rapid and not acting as rate limiting factors [Moiescu, 1976; Cannell and Allen, 1984; Stein et al., 1988]. The active state of the muscle was thus expressed by the following two dynamic variables:

1. **Ca^{+2} concentration:**

    The temporal intracellular (myoplasm) free concentration of Ca^{+2} ions, $[Ca]_i$, is governed by the release and uptake of calcium from and into the SR. The simplest assumption that one can make about calcium injection into cytoplasm is that each muscle action potential releases a fixed quantity of calcium during a certain time course [Zahalak and Ma, 1990]. Since the SR contains about five to ten times the calcium injected during the first action potential, and since experiments show a decrease in the free calcium concentration in the SR during repeated trains of electrical stimuli [Cannell and Allen, 1984; Blinks et al., 1977], we assume that the calcium injection from the SR decreases linearly with the free calcium concentration outside the SR [Zahalak and Ma, 1990]. We used a dimensionless first-order differential equation to express the calcium kinetics within the myoplasm, as presented by (3.19)

$$\frac{d[Ca]_i}{dt} = R_0 \left(1 - \frac{[Ca]_i}{[Ca]_s} \right) u(t) - V_m \frac{[Ca]_i}{[Ca]_i + K_m}, \qquad (3.19)$$

    where R_0 is the maximal rate of calcium efflux from the SR into the sarcoplasm; $[Ca]_s$ is the dimensionless peak of myoplasmic calcium concentration at which the gradient driving calcium injection from SR would disappear. Calcium injection from the SR in response to a single action potential is expressed by the first term in the right hand part of (3.19). The return of calcium from the cytoplasm to the SR was assumed, for simplicity, to result from a saturated first-order pump [Cannell and Allen, 1984]. The uptake of calcium into the SR as consequence of SR-Ca^{+2} ATPase pumping activity is given by the second term in the right hand part of (3.19). Note that $0 < [Ca]_i/[Ca]_s < 1$ at any given time. V_m and K_m express, respectively, the maximum rate of calcium uptake by the SR-Ca^{+2} ATPase pump and the dimensionless

intracellular calcium concentration in which half-maximal pump rate occurs.

2. **Active state of the muscle:**

The active state of the muscle, $a(t)$, is governed by $[Ca]_i$. Full activation (i.e., $a = 1$) will occur when the maximal number of cross-bridges results from the interaction between Ca^{+2} and troponin [Giat et al., 1993]. We assume: 1) that Ca^{+2} ions bind independently to troponin, 2) troponin releases its inhibition over the actin binding sites only after it has bound two calcium ions, and 3) when the troponin-mediated inhibition is removed, myosin is free to bind actin. Let $y_o(t)$ be the fraction of regulatory sites on troponin without a Ca^{+2} bound, and let $y_1(t)$ be the fraction of troponin sites with Ca^{+2} bound (note that $y_o(t) + y_1(t) = 1$). If there is no cooperativity between the sites, then the reaction between calcium and troponin is mode led by the following differential equation [Stein et al., 1988]:

$$\frac{dy_1}{dt} = \frac{1}{T_{atc}}(1 - y_1(t))[Ca]_i - \frac{1}{T_{dtc}}y_1(t). \tag{3.20}$$

The rate constants T_{atc} and T_{dtc} express respectively, the forward and backward Ca^{+2}-troponin kinetics [Cannell and Allen, 1984; Stein et al., 1988]. It was shown that force production is proportional to the number of Ca^{+2} ions (n) bound to each troponin molecule [Stein et al., 1988], hence, FCE is proportional to y_1^n, and $a(t) \equiv y_1(u(t))^n$ with $n = 2$.

Numerical values of the coefficients in (3.19) and (3.20) are given in Stephenson and Williams, [1981]; Ma and Zahalak, [1991], and Levin and Mizrahi, [1999].

B. Action potential waveform $\mathbf{u(t)}(= 1)$ is taken to be constant, whereas the recruitment function $\mathbf{r(t)}$ follows the EMG peak-to-peak amplitude (Fig. 3.10b)

Thus,

$$r(t) = c_1 + c_2 V_{EMG}(t). \tag{3.21}$$

Solution of the predicted force in the ascent phase of contraction by using each of the two activation algorithms gives the profiles presented in Fig. 3.11. It is noted that using model A, the post-tetanic potentiation phase is better predicted that the tetanic phase. Model B, however, gave good prediction of both the tetanic and the post-tetanic phases and this model is thus indicated for the ascent phase of muscle contraction.
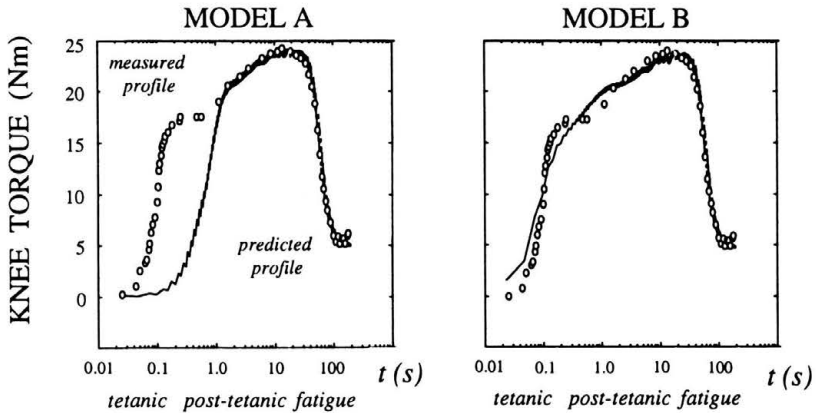
FIGURE 3.11. Prediction of the knee torque for each of the two muscle activation models

3.9. Comparison of Prediction of the Fatigue Phase Using Different Metabolic Predictors

Figure 3.12 presents the comparative results obtained for the first stimulation, i.e., activation from the initially unfatigued condition. The predicted force is depicted by the bolded curve and the measured one by the solid one. It is noted that better agreement (as expressed by the sum of the square of the errors, SSE) between model and experimental forces is obtained with Pi and $H_2PO_4^-$ rather than with pH.
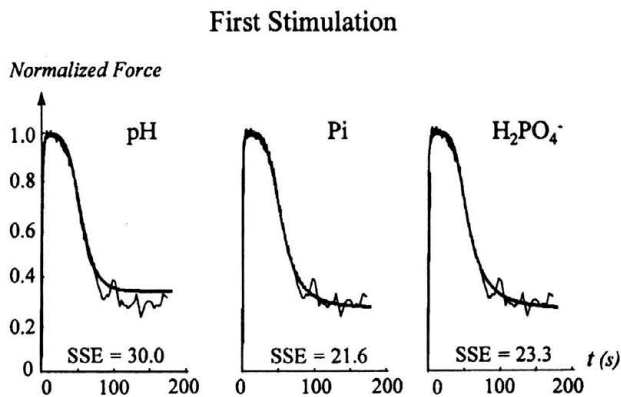
FIGURE 3.12. Prediction of the quadriceps force at first stimulation for each of the metabolic predictors
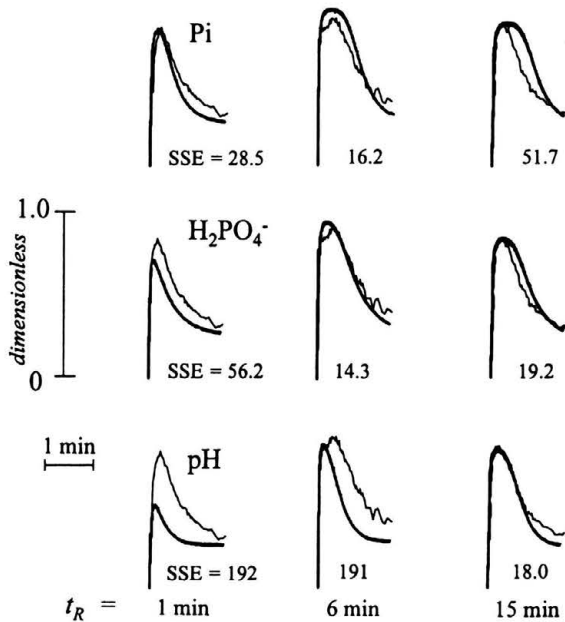
FIGURE 3.13. Post-rest stimulation fatigue: prediction of the quadriceps force for each of the metabolic predictors and for different resting durations

In post-rest stimulation fatigue, shown in Fig. 3.13, it is noted that for short rest periods (~ 1 min.), Pi is superior for predicting the decay due to fatigue. For intermediate rest time periods (~ 6 min.), $H_2PO_4^-$ is preferable among the metabolites. For long periods of recovery (~ 15 min.), pH provides the best predictability of the fatigue phase of the muscle force.

3.10. Conclusions

Learning the dynamics of muscle contraction should help us in designing strategies for reducing fatigue. Furthermore, by modeling muscle dynamics, prediction of the muscle forces can help us in reducing the errors in a feedback controller task. Thus, a reference-based open loop (pre-computed stimulation) can be more easily designed, or alternatively the model can provide the basis for closed loop computed-torque controller.

The results of the presented model demonstrated that EMG can be used to predict muscle activation (or recruitment level) in the ascending phase of force.

For the decaying (fatiguing/recovering) phase of force, metabolite-based prediction was indicated in intermittent stimulation, with different prediction capacities of the various metabolites, depending on the resting period between the stimulations.

References for Chapter 3

1. R.S. ALEXANDER and P.D. JOHNSON, *Muscle stretch and theories of contraction*, Amer. J. Physiol., **204**:412–416, 1965.

2. B.J. ANDREWS, R.H. BAXENDALE, R. BARNETT, G.F. PHILLIPS, T. YAMAZAKI, J.P. PAUL, and P. FREEMAN, *Hybrid FES orthosis incorporating closed loop control and sensory feedback*, J. Biomed. Eng., **10**:189–195, 1988.

3. A.S. BAHLER, *Series elastic component of mammalian skeletal muscle*, Amer. J. Physiol., **213**:1560–1564, 1967.

4. J.R. BLINKS, R. RUDEL, and S.R. TAYLOR, *Calcium transients in isolated amphibian skeletal muscle fibers: Detection with aeqorin*, J. Physiol. (London), **277**:291–323, 1977.

5. G.L. BROWN and B.D. BURNS, *Fatigue and neuro-muscular block in mammalian skeletal muscle*, Proc. R. Soc. London Ser. B, **136**:182–195, 1949.

6. F. BUCHTHAL and E. KAISER, *The rheology of the cross striated muscle fiber with particular reference to isotonic conditions*, Dan. Bio. Med., **21**:318, 1951.

7. R.E. BURKE, D.N. LEVINE, P. TSAIRIS, and F.E. ZAJAC, *Physiological types and histochemical profiles in motor units of the cat gastrocnemius*, J. Physiol. (London), **234**:723–748, 1973.

8. M.B. CANNELL and D. ALLEN, *Model of calcium movements during activation in the sarcomer of frog skeletal muscle*, Biophys. J., **45**:913–925, 1984.

9. H.J. CHIZECK, R. KOBETIC, E.B. MARSOLAIS, J.J. ABBAS, I.H. DONNER, and E. SIMON, *Control of functional neuromuscular stimulation systems for standing and locomotion in paraplegics*, IEEE Proc., **76**(9):1155–1165, 1988.

10. P. CRAGO, J.T. MORTIMER, and P.H. PECKHAM, *Closed-loop control of force during electrical stimulation of muscle*, IEEE Trans. Biomed. Eng., **27**:306–312, 1980.

11. R.D. CROWNINSHIELD and A. BRAND, *A physiologically based criterion of muscle force prediction in locomotion*, J. Biomech., **14**:793–801, 1981.

12. G.R. CYBULSKI, R.D. PENN, and T.J. JAEGER, *Lower extremity functional neuromuscular stimulation in cases of spinal cord injury*, Neurosurgery, **15**:132–146, 1984.

13. M. DORNAY, O. YADID-PECHT, J. MIZRAHI, E. ISAKOV, and Z. SUSAK, *Learning by artificial neural networks the development of fatigue in paralyzed human muscle during isometric functional electrical stimulation*, in: Proc. of The 25th Israel Conference on Mechanical Engineering, Technion City, Haifa, Israel, May 25–26, pp.82–84, 1994.

14. S. EBASHI and M. ENDO, *Calcium ion and muscle contraction*, Progr. Biophys. Molec. Biol., **18**:123–183, 1968.

15. R.H.T. EDWARDS, R.C. HARRIS, E. HULTMAN, and L.O. NORDESJO, *Phosphagen utilization and resynthesis in successive isometric contractions, sustained to fatigue of the quadriceps muscle in man*, J. Physiol., **224**:40P–41P, 1972.

16. Y.C.B. FUNG, *Mathematical representation of the mechanical properties of heart muscle*, J. Biomech., **3**:381–404, 1970.

17. C. GANS and W.J. BOCK, *The functional significance of muscle architecture: A theoretical analysis*, Ergebnisse der Anatomie und Entwicklungsgeschintle, **38**:H5–142, 1965.

18. Y. GIAT, J. MIZRAHI, and M. LEVY, *A musculotendon model of the fatigue profiles of paralyzed quadriceps muscle under PES*, IEEE Trans. Biomed. Eng., **40**:664–674, 1993.

19. Y. GIAT, J. MIZRAHI, and M. LEVY, *Fatigue and recovery in paraplegic's quadriceps muscle when subjected to intermittent stimulation*, ASME J. Biomech. Eng., **118**:357–366, 1996.

20. J. HE, *A feedback control analysis of the neuro-musculo-skeletal system of a cat hindlimb*, Ph.D. dissertation, Univ. Maryland, 1988.

21. J.A. HOFFER and M.K. HAUGLAND, *Signals from tactile sensors in glabrous skin suitable for restoring motor function in paralyzed humans*, in: Neural Prostheses, Replacing Motor Function After Disease or Disability, R.B. Stein, P.H. Peckhman, and D.P. Popovic (Eds.), Oxford University Press, New York, pp.99–125, 1992.

22. A.F. HUXLEY and R.M. SIMMONS, *Proposed mechanism of force generation in striated muscle*, Nature, **233**:533–538, 1971.

23. C. JUEL, *Muscle action potential propagation velocity changes during activity*, Muscle Nerve, **11**:714–719, 1988.

24. O. LEVIN and J. MIZRAHI, *EMG and metabolic-based prediction of force in paralyzed quadriceps muscle under interrupted simulation*, IEEE Trans. Rehab. Eng., **7**:301–314, 1999.

25. M. LEVY, J. MIZRAHI, and Z. SUSAK, *Recruitment, force and fatigue charac-
    teristics of quadriceps muscle of paraplegics isometrically activated by surface
    functional electrical stimulation*, J. Biomed. Eng., **12**:150–156, 1990.

26. M. LEVY, T. KUSHNIR, J. MIZRAHI, and Y. ITZCHAK, *In vivo 31P NMR stu-
    dies of paraplegic's muscles activated by functional electrical stimulation*, Magn.
    Res. Med., **29**:53–58, 1993.

27. A.R. LIND and J.S. PETROFSKY, *Amplitude of the surface electromyograms
    during fatiguing isometric contractions*, Muscle Nerve, **2**:257–264, 1979.

28. S.-P. MA and G.I. ZAHALAK, *A distribution-moment model of energetics in
    skeletal muscle*, J. Biomech., **24**:21–35, 1991.

29. J. MIZRAHI, Y. GIAT, and M. LEVY, *A dynamically determinate model of
    fatigue and recovery of electrically stimulated paralysed muscles*, XVIIIth Inter-
    national Congress of Theoretical and Applied Mechanics, Haifa, Israel, August
    22 to 28, p.106, 1992.

30. J. MIZRAHI, M. LEVY, H. RING, K. ISAKOV, and A. LIBERSON, *EMG as
    an indicator of fatigue in isometrically FES-activated paralyzed muscles*, IEEE
    Trans. Rehab. Eng., **2**:57–65, 1994.

31. J. MIZRAHI, *FES-activated paralyzed muscles: a model of peripheral fatigue*, in:
    Proc. Symposium on Neural and Neuromuscular Aspects of Muscle Fatigue,
    Miami, Florida, November 1994, published in Muscle and Nerve, Suppl. 4:530,
    1996.

32. J. MIZRAHI, *Fatigue in muscles activity by functional electrical stimulation*,
    Crit. Rev. Phys. Rehab. Med., **9**:93–129, 1997.

33. J. MIZRAHI, O. LEVIN, A. AVIRAM, E. ISAKOV, and Z. SUSAK, *Muscle fa-
    tigue in interrupted stimulation: Effect of partial recovery on force and EMG
    dynamics*, J. Electromyogr. Kinesiol., **7**:51–65, 1997.

34. D.G. MOIESCU, *Kinetics of reaction in calcium-activated skinned muscle fibers*,
    Nature, **262**:610–613, 1976.

35. A.G. PATRIARCO, R.W. MANN, S.R. SIMON and J.M. MANSOUR, *An evalua-
    tion of the approaches of optimization models in the prediction of muscle forces
    during human gait*, J. Biomech., **14**:513–525, 1981.

36. J.S. PETROFSKY, *Sequential motor unit stimulation through peripheral motor
    nerves in the cat*, Med. Biol. Eng. Comp., **17**:87–93, 1979.

37. B.D. POPOVIC, *Functional electrical stimulation for lower extremities*, (in:)
    Neural Prostheses: Replacing Motor Function After Disease or Disability, R.B.
    Stein, P.H. Peckham, and D.B. Popovic (Eds.), Oxford University Press, New
    York, pp.233–251, 1992.

38. T.G. SANDERCOCK, J.A. FAULKNER, J.W. ALBERS, and P.H. ALBRECHT, *Single motor unit and fiber action potential during fatigue*, J. Appl. Physiol., **58**:1073–1079, 1985.

39. A. SEIREG and R.J. ARVIKAR, *The prediction of muscular load sharing and joint forces in the lower extremities during walking*, J. Biomech., **8**:89–102, 1975.

40. T. SINKJAER, N. GANTCHEV, and L. ARENDT-NIELSEN, *Mechanical properties of human ankle extensors after muscle potentiation*, Electroenceph. Clin. Neurophysiol., **85**:412–418, 1992.

41. G. SJOGAARD and A.J. MCCOMAS, *Role of interstitial potassium*, in: Fatigue: Neural and Muscular Mechanisms, Advanc., S.C. Gandevia, R.M. Enoka, A.J. McComas, D.G. Stuart, and C.K. Thomas (Eds.), Experi. Med. Biol. **384**:69–80, 1995.

42. R.B. STEIN, J.M. BOBET, N. OGUZTORELI, and M. FRYER, *The kinetics relating calcium and force in skeletal muscle*, Biophys. J., **54**:705–717, 1988.

43. D.G. STEPHENSON and D.A. WILLIAMS, *Calcium-activated force responses in fast-and slow-twitch skinned muscle of the rat at different temperatures*, J. Physiol. (Lond.), **317**:284–302, 1981.

44. S. TASHMAN and F.K. ZAJAC, *Control of multijoint lower limb motor tasks with functional neuromuscular stimulation*, in: Neural Prostheses, Replacing Motor Function After Disease or Disability, R.B. Stein, P.H. Peckham, and D.P. Popovic (Eds.), Oxford University Press, New York, pp.252–278, 1992.

45. C.L. VAUGHAN, B.L. DAVIS and J.C. O'CONNOR, *Dynamics of Human Gait*, Human Kinetic Publishers, Champaign, 1992.

46. S.M. WALKER, *Potentiation and hysteresis induced by stretch and subsequent release of papillary muscle of the dog*, Amer. J. Physiol., **198**:519–522, 1960.

47. J.G. WEBSTER, *Artificial sensors suitable for closed–loop control of FNS*, (in:) Neural Prostheses: Replacing Motor Function After Disease or Disability, R.B. Stein, P.H. Peckham, and D.B. Popovic, Oxford University Press, New York, pp.88–98, 1992.

48. R.C. WOLEDGE, *The thermoelastic effect of change of tension in active muscle*, J. Physiol., **155**:187–208, 1961.

49. G.I. ZAHALAK and S.-P. MA, *Muscle activation and contraction: Constitutive regulation based directly on cross-bridge kinetics*, ASME J. Biomed. Eng., **112**:52–62, 1990.

Chapter 4

Biomechanical Interactions
between Muscle and Bone

4.1. Muscle and Bone Loading

The mechanical activity of contracting muscles is greatly responsible for the loading of the bones and joints. With the exception of trauma and jumping from heights, *muscles*, not body weight, put the largest loads on bone [Currey, 1984; Martin and Burr, 1989; Nordin and Frankel, 1989]. The significance of impact loading has been discussed in Chapter 1. Impact loading in the human body occurs at heel-strike during walking or running. More severely, it is found in fast or impulsive walking, stair climbing, jumping, falling or in collision. The shock impacts from each walking or running cycle are transmitted from the feet vertically upwards the skeleton to the different parts of the body and are often associated with damage. The *short-term damage* is associated with stress fractures of the bones. Fatigue, or stress fractures occur in bones in response to repetitive stresses over multiple cycles, when the body's ability to adapt is exceeded [Beck 1998]. In athletes 72% of the stress fractures were reported in running, 60% of which in long and middle distance running [Hulkko and Orava, 1987]. An important factor affecting the incidence of bone stress injury, is exposure to abrupt changes in the bone loading [Andersen et al., 1999].

The *long-term damage* is associated with accumulative damage to articular cartilage and intervertebral disc and the resulting degeneration of the joints [Radin, 1975] and spine [Wosk and Voloshin, 1981].

4.2. Muscle, Bone and Aging

Both muscle and bone have been reported to deteriorate with aging. By 80 years of age muscle strength can reduce to about 40% of its young-adult value [Buckwalter et al., 1993]. Bone strength and "mass" show long-known corresponding age-related changes [Riggs and Melton, 1995; Smith et al., 1989].

4.3. Bone Fractures

Clinical and experimental evidence suggests that stress injuries take place at the site in which the maximum tensile stress due to bending is present [Daffner, 1984; Milgrom, 1989].

4.4. Muscle and Shock Absorption

Apart from its function as a joint actuator, muscle acts also as an active shock absorber. It has been hypothesized that muscle fatigue can reduce the dampening effect and accelerate the initiation of stress fractures [Beck, 1998; Burr et al., 1985; Milgrom, 1989; Schaffler et al., 1990]. Recent studies have shown that, as a result of muscle fatigue, there is an increase in the strain rate (i.e., rate of strain development) in the tibia, rather than in the maximal strain [Fyhrie et al., 1998] suggesting that loading of the tibia during running becomes more impulsive as fatigue progresses.

Thus, in situations of fatigue or, more severely, muscle impairment, both functions of the muscle, i.e. actuator and shock absorber, are hampered and the following may take place: (a) increased transmission of shock loads along the skeleton; (b) loading imbalance on the bones, resulting of increased stresses there; (c) altered kinematics; and (d) increased risk of overload injuries and of joint degeneration. Information of the impulsive loading on the bone in long-distance running can be obtained non-invasively either by means of the foot-ground reactive forces [Dickinson et al., 1985] or, directly, by measuring the transient accelerations on the shank caused by impact.

By attaching an accelerometer externally on the tibial tuberosity, it has been shown that the impact acceleration increases with developing of muscle fatigue [Mizrahi et al., 1997, 2000a,b,c; Verbitsky et al., 1998; Voloshin et al., 1998]. Accelerometer measurement of the shock wave (or impulse load)

[Mizrahi and Susak, 1982] provides a dynamic quantity closer to *strain rate* than to strain (Implicated in the etiology of stress fractures, Fyhrie et al., [1998]). A light-weight (4.2 grams) accelerometer (Kistler PiezoBeam, type 8634B50, Kistler, Winterthur, Switzerland), connected to a coupler (Kistler Piezotron, type 5122) is used [Mizrahi and Susak, 1982; Mizrahi et al., 1997, 2000a,b,c, 2001; Verbitsky et al., 1998; Voloshin et al., 1998]. It is externally attached by a metal holder (1.4 grams) above the tibial tuberosity of the right leg of each subject and aligned with the longitudinal axis of the tibia to provide the axial component of the shank acceleration. The accelerometer is pressed onto the skin in closest position to the bony prominence of the tibial tuberosity by means of an elastic belt around the shank (Fig. 4.1). The tension of the belt as measured by a spring dynamometer is approximately 50 N, which corresponds to an accelerometer preload of about 25 N. This is well above the 14 N level we found in which the acceleration trace for a given impact force became insensitive to the accelerometer attachment force, thus ensuring reproducibility of the measurements [Mizrahi and Susak, 1982].

Dual attachment on the tibial tuberosity and the sacrum area (Fig. 4.1 a and b) enables to calculate the transmission ratio between these two levels.
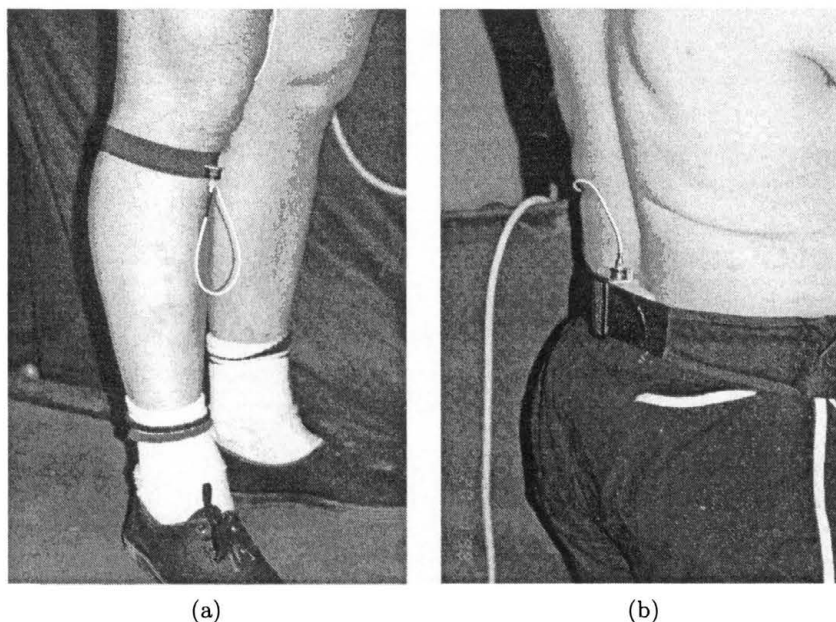

(a)   (b)

FIGURE 4.1. Attachment of accelerometer: (a) the accelerometer is pressed onto the skin in closest position to the bony prominence of the tibial tuberosity by means of an elastic belt around the shank; (b) attachment on sacrum

Fatigue can be either global or local in nature. Global, or metabolic fatigue is associated with the development of metabolic acidosis following an endurance exercise and is accompanied by a decrease in the end tidal carbon dioxide pressure (PETCO$_2$) [Wasserman, 1987]. In long distance running, for instance, metabolic fatigue is reached when the running speed exceeds the anaerobic threshold. Local fatigue in a muscle takes place as a result of an intensive activity of this muscle and is reflected by certain changes in its electromyogram (EMG) signal in either the time or frequency domains [Edwards, 1981]. A possible model for studying the effects of fatigue, metabolic or local, on bone loading is continuous running for long distances

Figure 4.2 shows the simultaneous recording of the tibial and sacrum accelerations during three running cycles, along with the raw electromyograms of three muscles of the leg: quadriceps, gastrocnemius and tibialis anterior.
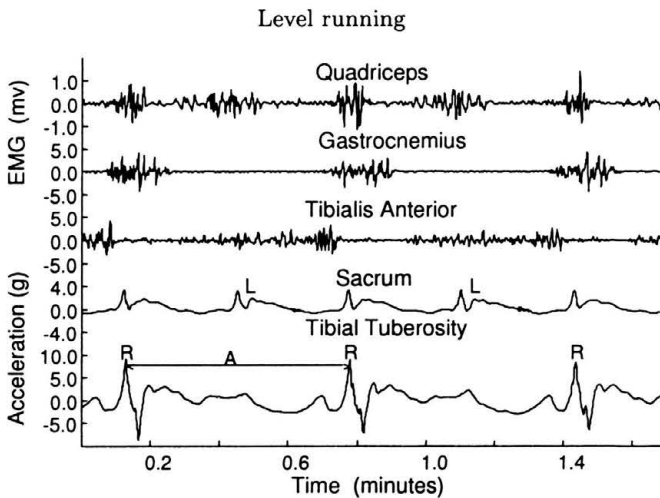
FIGURE 4.2. Simultaneous recording of the tibial and sacrum accelerations during three running cycles, along with the raw electromyograms of three muscles of the leg: quadriceps, gastrocnemius and tibialis anterior

4.5. Metabolic Fatigue and Impact Loading

To monitor metabolic fatigue during running, the tested subject is asked to breath through a mouthpiece attached to a turbine device [Verbitsky et al., 1998]. The respired gas is continuously sampled by a Sensor-Medics 4400 metabolic cart (Alpha Technologies, Inc., Laguna Hills, CA, USA) for breath-by-breath determination of the gas exchange and ventilatory variables. The

instrument is calibrated before every test using a standard 3 liters syringe and precision reference gases.

Exercise values for oxygen consumption ($\dot{V}O_2$), minute ventilation ($\dot{V}E$), carbon dioxide production ($\dot{V}CO_2$), end-tidal carbon dioxide pressure (PETCO$_2$), ventilatory equivalent for oxygen ($\dot{V}E/\dot{V}O_2$), and ventilatory equivalent for carbon dioxide ($\dot{V}E/\dot{V}CO_2$) are calculated as an average of the breath-by-breath data during a time span of 30 s. PETCO$_2$ is used as a measure for the assessment of global fatigue due to the development of metabolic acidosis as it is considered an established and reliable measure for indicating both the anaerobic threshold (AT) and global fatigue [Wasserman, 1987]. It is also more sensitive than the changes in lactic acid during 30 min. running [McEllan and Cheung, 1992].

The running tests are performed on a treadmill (Quinton Q55, Seattle, Washington, USA) to allow repetitive monitoring of the data. Prior to each running test, the subjects undergoes a 15-minute warming-up running at an individually selected and comfortable speed to get used to the treadmill and the measuring equipment. One week prior to the experiment, a pre-test is conducted for each subject to determine the AT using the following procedure. The subject is exposed to an incremental load by increasing the running speed on the treadmill from an initial 8 km/h to a maximum of 15 km/h. The speed increments were of 1 km/h every 2 minutes and were given until PETCO$_2$ reached the decline phase. The decline phase was confirmed if it persisted for at least one minute. AT is then determined as the point of initial increase of $\dot{V}E/\dot{V}O_2$ and $\dot{V}E/\dot{V}CO_2$, which just precedes the initial decline of PETCO$_2$ [Wasserman, 1987]. The running test is performed for a duration of 30 min. at a steady speed exceeding the AT level of each subject by 5%.

Figure 4.3 shows two groups of subjects as follows. Ten subjects whose PETCO$_2$ significantly decreased ($p < 0.05$) at the end of the 30-min. run ran above the AT speed and were defined as the fatigue group. Twelve subjects who did not show a significant change in the amount of PETCO$_2$ at the end of the test ran below the AT speed and were defined as the nonfatigue group. It is obvious that 30 min. running at a speed exceeding the AT is a sufficient time to induce general fatigue.

Averages for all subjects of $\dot{V}E$, PETCO$_2$, and $\dot{V}O_2$ at selected time points in the course of running are presented graphically in Fig. 4.4. A steady rate of O$_2$ uptake was achieved after 10 min. of running. Thus, the values obtained on the 15th, 20th, 25th, and 30th min. were compared to those of

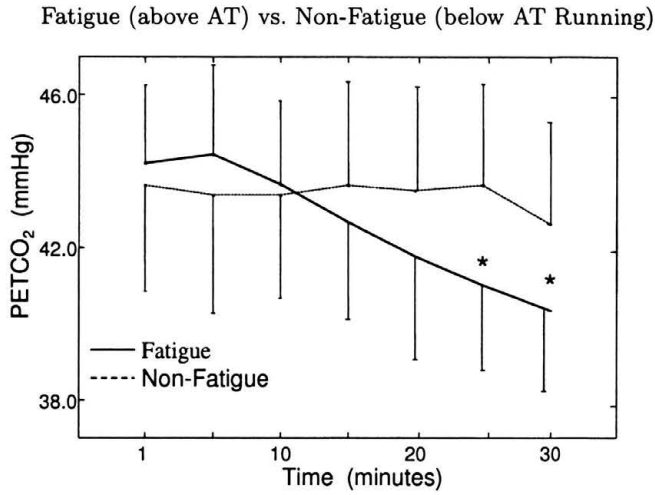Fatigue (above AT) vs. Non-Fatigue (below AT Running)

FIGURE 4.3. The effect of fatigue on end-tidal carbon dioxide pressure ($PETCO_2$) in fatigue (above anaerobic threshold running speed, AT) and non-fatigue (below AT)
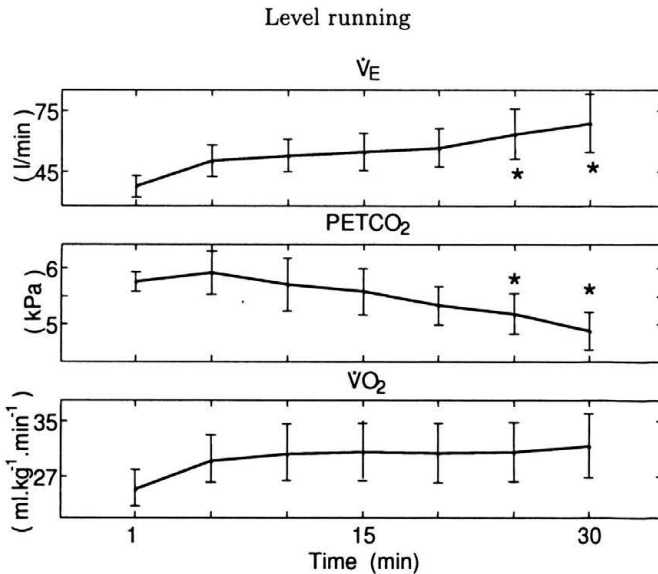
Level running

FIGURE 4.4. Averages for all subjects of $\dot{V}E$, $PETCO_2$, and $\dot{V}O_2$ at selected time points in the course of running above the anaerobic threshold
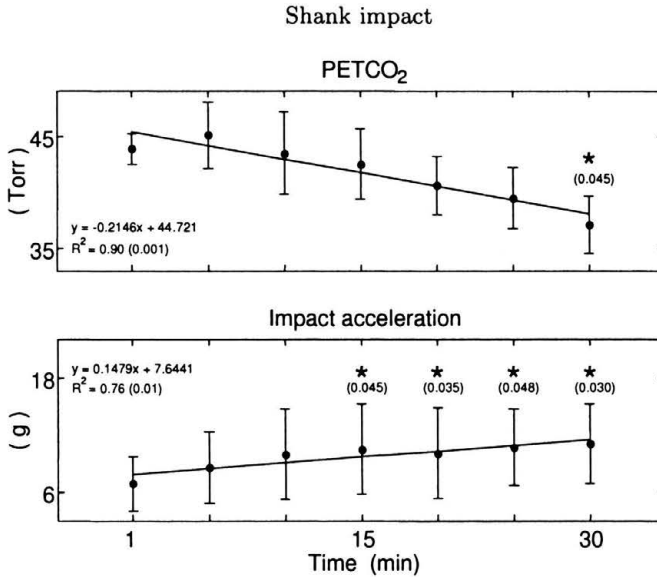
Shank impact

FIGURE 4.5. Average $PETCO_2$ and impact acceleration on the shank during the course of running above the anaerobic threshold

the 10th min. While the values of $\dot{V}E$ increased and $PETCO_2$ decreased significantly from the 25th min. onwards, those of $\dot{V}O_2$ remained unchanged during the running test.

Summarized values of the average $PETCO_2$, and impact acceleration on the shank are presented in Fig. 4.5. $PETCO_2$ decreased significantly from the 30th min. compared to the 1st min. ($P = 0.045$), indicating that global fatigue developed. The impact acceleration at heel strike increased significantly from the 15th min, compared to the 1st min. ($P \leqslant 0.048$).

Figure 4.6 presents the results of the spectral analysis of the accelerometer signal at shank level. The top part of the figure shows the average of the PSD of the accelerometer traces during the contact phase of running at four time stages. In the first minute of running, the PSD demonstrates a two-peak pattern, in accordance with previous reports [Mizrahi et al. 2000a; Shorten and Winslow, 1992). The impact peak (12–20 Hz zone), higher than the active peak (4–9 Hz zone), is associated with the high-frequency content of the foot-ground impact and corresponds to the initial 15% of the stance phase. As fatigue develops, in the later stages of running, an additional peak within the 25–35 Hz range level becomes noticeable, in parallel to the increase in the peak of the impact region. The possibility that this increase was an artifact is
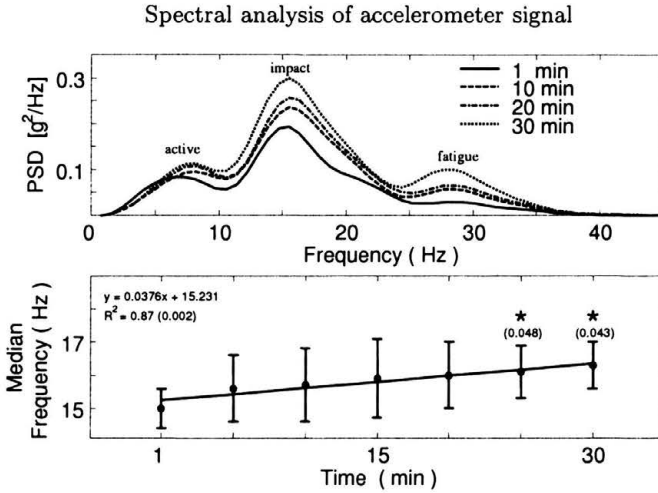
FIGURE 4.6. Spectral analysis of the accelerometer signal at shank level; top: average of the PSD of the accelerometer traces during the contact phase of running at four time stages of the running time; bottom: MDF of the PSD

ruled out since the resonance frequency of a 4 gr. skin-mounted accelerometer is well above 35 Hz [Smeathers, 1989]. Changes in the average peak frequencies from the first to the 30th min. of running for both the active and the impact frequency regions were not significant. Nevertheless, the average MDF of the PSD acceleration signal in the shank significantly increased from the 25th min. of running and onwards ($P \leqslant 0.048$) as compared to the beginning of running (bottom part of Fig. 4.6).

4.6. Metabolic Fatigue and Shock Attenuation along the Skeleton

Previous studies have demonstrated that in increased eccentric activity, e.g. in downhill running or walking or on a bicycle ergometer modified for use in eccentric work, ultra-structural and morphological low-frequency fatigue related damage is caused to the muscle [Nurenberg et al., 1992; Friden et al., 1983; Friden and Lieber, 1992; Sargeant and Dolan, 1987; Balnave and Thompson, 1993]. More recently, Lieber et al., [1996] reported in experimental animal models that cyto-skeletal disruption occurs within the first 15 min. of cyclic eccentric contraction. It can thus be assumed that, due to the structural disruption that results from repetitive intensive eccentric

muscle activity, and despite the above-mentioned reduced metabolic cost, a decreased ability of the muscle to attenuate and dissipate the heel-strike induced shock accelerations may be expected.

We have earlier seen the characteristics of spectral analysis of the acceleration signal. Frequency analysis was also used to study vertical transmission of the acceleration signal from the shank upwards along the body. Thus, it has been reported that the range of the median frequency (MDF) of the entire PSD at the sacrum is 7–9 Hz [Voloshin et al., 1998], as compared to 11–13 Hz at the shank level [Voloshin et al., 1998; Mahar et al., 1997] and to 3–4 Hz at the head level [Mahar et al., 1997]. It has been suggested that the elimination of higher frequencies in higher body positions is associated with the low-pass filter properties of the body.

For each given frequency, the following transfer function (TF) is defined [Shorten and Winslow 1992]:

$$TF = 10 \log_{10} (PSD_{sacrum}/PSD_{shank}) \qquad (4.1)$$

where PSD_{sacrum} and PSD_{shank} designate the PSD functions for the sacrum and shank, respectively. The transfer function assumes a positive value if PSD_{sacrum} is larger than PSD_{shank} (amplified signal) and a negative value if PSD_{sacrum} is smaller than PSD_{shank} (attenuated signal).

From the PSD versus frequency plots, three frequency measures were used for the statistical analyses: (a) peak frequency of the active, low-frequency, region; (b) peak frequency of the impact shock region; and (c) median frequency of the entire PSD.

4.7. Shank and Sacrum Shock Acceleration and Sacrum / Shank Attenuation Ratio

Variations of the shock acceleration and of the attenuation ratio during the course of running are presented in Fig. 4.7. On the shank, the shock acceleration increased in level running, but did not vary in decline running (top panel). At the sacrum level the shock acceleration increased in both level and decline running (central panel). The average sacrum shock acceleration was higher in decline compared to level running. The average sacrum/shank shock acceleration ratio decreased in level running (bottom panel), but increased in decline running. The attenuation ratio was significantly higher in decline compared to level running.
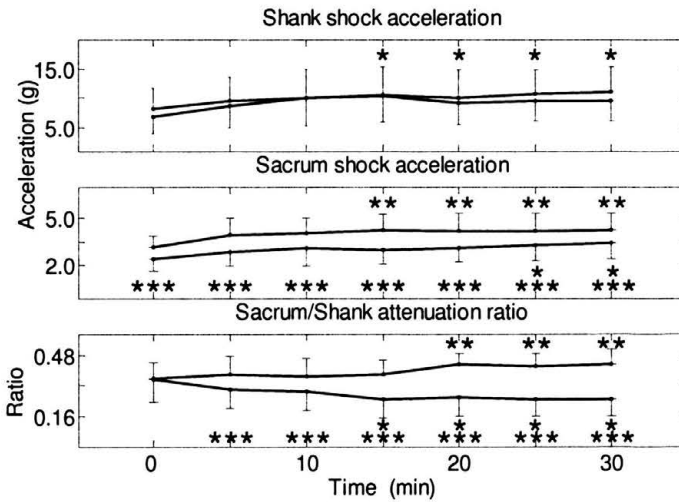
FIGURE 4.7. Variations of the shock acceleration and of the attenuation ratio during the course of running

It is concluded that during decline running, when metabolic fatigue was not attained, a significantly increased shock acceleration was found at the sacrum level, while the shock acceleration at the tibial tuberosity level did not change. Of special interest was to compare the sacrum/shank acceleration attenuation ratio, as presented in Fig. 4.7, bottom panel. In level running this ratio decreased significantly with the development of metabolic fatigue while in decline running, it significantly increased.

4.7.1. Transfer function (TF)

The mean transfer function, equation (4.1), for all the subjects versus frequency is presented in Fig. 4.8 for level and decline running, at different stages of running [Mizrahi et al., 2000a]. Frequencies above 5 Hz were attenuated between the shank and sacrum levels (negative TF values). Peak attenuation was noticed at nearly 9 Hz in both level and decline running. The effect of time during running on frequency attenuation was less accentuated in decline running when compared to level running. In level running the peak at 9 Hz was found to increase over the course of running, hence improving the attenuation between shank and sacrum. In decline running the opposite was noticed demonstrating, in the frequency domain, that the attenuation properties were more inferior in downhill compared to level running.
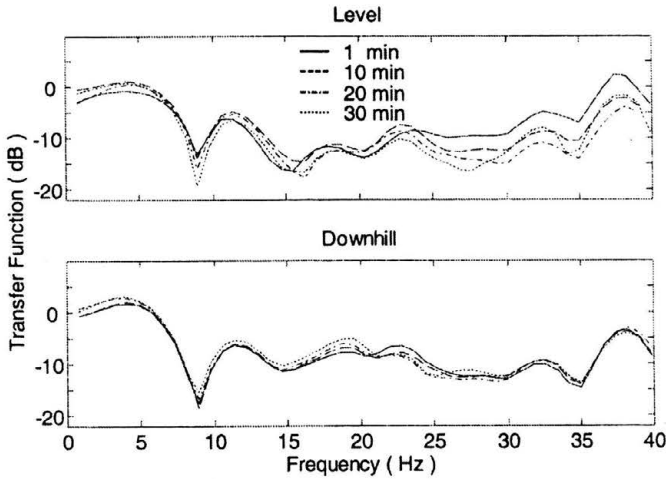
FIGURE 4.8. Transfer function, expressing the attenuation between shank and sacrum, equation

It has been reported that downhill running was associated with an increased mechanical stress [Iversen and McMahon, 1992] and muscular damage due to eccentric muscular contractions [Nurenberg et al., 1992]. It is also well known that one of the major functions of lower limb muscle tissues is the dissipation of shock loadings during human locomotion [Paul et al., 1978; Radin, 1986; Jefferson et al., 1990]. Milgrom, [1989] reported that an increased shock loading on the bone results in an enhanced risk of stress fractures, due to inability of the muscle tissues to effectively dissipate and attenuate the heel strike induced shock loads. It can therefore be hypothesized that the increased shock transmission from the tibial tuberosity to the sacrum level is associated with an increased muscular damage and, consequently, an inability of the lower limb muscle tissues to dissipate and attenuate shock wave propagation. Interestingly downhill running, which involves eccentric contraction, was found to be associated with increased shock propagation from the tibial tuberosity level to the sacrum levels without the development of metabolic fatigue.

4.7.2. Power Spectral Density (PSD)

Figure 4.9 shows typical spectra for one subject of the shank and sacrum accelerometer traces during the contact phase of running. In level running, the shank PSD demonstrates in the first minute of running a two-peak pat-
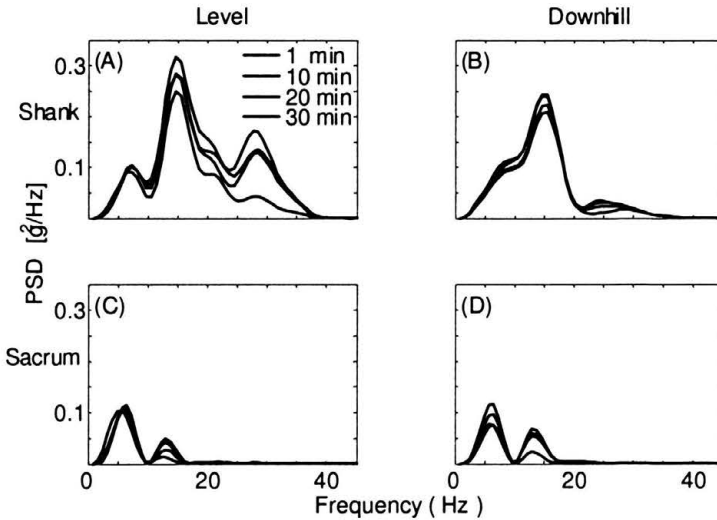
FIGURE 4.9. Typical spectra for one subject of the shank and sacrum accelerometer traces during the contact phase of running

tern (Fig. 4.9a). The impact peak (12–20 Hz zone) is higher than the active one (4–9 Hz zone). As fatigue develops the peak in the impact region increases and, in parallel, an additional peak within the 25–35 Hz range level becomes noticeable. The sacrum PSD in level running demonstrates a double-peak pattern throughout the running time (Fig. 4.9c), with the active peak at a higher level than the impact peak.

In decline running the shank PSD has a single peak at the impact frequency region, and a shallow inflection zone in the active frequency region (Fig. 4.9b). The sacrum PSD demonstrates again a double-peak pattern, with a higher peak in the active frequency region. As fatigue develops, the peak magnitudes increase (Fig. 4.9d).

4.8. Global Fatigue Versus Local Fatigue

The EMG signal is used for the online monitoring of muscle fatigue. Figure 4.10 presents a typical output of the shank acceleration, and of the integrated electromyogram (iEMG) of the gastrocnemius and tibialis anterior muscles in the 1st min. (non-fatigue) and in the 30th min. (fatigue). A stick diagram of the leg is presented in the lower part of the figure, showing one running cycle of the right leg.

Shank Acceleration and iEMG for Typical Cycle

FIGURE 4.10. Typical output of the shank acceleration, and of the integrated electromyogram (iEMG) of the gastrocnemius and tibialis anterior muscles in the 1st min. (non-fatigue) and in the 30th min. (fatigue); a stick diagram of the leg is presented in the lower part of the figure, showing one running cycle of the right leg
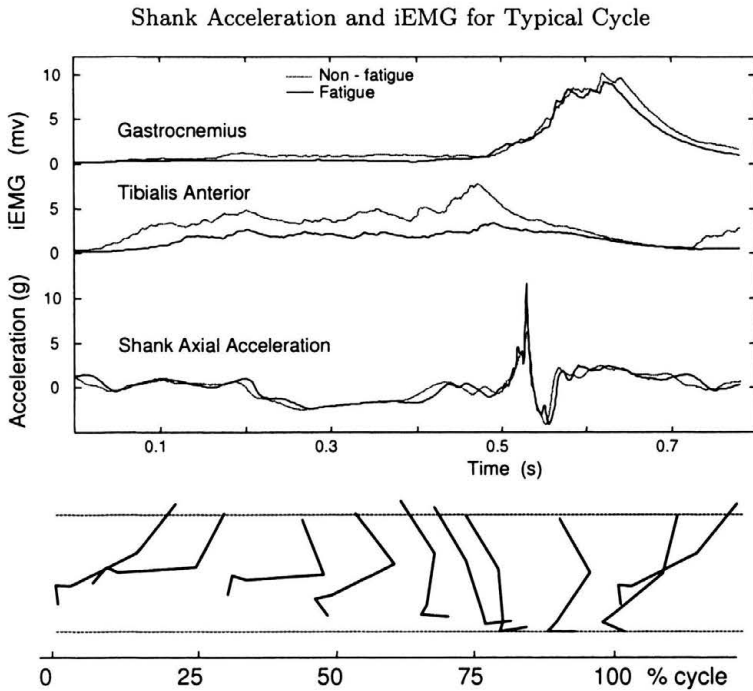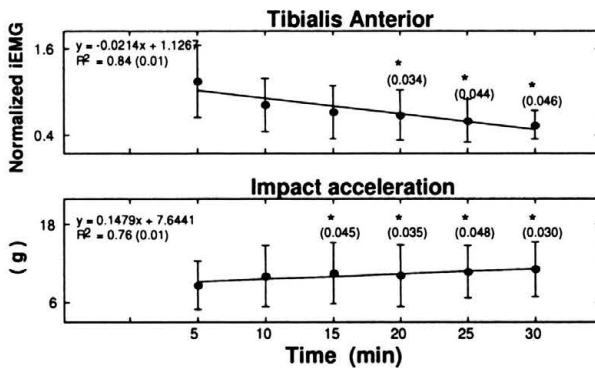

FIGURE 4.11. Averages of the integrated EMG (iEMG) data of the tibialis anterior muscle (top) and impact acceleration (bottom)

Averages of the iEMG data of the tibialis anterior muscle are presented along with the impact acceleration (in time domain) in Fig. 4.11. It is seen that the tibialis anterior iEMG significantly decreased from the 20th min. onwards compared to the 5th min. of running ($P \leqslant 0.046$). The MPF of the EMG data of the tibialis anterior muscle along with the MPF of the impact acceleration (in frequency domain) is presented in Fig. 4.12. MPF of the tibialis anterior significantly decreased from the 20th min. and onwards compared to the 1st min. of running ($P \leqslant 0.048$). The results obtained in this study revealed an increased MPF of the acceleration signal that indicated that during running the heel strike became more impulsive as general fatigue developed. Impact intensity also increased. As previously suggested, this may result in an increased fracture risk due to the muscles' inability to dissipate and attenuate the heel strike induced impact acceleration [Milgrom, 1989].
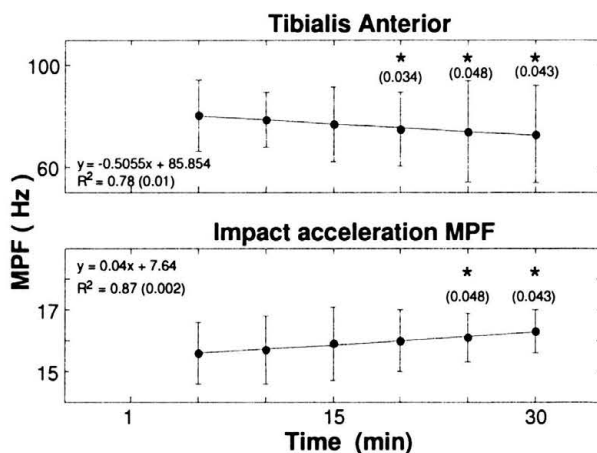
FIGURE 4.12. MPF of the EMG data of the tibialis anterior muscle (top) along with the MPF of the impact acceleration (bottom)

Two major fatigue-related factors taking part in exposing the shank to stress fractures risk are to this point obvious. One is increased intensity and mean frequency (MPF) of the impact acceleration on the shank accompanying the decline in end tidal carbon dioxide pressure ($PETCO_2$), the latter expressing metabolic fatigue [Wasserman 1987]. The second is the developing imbalance between the ankle's antagonistic flexor muscles resulting from changes in the activities of these muscles, as demonstrated in Fig. 4.13. Along with the prominent decrease in the iEMG of the tibialis anterior, there is an
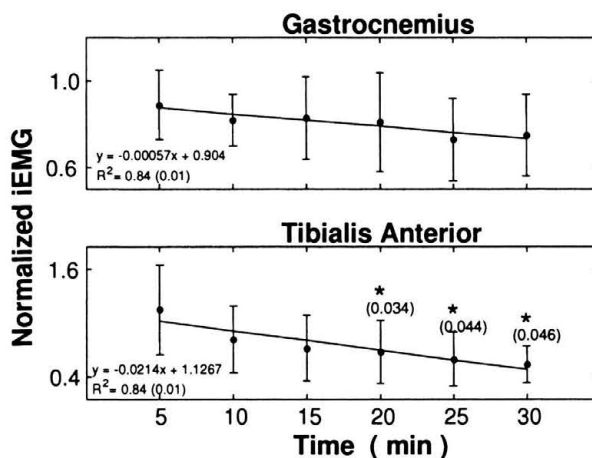
FIGURE 4.13. Differences in the activities of the gastrocnemius and tibialis anterior muscles during the course of running
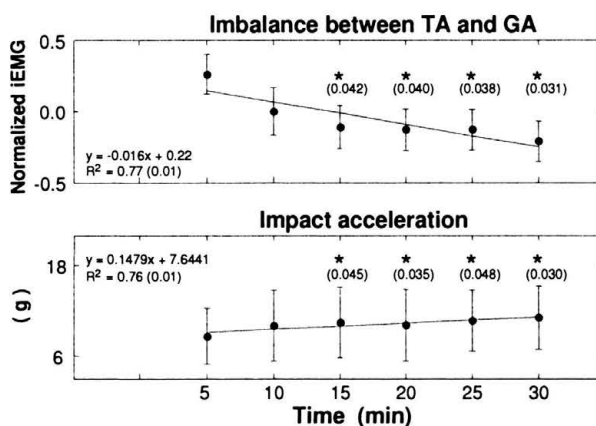
FIGURE 4.14. Developing imbalance between the gastrocnemius and tibialis anterior muscle

insignificant change in the iEMG of the gastrocnemius, reflecting developing imbalance. The developing imbalance between the two muscles in parallel to the increasing impact is shown in Fig. 4.14.

The question whether the disturbance in activation between the agonistic and antagonist ankle muscles combines with the increased impact acceleration on the shank is an important issue due to the following reason. Muscles have an important role in bone loading, particularly bending [Baker et al.; 1972, Nordin and Frankel, 1989]. When purely bent, one surface of the bone

is subject to compression and the opposite surface to tension. Since bone is weaker in tension than compression [Yamada, 1970], it should be of interest to protect the bone from excessive tensile stresses [Herrmann and Leibowitz, 1972].

Co-contraction of antagonistic muscles do help in providing that protection by: (a) compound bending, i.e. converting non-axial bending stresses into more axial and compressive stresses, therefore lowering the tensile stresses on the bone [Baker et al., 1972; Nordin and Frankel, 1989]; (b) stabilizing the lower leg at heel strike while loading occurs [Elliot and Blanksby, 1979]; and (c) serving as effective shock absorbers to lessen the impact on the shank due to the initial heel contact [Milgrom, 1989]. Thus, when imbalance between the muscles develops and the muscles that span the tensile surface of the bone become less active than those of the opposite side, the result is a decrease in the protection abilities of the muscles.

The development of loading imbalance was demonstrated by the myoelectric signals of the gastrocnemius and tibialis anterior muscles. The iEMG of the gastrocnemius muscle did not change suggesting a maintained activity of this muscle. This situation can be possible due to an enhanced firing rate of the working motor units, as reflected by the increase in the MPF, as was the case in our results. In the tibialis anterior muscle, however, both MPF and iEMG decreased substantially. The resulting reduction in the number of active motor units (reflected by the iEMG decrease) and in the motor unit firing rate (reflected by both decreases in MPF and iEMG) indicates that activity of this muscle is reduced due to fatigue [Edwards, 1981]. It should be pointed out that, due to its relatively high rate of sustained activity in the running cycle, the tibialis anterior muscle is susceptible to overload fatigue [Reber et al., 1993].

Thus, the mechanical consequence of fatigue in long-distance running is two-fold: enhanced impact acceleration due to global fatigue and muscle activity imbalance due to local fatigue before and during foot contact, resulting in the development of excessive tibial bending stresses and higher risk of stress injury.

4.9. Fatigue and Kinematics

The effect of fatigue on kinematics in the running exercise can be monitored by using markers were attached to the leg for video data were collection. Digital filtering (4th order Butterworth, zero-lag) with a cut off frequency of
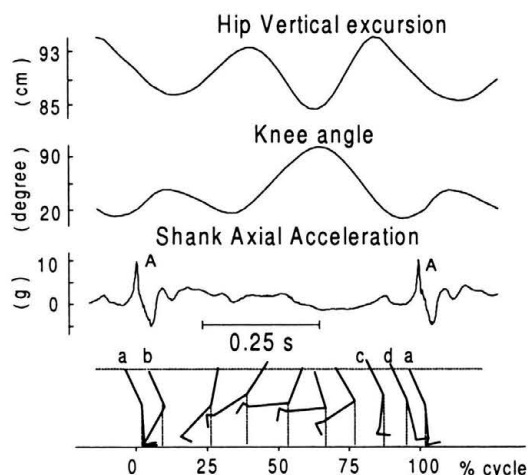
FIGURE 4.15. Examination of 2 additional kinematic factors: knee angle and hip vertical excursion, in addition to shank impact acceleration; a stick diagram of the leg is presented in the lower part of the figure, showing one running cycle of the right leg

10 Hz is necessary for smoothing the markers' data [Mizrahi et al., 2000c]. An external trigger is used to synchronize the accelerometer and video data.

Figure 4.15 presents a typical output of impact acceleration on the shank, knee angle and hip vertical excursion. A stick diagram of the leg is presented in the lower part of the figure, showing one running cycle of the right leg. The curves of the knee and hip were obtained by using cubic spline interpolation. The accelerometer spike was used to indicate knee and hip positions at foot strike.

The following kinematic parameters were measured: 1) Impact acceleration on the shank, defined as the maximal amplitude of the accelerometer transient at foot strike (position a); 2) Stride rate from the times between the impact accelerations; 3) Angle at the maximum knee extension position (position d, preceding heel strike, slide 41), at peak acceleration (position a), and at maximal stance flexion (cushioning flexion, position b). The range of knee flexion between the positions d and a was also calculated; 4) Hip level at the following time points: maximum flight (position c), peak acceleration (position a) and cushioning flexion (position b). The hip height at these three positions was approximated by the marker attached to the greater trochanter. Differences between the 3 hip positions were calculated in order to establish the amplitudes of vertical excursion.
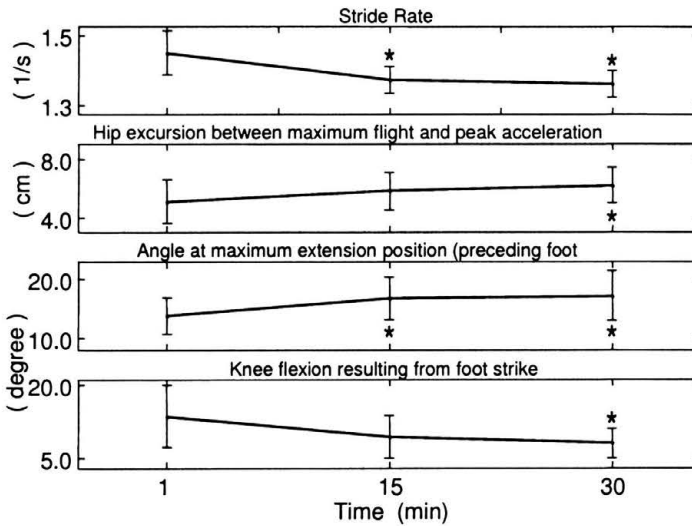
FIGURE 4.16. Summarized values of average stride rate, hip marker excursion and knee angle

Summarized values of average stride rate, hip marker excursion and knee angle are presented in Fig. 4.16. Initially, the average stride rate was $1.46 \pm 0.05\,\mathrm{s}^{-1}$ and a significant decrease was measured from the 15th min. onwards reaching the value of $1.39 \pm 0.03\,\mathrm{s}^{-1}$ (Fig. 4.16, top panel). The observed changes in stride rate are somewhat intriguing because, as has been reported in the non-fatigued state, at a given running speed, subjects select approximately the same optimal stride rate, corresponding to minimal metabolic cost [Cavanagh and Williams, 1982]. However, with progressing fatigue the subjects shift to a different stride rate than the optimal one [Verbitsky et al., 1998; Candau et al., 1998]. Thus, the observed reduction in stride rate is at the expense of an increase in metabolic cost.

The average hip heights at the maximal flight instant did not change significantly in the course of running. The average differences between the hip heights at maximal flight instant and maximum acceleration at the end of running were found significantly higher than those at the beginning of running, $6.2 \pm 1.2\,\mathrm{cm}$ versus $5.1 \pm 1.5\,\mathrm{cm}$, respectively (Fig. 4.16, 2nd panel). Differences between the hip heights at maximum acceleration and cushioning flexion did not change significantly. In the present study, speed was constrained by the treadmill to remain constant throughout running. The decreased stride rate at a constant running speed implies an increase in the

vertical displacement of the center of mass and of the hip [Anderson, 1996]. The hip vertical excursion analyzed in this study was found to increase significantly. It may be of interest to note in this respect the fatigue-related developing imbalance found between the ankle flexor and extensor muscles [Mizrahi et al., 2000b]. In the fatigued state the mean power frequency of the EMG of the tibialis anterior was found significantly reduced and that of the gastrocnemius significantly increased, as compared to the non-fatigued, state. However, the question whether increased hip excursion and fatigue of the flexor muscles are related to each other would require data on the fatigue of the flexor and extensor muscles at other joints as well and this remains to be studied.

The average for all subjects of the angle at maximum knee extension position (preceding touchdown, Fig. 4.16, 3rd panel) was 13.8±3.1° in the first min., and it increased significantly in the 15th and 30th min. ($16.8 \pm 3.7°$ and $17.2 \pm 4.2\circ$, respectively). The average knee angles at maximum acceleration and cushioning flexion did not change significantly.

Average of the ranges of knee flexion between the positions d (preceding heel strike) and a (during heel strike) are presented in Fig. 4.16, bottom panel. During the test, a significant decrease in the flexion range occurred between the first ($13.6 \pm 6.3°$) and the 30th minute ($8.1 \pm 3.0°$).

Of the kinematic variables shown, the knee angle is the more directly related to impact transmission and attenuation. With progressing fatigue, there is a gradual increase of the knee angle in the maximum extension position (i.e., just preceding the foot strike position) and a gradual decrease in the flexion range of the knee following foot-strike. It has been shown that increasing knee flexion at heel strike has different effects on the impact acceleration above and below the knee joint. On the shank, i.e. below the knee, the impact acceleration was reported to increase. Above the knee, impact attenuation was reported to improve [Hamill et al., 1995; Derrick et al., 1998]. This latter effect was studied in the following two situations: (a) "Groucho" running [McMahon et al., 1987], where the subjects are asked to run with their knees deliberately flexed, and (b) at foot strike, while the tested subjects were lying on their back [Lafortune et al., 1996]. It should be reminded that as a result of fatigue, the impact acceleration at the sacrum level also increases [Voloshin et al., 1998]. This increase however was to a lesser extent than that of the tibial tuberosity. Accordingly, the shank/sacrum attenuation ratio increased with increasing fatigue [Mizrahi et al., 2000a].

Thus, in parallel to the development of fatigue during steady-speed running on a treadmill, there is a gradual increase of the knee angle in the maximum extension position (i.e., preceding foot strike) and a gradual decrease in the flexion range accompanying foot-strike. Thus, fatiguing gradually approaches the "Groucho" style, which is characterized by an increased knee flexion and by an increased vertical acceleration measured at the shank and an improved attenuation [Mizrahi et al., 2000a], increasing the risk of overload injuries.

4.9.1. Aggravation

In the above results it has been shown that fatigue hampers the muscles from effectively fulfilling the important role of attenuating impact shocks therefore protecting the skeleton and joints from damage. Fatigue may be considered to be a muscle deficiency. While this usually is a temporary deficiency, more permanent deficiencies such as in situations of post-stroke, lower limb amputations or deterioration related to aging, muscle impairment presents a high-risk situation that may endanger the skeleton and joints. For instance, by 80 years of age muscle strength can reduce to about 40% of its young-adult value [Buckwalter et al., 1993] and bone strength and "mass" show long-known corresponding age-related changes [Riggs and Melton, 1995; Smith and Gilligan, 1989].

In the presence of musculo-skeletal deficiencies, a common consequence is reduced smoothness of motion, which characterizes normal gait and the appearance of stiff gait accompanied with bi-lateral asymmetry. Previous studies have indicated that following disability on one side of the body, there is a developing tendency to transfer loading forces from this affected side to the contra-lateral side. This leads to a two-fold problem: due to reduced loading, osteoporosis is likely to develop on the affected side [Burke et al., 1987], while joint degeneration and osteoarthritis develop on the over-loaded contra-lateral side [Burke et al., 1987, Kramer et al., 1979]. Moreover, due to the stiffer nature of locomotion higher dynamic components contribute to increased impact loading, contributing to enhanced joint degeneration. Further studies have indicated substantial damage also to the spine [Kramer et al., 1979].

Thus, the primary disability provides a predisposition for a secondary disability, both creating a vicious circle of severing the locomotion abilities.

The following question may then be asked: Are there means to *enhance*

muscle activity so as to increase its protective action under *fatigue* or other *deficient conditions*? Towards attempting to examine this question, it is of interest to note some facts about the mechanical activity of muscles while in contraction.

4.10. Mechanical Activity of a Contracting Muscle

In addition to the tension along their axes, muscles in action naturally vibrate (lateral vibrations) and thus produce detectable mechanical signals. These can be detected either by vibro-myography (VMG), or by the sound accompanying the muscle's activity, i.e., acoustic-myography (AMG). The origin of these mechanical signals should be distinguished from that of the electro-myographic (EMG) signals of the muscle. Previous studies have compared the correlation of each of those signals with muscle force and reported the existence of similar relations in some force ranges and differences in others [Zhang et al., 1992, Vaz et al., 1996, Herzog et al., 1994, Matheson et al., 1997]. It was concluded that either of the above (VMG or AMG) supplements EMG and provides further insight [Keidel and Keidel, 1989, Madeleine et al. 2001] to the muscle's activity.

The basic property of the mechanical signals from the contracting muscle is that its amplitude increases with tension and its frequency is rich in low frequencies, at the limit of recognition of tone, i.e. in the range of 10–50 Hz [Oster and Jaffe, 1980, Rhatigan et al., 1986]. It should be noted that, while this frequency component is an extremely low frequency from the electromagnetic point of view, it is considered very high from mechanical aspects. Interestingly, dynamic loading applied at this frequency has been found to be beneficial in bone remodeling [Adams et al., 1997, Fritton et al., 1997, McLeod et al., 1998. Qin et al., 1998]. With normal daily activities occurring at a frequency of ∼1 Hz, only muscle can provide the 10–50 Hz mechanical components, which are beneficial for bone remodeling. Thus, in addition to exerting the high-intensity loads on the bone and joint systems, muscles have two beneficial roles: (a) provide the high frequency components of the mechanical loading, which are important for mediating the physiologic response of bone tissue [Qin et al., 1998, McLeod et al., 1998], and (b) shock absorption, as already earlier discussed.

In a recent study it has also been reported that the 30–50 Hz activity components suffer a significant reduction with advancing age in humans [Huang

et al., 1999]. This observation is of utmost potential relevance due to the possible connection with other age-related changes. These include degradation in bone mass, postural stability as well as histologic changes in the muscle, such as the number of type II muscle fibers.

4.11. Properties of the Mechanical Signals

VMG signals are detectable by means of accelerometers, while the detection of AMG signals requires low-frequency microphones. Although both methods have been used to measure the mechanical activity of the contracting muscle, it has been argued that VMG is advantageous because the signal measured in this case can be calibrated in physiological/engineering units (m/s^2). At any case, since vibro- and acoustic-myography signals are linearly related [Barry et al., 1992], they may be considered equivalent.

As already mentioned, it is generally believed that the above-mentioned mechanical signals reflect the lateral vibrations of the muscle. Changes in muscle tension are the major determinants of changes in transverse resonant frequency. Muscles were found to be anisotropic (i.e., having different properties in different directions) with a much larger modulus of elasticity in the longitudinal than the transverse direction. This may be the cause for vibration, or sound production [Cole and Barry, 1994]. Muscle sounds are emitted at the resonant frequencies of skeletal muscle [Barry and Cole, 1990].

Various explanations have been suggested as to the origin of these signals. Some of these included intrinsic muscle events such as cross-bridge formation and breakage, physiological and biochemical processes within the sarcomere, such as ATP turnover [Oster and Jaffe, 1980; Fuchs, 1974; Taylor and Lymn, 1972; Huxley, 1974; Goldspink et al., 1970] and intramuscular visco-elastic characteristics [Orizio et al., 1999]. Other explanations suggested that these signals are related to motor control mechanisms rather than intrinsic contractile processes and thus maybe indicative of motor activation pattern [Orizio et al., 1999; Keidel and Keidel, 1989] and recruitment strategies (whenever force is considerably below full recruitment, [Goldenberg et al., 1991]).

Thus, VMG can provide means to evaluate muscle force contractions [Petitjean et al., 1992], as well as to provide information on the intrinsic properties of muscle, such as resonant frequency [Barry and Cole, 1990], muscle stiffness [Cole and Barry, 1994], information on fiber type composition and distribution [Akataki et al., 1999] which would help in monitoring muscle fa-

tigue [Orizio et al., 1999, Herzog et al., 1994] and in the diagnosis of pathology or disease [Madeleine et al., 2001; Zhang et al., 1992; Barry and Hill, 1992; Barry et al., 1985; Barry et al., 1990; Goldenberg et al., 1991; Wee and Ashley 1989].

An interesting fact is that with advancing age in humans the 30–50 Hz muscle activity is significantly reduced [Huang et al., 1999]. As already mentioned, bone density and strength also show age-related degradation (known as osteoporosis). It may thus be questioned whether these two changes are not correlated together?

4.12. Electrical Stimulation (ES) of Muscles

Chapters 2 and 3 have demonstrated the application of low-frequency (∼20–30 Hz) external ES on humans for the functional activation of handicaped muscles (FES) [Braun et al., 1985; Isakov and Mizrahi, 1993; Minzly et al., 1993a]. While it is generally accepted that long-term ES training can modify the fiber type distribution and partly reverse disuse atrophy in those muscles, the possible reduction of osteopenia by using ES has been less conclusive. Nevertheless, a number of research groups have demonstrated that bone mineral density can increase by ES training [Belanger et al., 2000; Bloomfield et al., 1996; Hangartner et al., 1994; Mohr et al., 1997; Stein, 1999]. It can therefore be assumed that external ES in the 30–50 Hz range may compensate for the reduced activity in that frequency. When the muscle is activated by electrical stimulation it becomes problematic to monitor its activity by means of the EMG signal because of the stimulus artifact. The latter may severely affect the signal unless appropriate measures to suppress the stimulus artifact are taken [Minzly et al., 1993b], as discussed in Chapter 2.

A relevant question is then whether by stimulation of the *muscle*, one can create the required mechanical environment on the neighboring *bone*. Bone and muscle are not only in the same vicinity, thus potentially influencing each other, but also functionally coupled together. Muscle stimulation can provide the mechanical environment to the bone. This same stimulation can also have a direct effect on bone through the electric field created. Thus the next question is whether stimulation can be designed to optimally satisfy *both* the mechanical component (through muscle stimulation) *and* direct electromagnetic component (to the bone cells).

For that purpose, studies into the effects of stimulation on the muscle/bone complex would have to be conducted. These studies should include modeling of the effects of stimulation parameters on the electric field distribution within the muscle/bone complex. In addition, experiments to monitor the changes taking place would have to be made in vitro and in vivo (on experimental animals and human beings). A major goal of this study will be to determine whether stimulation modes that can optimally activate the muscle/bone complex do exist, and to determine these modes.

4.13. Proposed Mode of Activation and Expected Significance

It is proposed that the muscles be selectively activated to serve either as shock absorbers or as limb actuators, to augment weakened functions due to musculo-skeletal impairment or to compensate for fatigue. In the first case, muscle activation will serve to reduce impact loads. In the second case, activation is intended to achieve better load balance between the 2 legs. The expected outcome is reduction of shock load on the skeleton and reduction of symmetry imbalance. The ultimate expected outcome will be reduction of bone fractures (short-term damage) and the risk of osteoporosis and osteoarthritis of the bones and joints of the affected and contra-lateral legs (long-term damage).

References for Chapter 4

1. D.J. ADAMS, A.A. SPIRT, T.D. BROWN, S.P. FRITTON, C.T. RUBIN, and R.A. BRAND, *Testing the daily stress stimulus theory of bone adaptation with natural and experimentally controlled strain histories*, J. Biomech., **30**:671–678, 1997.

2. K. AKATAKI, K. MITA, and Y. ITOH, *Relationship between mechamyogram and force during voluntary contractions reinvestigated using spectral decomposition*, Eur. J. Appl. Physiol., **80**:173–179, 1999.

3. O.K. ANDERSEN, F.A. SONNENBORG, and T. ARENDT-NIELSEN, *Modular organization of human leg withdrawal reflexes elicited by electrical stimulation of the foot sole*, Muscle Nerve, **22**:1520–1530, 1999.

4. T. ANDERSON, *Biomechanics and running economy*, Sports Medicine, **22**:76–89, 1996.

5. J. Baker, V. H. Frankel and A. Burstein, *Fatigue fractures: biomechanical considerations*, J. Bone Joint Surg., **54A**1345–1346, 1972.

6. C.D. Balnave and M.W. Thompson, *Effect of training on eccentric exercise-induced muscle damage*, J. Appl. Physiol., **75**:1545–1551, 1993.

7. D.T. Barry, S.R. Geiringer, and R.D. Ball, *Acoustic myography: a non-invasive monitor of motor unit fatigue*, Muscle Nerve, **8**:189–194, 1985.

8. D.T. Barry, K.E. Gordon, and G.G. Hinton, *Acoustic and surface EMG diagnosis of pediatric muscle disease*, Muscle Nerve, **13**:286–290, 1990.

9. D.T. Barry and N.M. Cole, *Muscle sounds at the resonant frequencies of skeletal muscle*, IEEE Trans. Biomed. Engng., **37**:525–531, 1990.

10. D.T. Barry, T. Hill, and D. Im, *Muscle fatigue measured with evoked muscle vibrations*, Muscle & Nerve, **15**:303–309, 1992.

11. B.R. Beck, *Tibial stress injuries - An aetiological review for the purposes of guiding management*, Sports Medicine, **26**:265–279, 1998.

12. M. Belanger, R.B. Stein, G.D. Wheeler, T. Gordon, and B. Leduc, *Electrical stimulation: can it increase muscle strength and reverse osteopenia in spinal cord injured individuals?*, Arch. Phys. Med. Rehab., **81**:1090–1098, 2000.

13. S.A. Bloomfield, W.J. Mysiw, and R.D. Jackson, *Mone mass and endocrine adaptations to training in spinal cord injured individuals*, Bone, **19**:61–68, 1996.

14. Z. Braun, J. Mizrahi, T. Najenson, and D. Graupe, *Activation of paraplegics by functional electrical stimulation: training and biomechanical evaluation*, Scand. J. Rehab. Med., Suppl. **12**:93–101, 1985.

15. J.A. Buckwalter, Woo Sly, V.M. Goldberg, E.C. Hadley, F. Booth, T.R. Oegema, and D.R. Eyre, Current concepts review - soft-tissue aging and musculoskeletal function, J. Bone Joint Surg., [Am.] **75A**(10):1533–1548, 1993

16. M.J. Burke, V. Roman, and V. Wright, *Bone and joint changes in lower limb amputees*, Ann. Rheum. Dis., **37**:252, 1987.

17. D.B. Burr, R.B. Martin, M. B. Schaffler, and E. L. Radin, *Bone remodeling in response to in vivo fatigue microdamage*, J. Biomech., **18**:189–200, 1985.

18. R. Candau, A. Belli, G.Y. Millet, D. Georges, B. Barbier, and J.D. Rouillon, *Energy cost and running mechanics during a treadmill run to voluntary exhaustion in humans*, Europ. J. Applied Physiology, **77**:479–485, 1998.

19. P.R. CAVANAGH, and K.R. WILLIAMS, *The effect of stride length variation on oxygen uptake during distance running*, Medicine and Science in Sports and Exercise, **14**:30–35, 1982.

20. N.M. COLE and D.T. BARRY, *Muscle sound frequencies of the frog are modulated by skeletal muscle tension*, Biophys. J., **66**:1104–1114, 1994.

21. J.D. CURREY, *The Mechanical Adaptations of Bones*, Princeton University Press, Princeton, 1984.

22. R.H. DAFFNER, *Anterior tibial striations*, Am. J. Roengenology, **143**:651–653, 1984.

23. T.R. DERRICK, J. HAMILL, and G.E. CALDWELL, *Energy absorption of impacts during running at various stride lengths*, Medicine and Science in Sports and Exercise, **30**:128–135, 1998.

24. J.A. DICKINSON, S. D. COOK, and T. M. LEINHARDT, *The measurement of shock waves following heel strike while running*, J. Biomech., **18**:415–422, 1985.

25. R.H. EDWARDS, *Human muscle function and fatigue. Human muscle fatigue: physiological mechanisms*, Pitman Medical, London (Ciba Foundation symposium 82) pp. 1–18, 1981.

26. B.C. ELLIOT and B. A. BLANKSBY, *The synchronization of muscle activity and body segment movements during a running cycle*, Med. Sci Sports., **11**:322–327, 1979.

27. J. FRIDÉN, M. SJŠTRÖM, and B. EKBLOM, *Myofibriallar damage following intense eccentric exercise in man*, Int. J. Sports Med., **4**:170–176, 1983.

28. J. FRIDÉN and R.L. LIEBER, *Structural and mechanical basis of exercise-induced muscle injury*, Med. Sci. Sports Exercise, **24**:521–530, 1992.

29. J.C. FRITTON, C.T. RUBIN, Y.X. QIN, and K.J. MCLEOD, *Whole-body vibration in the skeleton: development of a resonance-based testing device*, Ann. Biomed. Engng., **25**:831–839, 1997.

30. F. FUCHS, *Striated muscle*, Ann. Rev. Physiol., **36**:461–502, 1974.

31. D.P. FYHRIE, C. MILGROM, S.J. HOSHAW, A. SIMKIN, S. DAR, D. DRUMB, and D.B. BURR, *Effect of fatiguing exercise on longitudinal bone strain as related to stress fracture in humans*, Ann. Biomed. Eng., **26**:660–665, 1998.

32. S.M. GOLDENBERG, H.J. YACK, F.J. CERNY, and H.W. BURTON, *Acoustic myography as an indicator of force during sustained contractions of a small hand muscle*, J. Appl. Physiol., **70**:87–91, 1991.

33. G. GOLDSPINK, R.E. LARSON, and R.E. DAVIES, *Fluctuations in sarcomere length in chick anterior and posterior latissimus dorsi muscles during isometric contraction*, Experimentia, **26**:16–18, 1970.

34. J. Hamill, T.R. Derrick, and K.G. Holt, *Shock attenuation and stride frequency during running*, Human Movement Science, **14**:45–60, 1995.

35. T.N. Hangartner, M.M. Rodgers, R.M. Glaser, and P.S. Barre, *Tibial bone-density loss in spinal-cord injured patients – effects of FES exercise*, J. Rehab. Res. Dev., **31**:50–61, 1994.

36. G. Herrmann, and H. Leibowitz, *Mechanics of bone fracture*, in: H. Leibowitz, [ed.] Fracture, vol. VII, Fracture of Nonmetals and Composites, New York: Academic Press, pp. 771–840, 1972.

37. W. Herzog, Y.T. Zhang, M.A. Vaz, A.C. Guimaraes, and C. Janssen, *Assessment of muscular fatigue using vibromyography*, Muscle Nerve, **17**:1156–1161, 1994.

38. R.P. Huang, C.T. Rubin, K.J. McLeod, *Changes in postural muscle dynamics as a function of age*, J. Geronto. A Biol. Sci. Med. Sci., **54**:352–357, 1999.

39. A.F. Huxley, *Muscular contraction*, J. Physiol., 243:1–43, 1974.

40. A. Hulkko and S. Orava, *Stress fractures in Athletes*, Int. J. Sports Med., **8**:221–226, 1987.

41. E. Isakov and J. Mizrahi, *FES system for self-activation: An electrical stimulator and instrumented walker*, Clin. Rehab., **7**:39–44, 1993.

42. J.R. Iversen, T.A. MacMahon, *Running on an incline*, J. Biomech. Eng., **114**:435–441, 1992.

43. R.J. Jefferson, J.J. Collins, M.W. Whittle, E.L. Radin, and J.J. O'Connor, *The role of the quadriceps in controlling impulsive forces around heel strike*, Proc. Inst. Mech. Engrs., **204**:21–28, 1990.

44. M. Keidel and W.D. Keidel, *The computer vibromyography as a biometric progress in studying muscle function*, Biomed. Tech., (Berl) **34**:107–116, 1989.

45. J. Kramer, J.M. Heisel, and C.H. Ullrich, *Spatschaden am Bewegungsapparat bei Oberschenkelamputierten und deren Begutachtung*, Z. Orthop., **117**:801, 1979.

46. M.A. Lafortune, E.M. Hennig, and M.J. Lake, *Dominant role of interface over knee angle for cushioning impact loading and regulating initial leg stiffness*, J. Biomech., **29**:1523–1529, 1996.

47. R.L. Lieber, L.A. Thornell, and J. Friden, *Muscle cytoskeletal disruption occurs within the first 15 min. of cyclic eccentric contraction*, J. Appl. Physiol., **80**:278–284, 1996.

48. P. Madeleine, P. Bajaj, K. Sogaard, and L. Arendt-Nielsen, *Mechanomyography and electromyography force relationships during concentric, isometric and eccentric contractions*, J. Electromyo & Kinesiol., **11**:113–121, 2001.

49. A.T. Mahar, T.R. Derrick, J. Hamill, and G.E. Caldwell, *Impact shock and attenuation during in-line skating*, Med. Sci. Sports Exercise, **29**:1069–1075, 1997.

50. R.B. Martin and D.B. Burr, *Structure, Function and Adaptation of Compact Bone*, Raven Press, New York, 1989.

51. G.O. Matheson, L. Maffey-Ward, M. Mooney, K. Ladly, T. Fung, and Y.T. Zhang, *Vibromyography as a quantitative measure of muscle force production*, Scand. J. Rehab. Med., **29**:29–35, 1997.

52. T.M. McLellan and K.S. Cheung, *A comparative evaluation of the individual anaerobic threshold and the critical power*, Med. Sci. Sports Exerc., **24**:543–50, 1992.

53. K.J. McLeod, C.T. Rubin, M.W. Otter, and Y.X. Qin, *Skeletal cell stresses and bone adaptation*, Am. J. Med. Sciences, **316**:176–183, 1998.

54. T.A. McMahon, G. Valiant, and E. Frederick, *Croucho running*, J. Appl. Physiol., **62**:2326–2337, 1987.

55. C. Milgrom, *The Israeli elite infantry recruit: a model for understanding the biomechanics of stress fractures*, Journal of the Royal College of Surgeons of Edinburgh, **34**(6 Suppl):S18–S21, 1989.

56. J. Minzly, J. Mizrahi, E. Isakov, Z. Susak, and M. Verbeke, *Computer controlled portable stimulator for paraplegic patients*, J. Biomed. Eng., **15**:333–338, 1993a.

57. J. Minzly, J. Mizrahi, N. Hakim, and A. Liberson, *A stimulus artifact suppressor for EMG recording during FES by a constant current stimulator*, Med. Biol. Eng. and Comput., **31**:72–75, 1993b.

58. J. Mizrahi, and Z. Susak, *In-vivo elastic and damping response of the human leg to impact forces*, ASME J. Biomech. Eng., **104**:63–66, 1982.

59. J. Mizrahi, A. Voloshin, D. Russek, O. Verbitsky, and E. Isakov, *The influence of fatigue on EMG and impact acceleration in running*, Basic Appl. Myol., **7**:111–118, 1997.

60. J. Mizrahi, O. Verbitsky, and E. Isakov, *Shock accelerations and attenuation in downhill and level running*, Clinical Biomech., **15**:15–20, 2000a.

61. J. MIZRAHI, O. VERBITSKY, and E. ISAKOV, *Fatigue-related loading imbalance on the shank in running: a possible factor in stress fractures*, Annals Biomed. Eng., **28**:463–469, 2000b.

62. J. MIZRAHI, O. VERBITSKY, E. ISAKOV, and D. DAILY, *Effect of fatigue on leg kinematics and shank shock in long distance running*, Human Movem. Science, **19**(2):139–151, 2000c.

63. J. MIZRAHI, O. VERBITSKY, and E. ISAKOV, *Fatigue-induced changes in decline running*, Clinical Biomechanics, **16**(3):207–212, 2001.

64. T. MOHR, J. PODENPHANT, F. BIERING SORENSEN, H. GALBO, G. THAMSBORG, and M. KJAER, Calc. Tissue Intnl., **61**:22–25, 1997.

65. M. NORDIN and V. FRANKEL, *Biomechanics of bone*, in: M. Nordin, V. Frankel [Eds.] Basic Biomechanics of the Musculoskeletal System, Philadelphia (PA): Lea and Febiger, pp.3–29, 1989.

66. P. NURENBERG, C.J. GIDDINGS, J. STRAY-GUNDERSEN, J.L. FLECKENSTEIN, W.J. GONYEA, and R.M. PESHOCK, *MR Imaging-guided muscle biopsy for correlation of increased signal intensity with ultrastructural change and delayed-onset muscle soreness after exercise*, Radiology, **184**:865–869, 1992.

67. C. ORIZIO, B. DIEMONT, F. ESPOSITO, E. ALFONSI, G. PARRINELLO, A. MOGLIA, and A. VEICSTEINAS, *Surface mechanomyogram reflects the changes in the mechanical properties of muscle at fatigue*, Eur. J. Appl. Physiol. & Occup. Physiol., **80**:276–284, 1999.

68. G. OSTER and J.S. JAFFE, *Low frequency sounds from sustained contraction of human skeletal muscle*, Biophys. J., **30**:119–128, 1980.

69. I.L. PAUL, M.B. MUNRO, S.S.R. ABERNETHY, E.L. RADIN, and R.M. ROSE, Musculo-skeletal shock absorption: Relative contribution of bone and sort tissue at various frequencies, J. Biomech., **11**:237–239, 1978.

70. M. PETITJEAN, B. MATON, J.C. CNOCKAERT, *Evaluation of human dynamic contraction by phonomyography*, J. Appl. Physiol., **73**:2567–2573, 1992.

71. Y.X. QIN, C.T. RUBIN, and K.J. MCLEOD, *Nonlinear dependence of loading intensity and cycle number in the maintenance of bone mass and morphology*, J. Orthop. Res., **16**:482–489, 1998.

72. E.L. RADIN ET AL., Annals of Rheumatic Diseases, **34**:132–133, 1975.

73. E.L. RADIN, *Role of muscles in protecting athletes from injury*, Acta Med Scand Suppl., **711**:143–147, 1986.

74. L. REBER, J. PERRY, and M. PINK, *Muscular control of the ankle in running*, Am. J. Sports Med., **21**:805–810, 1993.

75. B.A. RHATIGAN, K.C. MYLREA, E. LONDSALE, and L.Z. STERN, *Investigation of sounds produced by healthy and diseased human muscular contraction*, IEEE Trans. Biomed. Engng., **33**:967–971, 1986.

76. B. RIGGS and L. MELTON, *The Worldwide problem of osteoporosis – insights afforded by epidemiology*, Bone, **17**(5):S505–S511, Suppl. S, 1995.

77. A.J. SARGEANT, P. DOLAN, *Human muscle function following prolonged eccentric exercise*, Eur. J. Appl. Physiol., **56**:704–711, 1987.

78. M.B. SCHAFFLER, E. L. RADIN, and D. B. BURR, *Long-term fatigue behavior of compact bone at low strain magnitude and rate*, Bone, **11**:321–326, 1990.

79. M.R. SHORTHEN and D.S. WINSLOW, *Spectral analysis of impact shock during running*, Int. J. Sport Biomech., **8**:288–304, 1992.

80. J.E. SMEATHERS, *Transient vibrations caused by heel strike*, J. Engineering Med., **203**:181–186, 1989.

81. E. SMITH, C. GILLIGAN, P. SMITH, C. SEMPOS, *Calcium supplementation and bone loss in middle-aged women*, Am. J. Clinical Nutrition, **50**(4):833–842, 1989.

82. R.B. STEIN, *Functional electrical stimulation after spinal cord injury*, J. Neurotrauma, **16**:713–717, 1999.

83. E.W. TAYLOR and R.W. LYMN, *Enzyme kinetics and the mechanism of muscle contraction*, in: R.G. Cassens [Ed.], Muscle Biology Vol 1, Dekker, NY pp.47–69, 1972.

84. M.A. VAZ, Y.T. ZHANG, W. HERZOG, A.C. GUIMARAES and B.R. MACINTOSH, *The behavior of rectus femoris and vastus lateralis during fatigue and recovery: an electromyographic and vibromyographic study*, Electomyogr. Cin. Neurophysiol., **36**:221–230, 1996.

85. O. VERBITSKY, J. MIZRAHI, A. VOLOSHIN, Y. TREIGER, and E. ISAKOV, *Shock transmission and fatigue in human running*, J. Appl. Biomechanics., **14**:300–311, 1998.

86. A. VOLOSHIN, J. MIZRAHI, O. VERBITSKY, and E. ISAKOV, *Dynamic loading on the human musculoskeletal system – effect of fatigue*, Clin. Biomech., **13**:515–520, 1998.

87. K. WASSERMAN, *Determinants and detection of anaerobic threshold and consequences of exercise above it*, Circulation, **76**(suppl VI):VI-29, 1987.

88. A.S. WEE and R.A. ASHLEY, *Vibrations and sounds produced during sistained muscle contraction*, Electromyogr. Clin. Neurophysiol., **29**:333–337, 1989.

89. J. Wosk and A.S. Voloshin, *Wave attenuation in the skeletons of young healthy persons*, J. Biomech., **14**:261–268, 1981.

90. H. Yamada, *Strength of Biological Materials*, Baltimore: Williams and Wilkins, 1970.

91. Y.T. Zhang, C.Y. Frank, R.M. Rangayyan and G.D. Bell, *A comparative study of simultaneous vibromyography and electromyography with active human quadriceps*, IEEE Trans. Biomed. Engng., **39**:1045–1052, 1992.